The Institute of Paper Chemistry

Appleton, Wisconsin

Doctor's Dissertation

The Dynamic Mechanical Shear Properties of Concentrated Solutions of Polystyrene in Tricresyl Phosphate

Richard B. Wasser

June, 1964

THE DYNAMIC MECHANICAL SHEAR PROPERTIES OF CONCENTRATED SOLUTIONS OF POLYSTYRENE IN TRICRESYL PHOSPHATE

A thesis submitted by

Richard B. Wasser

B.S. (Ch.E.) 1959, University of Wisconsin
M.S. 1961, Lawrence College

in partial fulfillment of the requirements
of The Institute of Paper Chemistry
for the degree of Doctor of Philosophy
from Lawrence College,
Appleton, Wisconsin

June, 1964

TABLE OF CONTENTS

SUMMARY

The real and imaginary components of the complex dynamic shear modulus were obtained for six polystyrene-tricresyl phosphate solutions of concentrations 5, 10, 21, 35, 52, and 67% polystyrene by weight. The data were obtained using a double electromagnetic transducer at frequencies between 6 and 1000 c.p.s. and over a temperature range where the solutions had dynamic properties characteristic of the glass-to-rubber transition region.

For all solutions the temperature dependence of relaxation times could be described by the Williams, Landel, and Ferry (WLF) equation. At the glass transition temperature the fractional free volume and the expansion coefficient of the fractional free volume, both calculated from the WLF equation, were found to be the same for all the solutions. This supports the theory that the glass transition temperature represents an iso-free volume state.

The method of reduced variables was used to obtain composite curves from the data at all temperatures. The relaxation spectra were calculated from the composite curves of both the real and imaginary components of the complex dynamic shear modulus for each solution. Agreement of the spectra as calculated from each component indicated that the applied shear strains were within the linear viscoelastic region where the Boltzmann superposition principle applies.

An equation was derived to relate the effect of concentration on relaxation times for the concentration range where the fractional free volume is not a linear function of concentration. The equation is of the form of the WLF equation and contains fractional free volume parameters which may be calculated from the WLF equation. This equation was applied to the transition regions of the relaxation spectra. Above a concentration of 10%, the relaxation spectra were proportional to the square of the concentration as opposed to the first power predicted by molecular theories for dilute solutions.

The loss tangent curves for each solution approached or passed through minima which are indicative of intermolecular entanglement coupling. The number of bonds between entanglements was estimated to be proportional to the -0.75 power of the concentration.

The real and imaginary components of the complex dynamic shear modulus for the 5 and 10% solutions were compared with the molecular theories of Rouse and Zimm modified for polymolecularity by Menefee and Peticolas. The shapes of the curves for the 5% solution appeared to be somewhere between that of the Zimm curve and Rouse curve while the curves for the 10% solution followed the Rouse theory more closely. The positions of the curves deviated from the theoretical curves in a direction which could be due to the effect of entanglement coupling on the steady-flow viscosity.

INTRODUCTION

Linear high molecular weight polymers are used extensively in the coating of paper because of the mechanical, optical, and resistant qualities they impart to the sheet. Polymers such as the cellulose derivatives and those of the vinyl type may be applied to paper by impregnation with a dilute solution of polymer in a suitable organic solvent. Various high boiling solvents known as plasticizers are incorporated in the coating formulation in order to give flexibility and toughness to the polymeric coating.

In a technological sense there is a wealth of information concerning the effect of plasticizers on the mechanical properties of high polymers. Unfortunately, most of the information has not been obtained in a form amenable to analysis according to current theories. In those instances where appropriate studies have been conducted, emphasis has been on examination of the undiluted polymer or its dilute solutions. Relatively little attention has been paid to the mechanical properties of concentrated polymer solutions.

It is the purpose of the present thesis to contribute to the knowledge about the mechanical properties of concentrated solutions which, for convenience, will be taken to include those solutions with a relative viscosity of the order of 100 or greater (1). The present investigation will be confined to a quantitative and theoretical interpretation of the effect of concentration, time, and temperature on the dynamic mechanical properties of solutions of polystyrene in tricresyl phosphate.

Polystyrene was chosen for the present work since it is a typical linear amorphous polymer. The polymer sample is of high molecular weight and has a

known molecular weight distribution. Tricresyl phosphate (TCP) was selected as the solvent because it is completely miscible with polystyrene at all concentrations and it has a very low volatility so that concentration changes of the solutions due to solvent losses are negligible. Also, a relatively simple and accurate analysis for TCP is available which makes it possible to determine the concentrations of the solutions after they have been prepared.

BACKGROUND

High polymers, such as polystyrene, have remarkable mechanical properties due to their great length and the fact that they have many degrees of freedom. When a dynamic mechanical property, such as the shear modulus, is investigated as a function of time, it is possible to define four characteristic regions in the experimental time scale. At the short time end of the scale there is a glassy region where the energy of deformation is stored in valence angle deformation and slight changes in interatomic distances. Characteristically, moduli of the order of 10^{11} to 10^{12} dynes/cm.^{2} are observed. At slightly longer times, where side groups on the polymer chain are able to respond, the modulus may drop to 10^{10} dynes/cm.^{2}.

By advancing along the time scale, the glass-to-rubber transition region is observed. Here sufficient time is available for segments of the polymer chain to change configurations and thereby relieve the applied stress. In this region the modulus will be extremely frequency dependent and will decrease from a value of the order of 10^{10} dynes/cm.^{2} to values of the order of 10^6 to 10^8 dynes/cm.^{2} which is characteristic of the rubbery region.

The rubbery region is next in order. This region is observed in those polymers that are of high enough molecular weight so that a network structure is present. This may be the result of actual chemical cross-linking or the result of entanglement coupling between the molecules.

In uncross-linked polymers a final region is observed in which the molecules disentangle from one another and the modulus drops rapidly in this terminal zone.

A large amount of work has been conducted on the mechanical properties of undiluted polymers. The effect of diluting with solvents has not received nearly as much attention. Most of the investigations on polymer solutions have been concerned with the rubbery and terminal region of the time scale. Important advances have been made in the interpretation of the effects of temperature in the glass-to-rubber transition region, and it seems reasonable to expect that the effects of concentration in this region may be interpreted in a similar way. In fact, Fujita, et al. (2) have already shown this to be true for experimental data obtained on a polymer diluted with small amounts of solvent.

Extensive data in the region of moderately concentrated polymer solutions is noticeably lacking. The work of Saunders, et al. (3) on the viscoelastic properties in the transition region for solutions of poly-n-butyl methacrylate in diethyl phthalate appears to be the only comprehensive study in this area.

THEORY

THE COMPLEX DYNAMIC SHEAR MODULUS

The experimental method used in this study involves the determination of the complex dynamic shear modulus, which may be defined as the ratio of sinusoidal shear stress to sinusoidal shear strain. If the shear stress is represented by the equation

$$\sigma^* = \sigma_o \exp [j(\omega t + \delta)], \tag{1}$$

then the shear strain on a linear viscoelastic material will be given by,

$$\gamma^* = \gamma_o \exp (j\omega t) \tag{2}$$

where σ_o and γ_o are the maximum stress and strain values, respectively, ω is the circular frequency, δ is the phase angle, and $\underline{t}$ is the time. The stress and strain may be represented as vector quantities in the complex mathematical plane as shown in Fig. 1.

The complex shear modulus $\underline{G}^*$ is defined by,

$$G^* = \sigma^*/\gamma^* = G' + jG'' , \tag{3}$$

where $\underline{G}'$ and $\underline{G}''$ are the real and imaginary components, respectively. From Equations (1), (2), and (3) we see that,

$$G^* = (\sigma_o/\gamma_o) \exp (j\delta) = (\sigma_o/\gamma_o)(\cos \delta + j \sin \delta), \tag{4}$$

and

$$G' = (\sigma_o/\gamma_o) \cos \delta , \tag{5}$$

$$G'' = (\sigma_o/\gamma_o) \sin \delta. \tag{6}$$

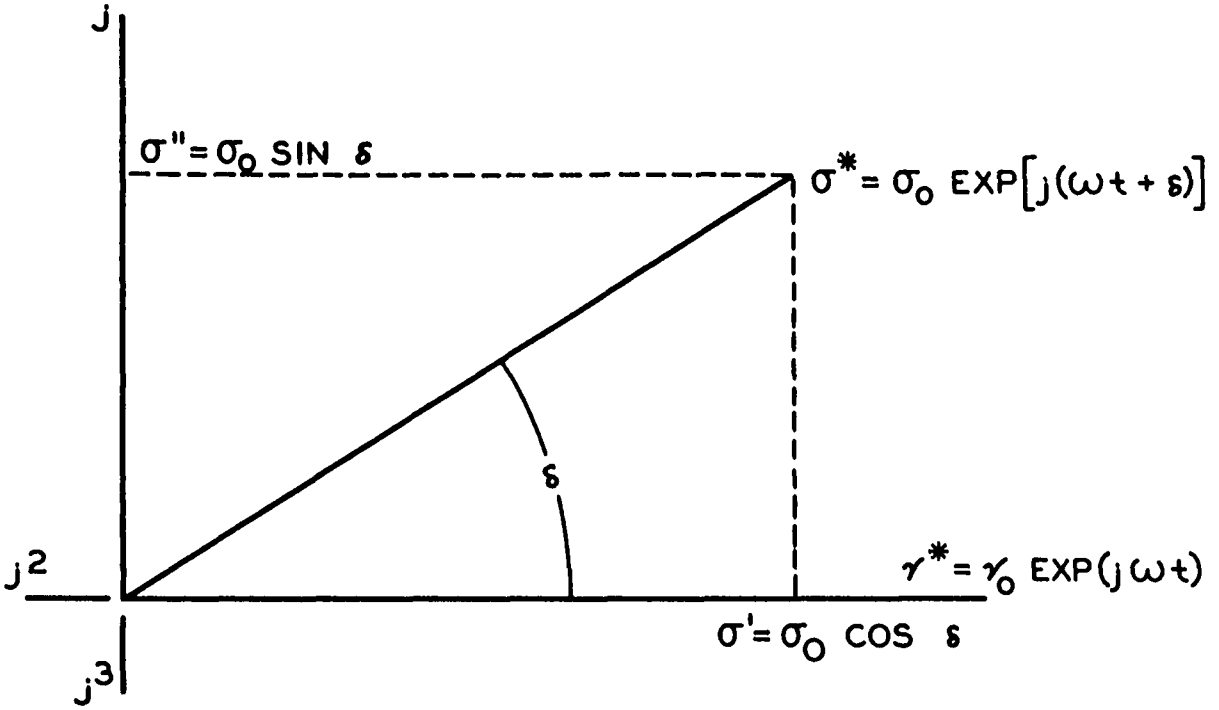

Figure 1. Graphic Representation of Sinusoidal Stress and Strain

The real component, $\underline{G}'$, is called the storage modulus since it is related to the energy stored in the sample per cycle, while the imaginary component, $\underline{G}''$, is called the loss modulus because it is related to the energy dissipated in the sample per cycle. The ratio, $\underline{G}''/\underline{G}' = \tan \delta$ is called the loss tangent.

PHENOMENOLOGICAL THEORY

In analysis of the frequency dependence of the complex dynamic shear modulus, use will be made of the phenomenological theory of viscoelasticity. Application of the theory will be limited to conditions which satisfy the Boltzmann principle of superposition (4, 5). This principle will apply only if all viscoelastic effects are linear (6). For the polymer solutions treated in the present work, these conditions are satisfied by restricting the examination of the complex dynamic modulus to small strains.

The real and imaginary components of the complex shear modulus can be written as,

$$G'(\omega) = \int_{-\infty}^{+\infty} H(\ln \tau) \left[\frac{\omega^2 \tau^2}{1 + \omega^2 \tau^2} \right] d(\ln \tau), \tag{4}$$

$$G''(\omega) = \int_{-\infty}^{+\infty} H(\ln \tau) \left[\frac{\omega \tau}{1 + \omega^2 \tau^2} \right] d(\ln \tau), \tag{5}$$

where $\underline{H}$ is the relaxation spectrum and $\underline{H}\, d(\ln \tau)$ is the contribution to the instantaneous shear modulus associated with relaxation times which lie between $\ln \tau$ and $\ln \tau + d(\ln \tau)$. If $\underline{H}$ were a line spectrum, that is, zero for all values of τ but one, then Equations (4) and (5) simplify to,

$$G'(\omega) = G_i \left[\frac{\omega^2 \tau_i^2}{1 + \omega^2 \tau_i^2} \right],$$

$$G''(\omega) = G_i \left[\frac{\omega \tau_i}{1 + \omega^2 \tau_i^2} \right],$$

where the kernels are multiplied by a constant, $\underline{G_i}$. These equations represent the mechanical properties of a Maxwell model, which consists of a spring of modulus $\underline{G_i}$ in series with a dissipative unit or "dashpot." The two units acting together have a characteristic relaxation time, $\tau_{\underline{i}}$. However, for the more complex mechanical properties of real viscoelastic materials, the kernels of Equations (4) and (5) must be multiplied by a continuous distribution function or relaxation spectrum.

It should be noted that ω appears on both sides of the equations. The components of the complex modulus on the left-hand sides of the equations are

the experimentally accessible quantities which are determined as a function of frequency. The relaxation spectrum is to be determined and can be recovered from under the integral sign by means of various methods of approximation.

The integral equations are not independent, and for a linear viscoelastic material the relaxation spectra obtained from the real and imaginary components of the complex modulus will be identical. This fact makes it possible to test the applicability of the Boltzmann superposition principle for any given material by experimental means.

MOLECULAR THEORIES

In addition to the phenomenologically based theory of viscoelasticity, use will be made of current molecular theories on the viscoelasticity of polymer solutions. The present section, therefore, contains a brief discussion of the theories of Rouse (7) and Zimm (8) and the extension of these theories to polymolecular systems.

THE ROUSE THEORY

In the Rouse theory an isolated flexible chain molecule is subdivided into a series of submolecules. The submolecules are long enough so that the distribution of their end-to-end separations may be described by a Gaussian probability function. The configuration of the submolecule is specified by the vector corresponding to the end-to-end separation. The configuration of the molecule is then described by the set of vectors corresponding to the submolecules.

In a velocity gradient the distribution of configurations of all the polymer molecules in the solution is continuously perturbed. As a result, free energy

will be stored in the molecules. The tendency for the free energy to seek a minimum provides the force tending to return the configurations of the molecules to their most probable distribution. The description of this process must take into account the co-ordinated thermal motions of the submolecules. Mathematically this results in a set of simultaneous partial differential equations in terms of the co-ordinates, gradients of chemical potential and mobility of the submolecules.

Solution of the equations by the methods of matrix algebra leads to the following equations for the storage and loss moduli. The storage modulus is given by,

$$G'(\omega) = \frac{cRT}{M} \sum_{p=1}^{N/5} \frac{\omega^2 \tau_p^2}{1 + \omega^2 \tau_p^2} \tag{6}$$

and the loss modulus by,

$$G''(\omega) - \omega\eta_s = \frac{cRT}{M} \sum_{p=1}^{N/5} \frac{\omega \tau_p}{1 + \omega^2 \tau_p^2} \tag{7}$$

where τ_p is the pth relaxation time given by,

$$\tau_p = \frac{6(\eta - \eta_s)M}{\pi^2 p^2 cRT} \tag{8}$$

Here, p is a running index, N is the number of submolecules, c the polymer concentration in grams of polymer per cubic centimeter of solution, R is the gas constant, M the molecular weight, η the steady-flow viscosity, and η_s the solvent viscosity.

Since the theory does not take into account configurational changes within segments of the chain shorter than the submolecule it is necessary to place an

upper limit on the value of p. Rouse imposes the requirement that $p < N/5$. This qualification then limits $\omega\tau_1$ to less than $N^2/250$.

The theory also does not take into account the intramolecular friction between the submolecules nor does it apply to polymer solutions with appreciable polymolecularity.

THE ZIMM THEORY

The Zimm theory (8) is based on a molecular model similar to that used by Rouse. It differs from the Rouse theory in that it specifically takes into account hydrodynamic interaction between submolecules. Hydrodynamic interaction was taken into account by using the method of Kirkwood and Riseman (9) for describing the hydrodynamic interaction between molecules in stationary flow.

The real and imaginary components of the complex shear modulus are given by Equations (6) and (7), respectively; however, the relaxation times obtained from the Zimm theory are different and are given by

$$\tau_p = 1.71\ (\eta - \eta_s)M/(\lambda_p'\ cRT) \tag{9}$$

where the λ_p' are numerical coefficients. The first seven values of λ_p' are 4.04, 12.8, 24.2, 37.9, 53.5, 70.7, and 89.4 (10). For p greater than seven the coefficients may be approximated by,

$$\lambda_p' = (\pi^2\ p^{3/2}/2)\ [1 - 1/(2\pi p)]. \tag{10}$$

MODIFICATIONS FOR POLYMOLECULARITY

Menefee and Peticolas (11) and Peticolas (12) have modified the Rouse and Zimm theories, which are for homogeneous polymers, to include polymolecularity.

The modifications for heterogeneity are introduced by assuming that the steady-flow viscosity of the whole polymer is a weighted sum of monodisperse viscosities;

$$\eta - \eta_s = \sum_i w_i(\eta - \eta_i)$$

$$= \sum w_i \sum_{p-1}^{N} (cRT/M_i)\tau_{pi}$$

where w_i and M_i are the weight fraction and molecular weight of the ith polymer molecule, respectively, and τ_{pi} is the pth relaxation time for that molecule.

For the Rouse theory the relaxation time becomes,

$$\tau_{pi} = \frac{6(\eta - \eta_s)}{\pi^2 p^2 cRT}\left(\frac{M_i^2}{\bar{M}_w}\right), \tag{11}$$

and the equation for the loss modulus in terms of a continuous molecular weight distribution becomes,

$$G'' - \eta_s = acRT \sum_{p=1}^{N} (1/p^2) \int_0^{\infty} \frac{\omega M\, W(M)\, dM}{1 + \left(\frac{\omega^2 a^2 M^4}{p^4}\right)}, \tag{12}$$

and for the storage modulus,

$$G' = a^2 cRT \sum_{p=1}^{N} (1/p^4) \int_0^{\infty} \frac{\omega^2 M^3 W(M)\, dM}{1 + \left(\frac{\omega^2 a^2 M^4}{p^4}\right)}, \tag{13}$$

where,

$$a = \frac{6(\eta - \eta_s)}{cRT\, \pi^2 \bar{M}_w},$$

and $\underline{W}(\underline{M})d\underline{M}$ is the weight fraction of polymer with molecular weight between $\underline{M}$ and $\underline{M} + d\underline{M}$, and $\bar{\underline{M}}_{\underline{w}}$ is the weight average molecular weight.

In the case of the Zimm theory, Peticolas (12) obtained for the loss modulus

$$G'' - \omega\eta_s = bcRT \sum_{1}^{N} (1/\lambda_p') \int_{0}^{\infty} \frac{\omega M^{1/2} W(M)\, dM}{1 + \left(\frac{\omega^2 b^2 M^3}{\lambda_p'^2}\right)}, \tag{14}$$

and for the storage modulus,

$$G' = b^2 cRT \sum_{1}^{N} (1/\lambda_p'^2) \int_{o}^{\infty} \frac{\omega^2 M^2 W(M)\, dM}{1 + \left(\frac{\omega^2 b^2 M^3}{\lambda_p'^2}\right)}, \tag{15}$$

where

$$b = \frac{1.71\ (\eta - \eta_s)}{cRT\ (\bar{M}_w)^{1/2}}.$$

TEMPERATURE AND CONCENTRATION DEPENDENCE OF RELAXATION TIMES

Since relaxation times are, in effect, rate constants, it would seem reasonable that their temperature dependence would fit an equation of the Arrhenius type. However, this has not been found to be true for glass-forming polymers and liquids. Apparent activation energies increase rapidly as the glass transition temperature is approached (13).

Williams, Landel, and Ferry (13) developed an empirical equation referred to as the WLF equation, for the temperature dependence of relaxation times. They found that this equation fitted experimental data of many polymer systems up to 100 degrees above their glass temperatures. The equation is of the form,

$$\log a_T = \frac{-C_1(T - T_o)}{C_2 + T - T_o} \tag{16}$$

where a_T is the ratio of the relaxation time at temperature T to the corresponding relaxation time at an arbitrary reference temperature T_o. The quantities C_1 and C_2 are empirical constants which are adjusted to fit the equation to the data.

Williams, Landel, and Ferry have shown that the WLF equation can be derived from a semiempirical equation developed by Doolittle (14). The Doolittle equation is used to describe the viscosity-temperature relationship of a homologous series of n-alkanes and is of the form,

$$\ln \eta = \ln A + B(v_o/v_f) \tag{17}$$

where A and B are constants, η is the viscosity, v_o the occupied volume of the molecules, and v_f the free volume. The free volume is defined as the decrease in specific volume that would be observed on going from a given temperature to absolute zero without encountering a change in phase. In order to obtain the WLF equation from the Doolittle equation, the constant B was set equal to unity, and the fractional free volume, f, was assumed to be a linear function of temperature,

$$f = v_f/(v_o + v_f) = f_o + \alpha_f(T - T_o), \tag{18}$$

where f_o is the fractional free volume at T_o and α_f is the expansion coefficient of the fractional free volume. The factor a_T was taken as the ratio of the viscosities at the two temperatures. It is apparent from the derivation that the constants in the WLF equation can be taken as

$$C_1 = 1/(2.303 f_o), \tag{19}$$

and,

$$C_2 = f_o/\alpha_f \ . \tag{20}$$

More recently, Cohen and Turnbull (15) derived a theoretical equation for self-diffusion in liquids. The equation has the same form as the Doolittle equation provided the self-diffusion coefficient is assumed to be inversely proportional to viscosity. This provides theoretical justification for the Doolittle equation and on this basis lends theoretical significance to the WLF equation.

Fujita and Kishimoto (2) have treated the effect of concentration on the shift in relaxation times by applying the concept of free volume in a manner similar to that used for temperature. The Doolittle equation was expressed in terms of fractional free volume, and the fractional free volume was assumed to be a linear function of the solvent concentration. For viscosity, diffusion, and viscoelastic data, (2, 16-19) this assumption was found to hold only at high concentrations, about 80% polymer or higher. Evidently, for lower polymer concentrations the fractional free volume is not a linear function of solvent concentration.

In the present work it was necessary to derive an equation for the effect of concentration on the relaxation times in the concentration range where the fractional free volume is a nonlinear function of concentration. Fujita and Kishimoto (19) have pointed out that the linear relationship between fractional free volume and concentration observed at high concentrations can be determined independently from the glass temperature-concentration relationship. An extension of this idea to include the nonlinear concentration range provides the basis for the following derivation.

Fox and Flory (20) suggest that the glass temperature is an iso-free volume state. This is supported by the fact that, for many polymer systems, the WLF constants, especially C_1 fall within a narrow range of values when the glass temperature of each system is chosen as its reference temperature (1).

Following Fox and Flory, assume that the fractional free volume at the glass temperature, f_g, is a constant independent of temperature. Furthermore, assume that the fractional free volume is a linear function of temperature and the expansion coefficient, α_f, is a constant over the range of concentrations considered. Then,

$$f(T,c) = f_g + \alpha_f [T - T_g(c)] \tag{21}$$

and for a reference polymer concentration c_o,

$$f(T,c_o) = f_g + \alpha_f [T - T_g(c_o)]. \tag{22}$$

Taking the difference between Equations (21) and (22),

$$f(T,c) = f(T,c_o) + \alpha_f [T_g(c_o) - T_g(c)] \tag{23}$$

and combining Equation (23) with the Doolittle viscosity Equation (17), an equation of the form of the WLF equation is obtained,

$$\log a_c = \frac{-[1/2.303\ f(T,c_o)][T_g(c_o) - T_g(c)]}{[f(T,c_o)/\alpha_f] + T_g(c_o) - T_g(c)} \tag{24}$$

where a_c is the ratio of relaxation times.

The right side of Equation (24) can be evaluated if the glass temperature is known as a function of concentration and $f(T,c_o)$ and α_f are known from

experimental log $\underline{a}_{\underline{T}}$ data. In this case log $\underline{a}_{\underline{c}}$ can then be calculated and compared directly with experimental results.

DISCRETE AND CONTINUOUS RELAXATION SPECTRA

According to Equations (8) and (9), the molecular theories of both Rouse and Zimm predict a discrete set of relaxation times. The relaxation spectrum defined by Equations (4) and (5) must then be a line spectrum rather than a continuous spectrum.

The relaxation spectrum for experimental data can only be obtained in continuous form; therefore, in order to compare experimental results with the molecular theories it is desirable to approximate the line spectrum with a continuous spectrum. Ferry (1) has shown that except for the two or three longest relaxation times, the line spectrum can be well approximated by a continuous spectrum. For the Rouse theory the spectrum has the form,

$$H = (\sqrt{6}/2)\,[(cRT/M)(\eta - \eta_s)]^{1/2}\,\tau^{-1/2} \tag{25}$$

and for the Zimm theory,

$$H = 0.626\,(cRT/M)^{1/3}(\eta - \eta_s)^{2/3}\,\tau^{-2/3}. \tag{26}$$

The limitations on these equations are, of course, the same as those for the Rouse and Zimm theories. Thus, they apply only to dilute solutions.

However, Ferry (1) has suggested that the forms of Equations (7) and (8) may apply to portions of relaxation spectra of concentrated and even undiluted polymers. This prediction is based on the assumption that for concentrated and undiluted polymers "each molecule executes much the same kind of motions that it

does in dilute solution, except that they are far slower because of higher frictional resistance."

THE INFLUENCE OF ENTANGLEMENT COUPLING ON RELAXATION SPECTRA

At polymer concentrations and molecular weights high enough to cause entanglement coupling between molecules, the transient network structure produces a plateau region in the relaxation spectrum and a minimum in the loss tangent.

Marvin (21) has derived a theory based on a ladder network model which takes into account entanglement coupling. Hoberg, et al. (22) have shown by a numerical evaluation of the Marvin theory that the minimum in the loss tangent can be expressed as

$$\tan \delta_{min} = 1.02 \left(\frac{2M}{\Lambda M_o} \right)^{-0.8} \qquad (27)$$

where M_o is the monomer molecular weight and Λ is the number of chain bonds between entanglement points. The equation only applies to homogeneous polymers; broad distribution polymers give minima which are too high (22). However, it has been assumed by Richards, et al. (23) that a broad distribution will not affect the concentration dependence of the minimum in the loss tangent, and they have found that for polyisobutylene the change in the number of bonds between entanglements is inversely proportional to the polymer concentration. This is what would be expected if there is a constant probability of entanglement of two juxtaposed monomer units in neighboring chains (23).

EXPERIMENTAL

THE DOUBLE ELECTROMAGNETIC TRANSDUCER

The present investigation of the dynamic mechanical properties of polystyrene solutions is based on the determination of the frequency dependence of the complex dynamic shear modulus. The complex dynamic shear modulus was determined by means of a double electromagnetic transducer which is a modified form of the instrument originally described by Marvin, et al. (24). A brief description of the modified instrument has been published (25); however, many of the operational details have been omitted. Information concerning the theory, construction, and recent modifications of the instrument is not readily available so that it is necessary to cover this material in some detail herein. This information was furnished by Kurath (26).

CONSTRUCTION

The central unit of the transducer is a rigid tube suspended by means of 8 steel wires as shown in Fig. 2 and 3. Basically, the unit consists of a 4 by 13/16 inch aluminum tube with 1/32-inch walls. The tube is of square cross section and is fitted at each end with magnesium inserts upon which are mounted Micarta coil forms. Double layers of No. 35 magnet wire are wound about each coil form and are attached to the forms by means of coil varnish. The total weight of the assembled tube is 43.23 g.

Each coil is situated in the magnetic field of a permanent magnet and the tube is mounted so as to translate freely in an axial direction (see Fig. 3). The pole faces of the magnets are shaped so as to supply the coils with a radial magnetic field. The pole faces of the magnet were machined from an annealed bar

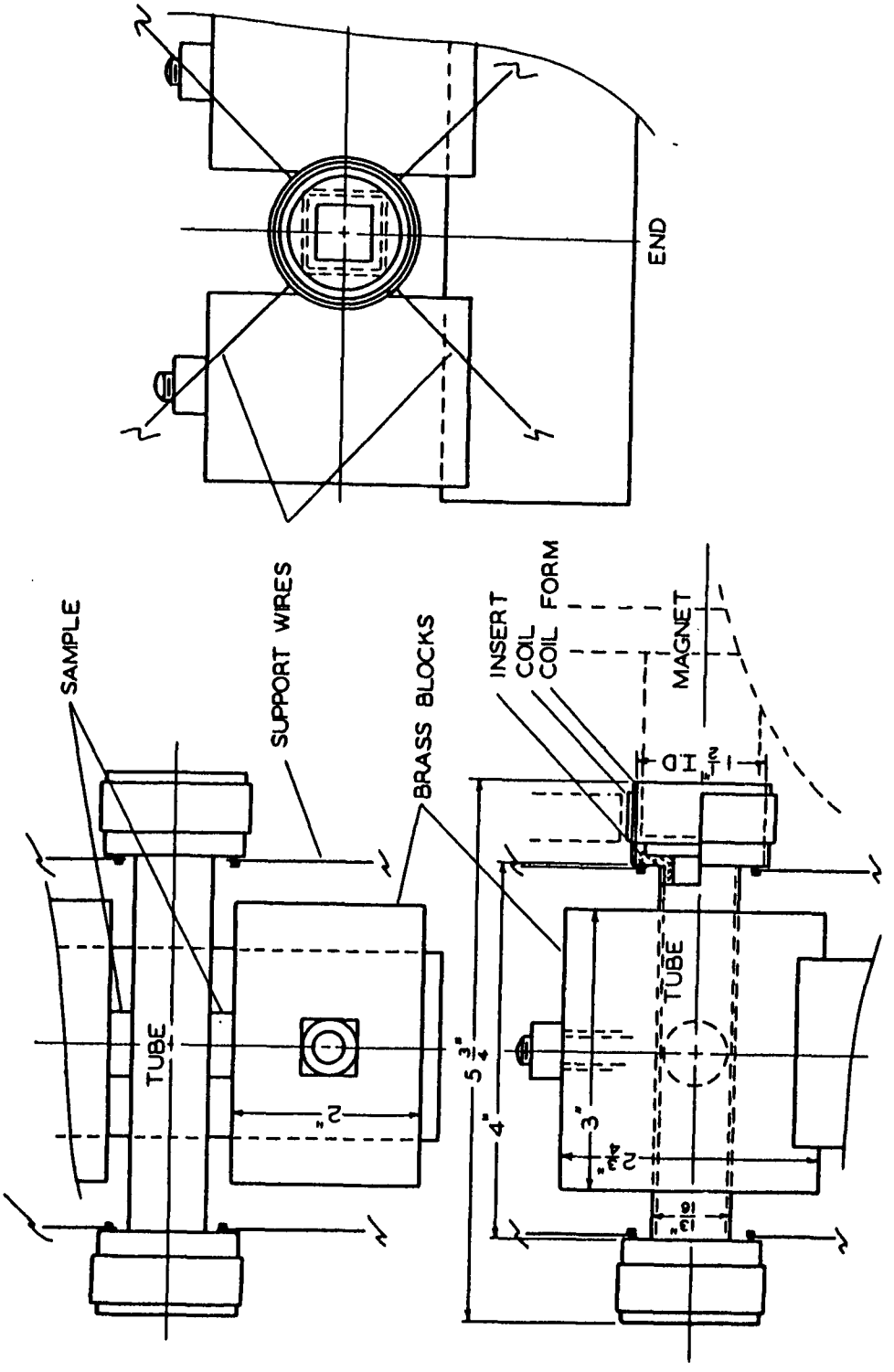

Figure 2. The Transducer Tube

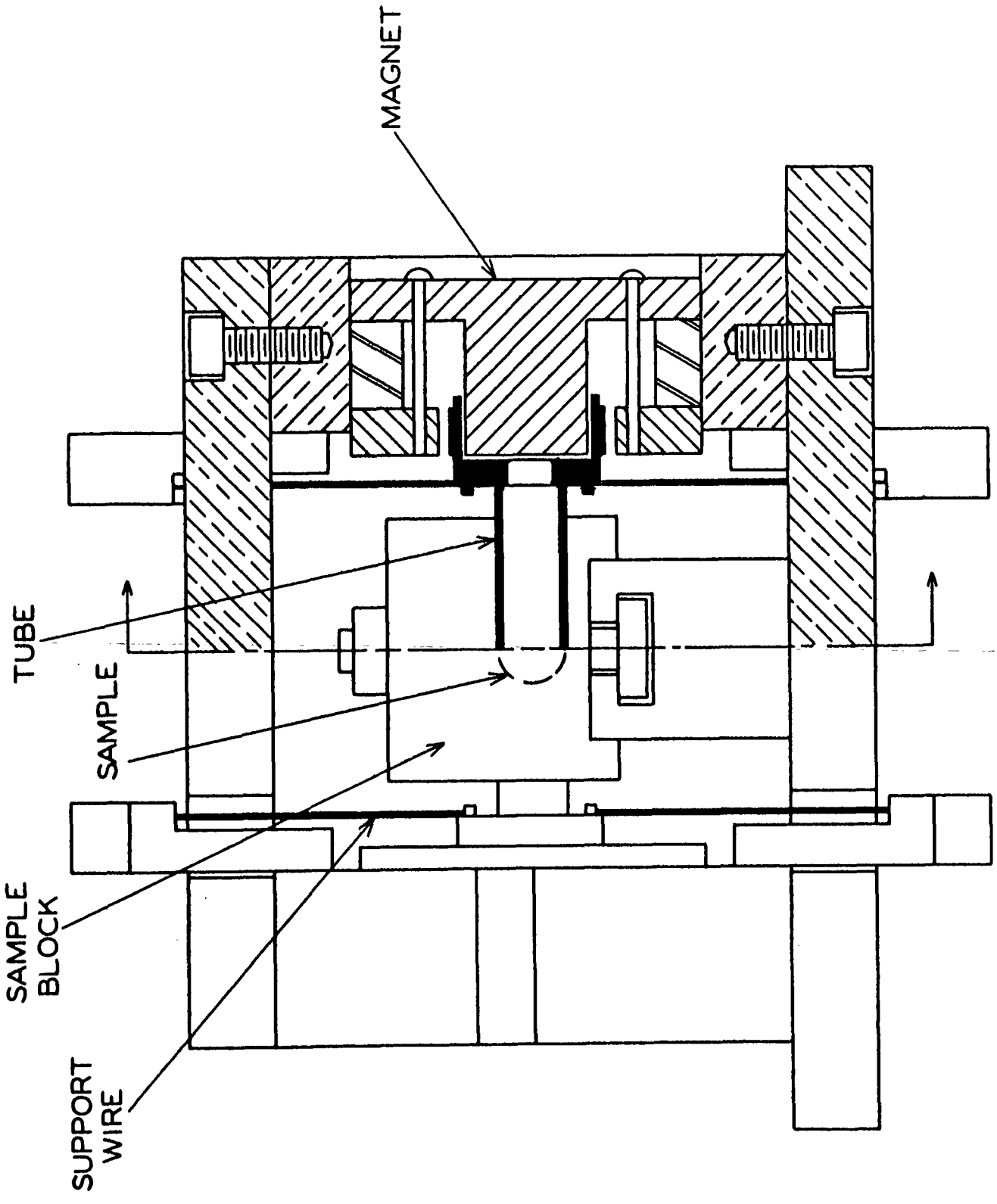

Figure 3. The Electromagnetic Transducer

of Armco ingot iron. The magnet proper is a cast Alnico 5 ring magnet 4.101 inches O.D. by 2.994 inches I.D. by 2 inches long. The direction of magnetization is parallel to the length.

The use of this particular tube and magnet arrangement has definite electrical advantages, since the specially shaped pole faces make it possible to eliminate electrical coupling between the two tube coils. The use of Micarta coil forms eliminates eddy current effects which would be encountered if aluminum coil forms were used.

A massive brass holder is used as a mounting for the tube and magnets. Sample pairs are strained in shear by pressing them between the flat faces of the tube and the two massive brass blocks. The blocks are mounted on a grooved track and may be clamped in any position along the track.

TRANSDUCER THEORY

When a sinusoidal alternating current $\underline{I}_1$ is supplied to Coil 1 of the tube (see Fig. 4) the tube will be subjected to a sinusoidal force,

$$F = B_1 I_1 \ell_1 \tag{28}$$

where $\underline{B}_1$ is the flux density at coil 1 and ℓ_1 is the length of wire in the coil. Since the magnetic field at the coils is radial, the sinusoidal force will act in the direction of the tube axis. Since the tube is free to translate in an axial direction, it will have an instantaneous velocity, $\underline{v}$, given by,

$$v = F/Z \tag{29}$$

where $\underline{Z}$ is the mechanical impedance of the tube and pair of samples.

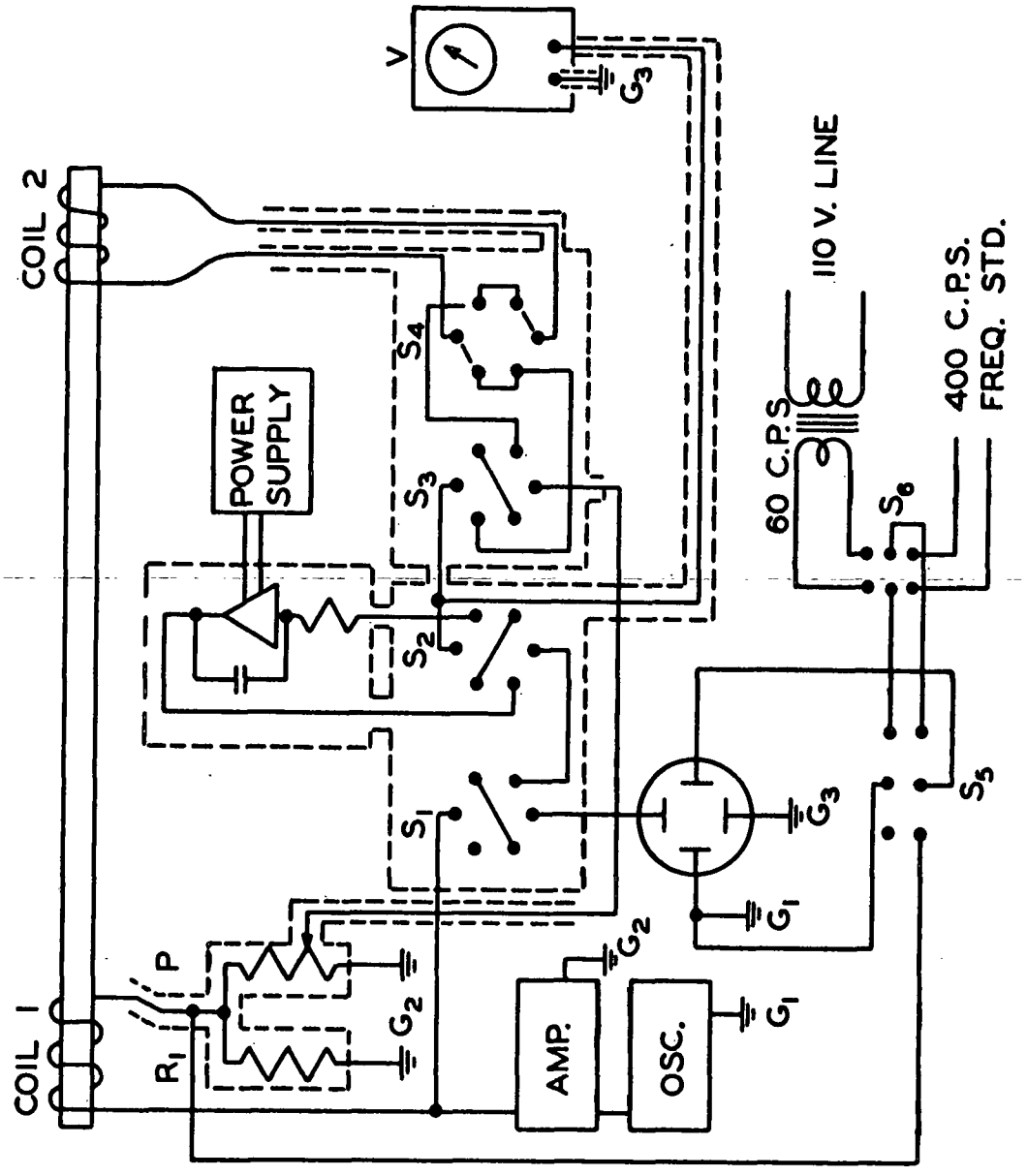

Figure 4. Wiring Diagram for the Double Electromagnetic Transducer

An open circuit voltage,

$$E_2 = B_2 \ell_2 v \tag{30}$$

will be induced in Coil 2. By combining Equations (28), (29), and (30) the mechanical impedance of the transducer is seen to be,

$$Z = F/v = (B_1 \ell_1)(B_2 \ell_2) I_1/E_2 . \tag{31}$$

This is the fundamental expression for the double transducer. For a given instrument the flux density and the length of wire in the coils will be constant quantities so that Equation (31) can be written,

$$Z = K^2 I_1/E_2 \tag{32}$$

where $\underline{K}^2$ is an instrument constant given by $\underline{K}^2 = (\underline{B}_1 \ell_1)(\underline{B}_2 \ell_2)$. The ratio, $\underline{I}_1/\underline{E}_2$ is known as the electrical transfer admittance. According to Equation (32) the measurement of mechanical impedance of a double transducer is reduced to a measurement of the electrical transfer admittance.

If $\underline{Z}_o$ represents the mechanical impedance of the transducer tube and $\underline{Z}$ is the impedance of the tube when shearing a pair of samples, then the sample impedance, $\underline{Z}_s$, is given by,

$$Z_s = Z - Z_o . \tag{33}$$

Noting that $\underline{v}/\gamma^* = j\omega\underline{h}$, then the complex shear modulus of the pair of samples may be calculated by means of the relation,

$$G^* = (F/A)/\gamma^* = (vZ_s/A)/\gamma^* = j\omega Z_s (h/A) \tag{34}$$

where $\underline{h}$ is the average thickness of the pair of samples and $\underline{A}$ their combined cross-sectional area.

ELECTRICAL MEASURING CIRCUITS

By measuring the electrical transfer admittance $\underline{I}_1/\underline{E}_2$, the impedance of the transducer may be determined from Equation (32). The electrical circuits used to make these measurements are shown in Fig. 4. The circuits are the same as those described by Kurath, et al. (24) except for the addition of a frequency standard and an integrating unit.

A Hewlett Packard model 200 J audio oscillator generates a voltage which is amplified by means of a McIntosh model MC-30, 30-watt power amplifier. The output power from the amplifier is supplied to Coil 1. Accurate settings of the oscillator frequency are obtained by displaying the oscillator frequency and either the 60 c.p.s. line frequency or the 400 c.p.s. reference frequency on a DuMont model 403-R oscilloscope and observing the resulting Lissajous patterns. The 400 c.p.s. reference frequency is supplied by an Industrial Equipment Co. Model JF 400 frequency standard. The potential divider $\underline{P}$ is an Electro-Measurements Dekavider model DV-411 and the resistance $\underline{R}_1$ is a 100 Ω General Radio type 1432 decade resistor. The voltmeter $\underline{V}$ is a Ballantine model 300 vacuum tube voltmeter. The integrating unit is composed of a Philbrick utility packaged amplifier Model UPA-2 powered by a Philbrick compound regulated power supply Model R-100B plus a precision resistor and capacitor.

Both Marvin, et al. (24) and Kurath, et al. (25) have described how the basic circuit can be used to determine the electrical transfer admittance. The resulting equation is given by,

$$Z = (K^2/R_1)\ (A_1 + jA_2) \tag{35}$$

where $\underline{A}_1 = \alpha_1/(\alpha_1^2 + \alpha_2^2)$ and $\underline{A}_2 = \alpha_2/(\alpha_1^2 + \alpha_2^2)$ and α_1 and α_2 are fractions of the voltage drop across the potential divider $\underline{P}$. The resistance $\underline{R}_1$ is known and $\underline{K}^2$ is determined by calibration.

An important step in the measurement operation involves adjustment of a potential divider until the phases of two particular voltages are in quadrature. This point can be detected by displaying the two voltages on the oscilloscope. A circle is formed when the balance point is reached; however, it is difficult to judge when a true circle is obtained. A more accurate technique, suggested by Dr. E. Passaglia of the National Bureau of Standards, is to shift the phase of one of the voltages 90 degrees so that a straight line is displayed on the oscilloscope at the balance point instead of a circle.

The phase shift is accomplished by the integrating unit. If the instantaneous input voltage $\underline{e}_i$ to the integrator is,

$$e_i = E_m \exp(j\omega t) \tag{36}$$

then upon integration the instantaneous output becomes,

$$\begin{aligned} e_o &= -(1/RC) \int E_m \exp(j\omega t)\, dt \\ &= -(E_m/j\omega RC) \exp(j\omega t) \end{aligned} \tag{37}$$

where $\underline{RC}$ is the time constant of the integrator. In terms of the effective voltages $\underline{E}_o$ and $\underline{E}_i$, Equations (36) and (37) combine to give,

$$E_o/E_i = -1/(j\omega RC). \tag{38}$$

Equation (38) shows that not only has a 90-degree phase shift occurred, but also the output voltage is inversely proportional to $\omega\underline{RC}$. The response of the

output voltage as a function of frequency was checked for linearity at two levels of the input voltage as shown in Fig. 5. The straight lines having slopes of -1 indicate that the integrating network operates satisfactorily between 6 and 6,000 c.p.s. The time constant, $\underline{RC}$, is 4.1×10^{-4} sec.$^{-1}$.

CALIBRATION

The method for determining the constant $\underline{K}^2$ involves measuring the mechanical impedance of the tube without samples, $\underline{Z}_o$. This impedance depends on the mass of the tube, $\underline{m}$, the elastance of the suspension wires, $\underline{k}$, and small frictional resistances, $\underline{f}$; and it is expressed by the relationship,

$$Z_o = f + j(\omega m - k/\omega), \tag{39}$$

where ω is the circular frequency at which the tube is being driven. Without samples in the transducer, Equation (35) may be written,

$$Z_o = (K^2/R_1)(A_{10} + jA_{20}), \tag{40}$$

and comparing Equations (39) and (40) it can be seen that,

$$(K^2/R_1)(A_{10} + jA_{20}) = f + j(\omega m - k/\omega). \tag{41}$$

The resonance frequency, where $\omega\underline{m} = \underline{k}/\omega$, is about 10 c.p.s. At much higher frequencies, $\omega\underline{m}$ will be much larger than $\underline{k}/\omega$ and the imaginary part of Equation (41) then becomes approximately, $(\underline{K}^2/\underline{R}_1)\underline{A}_{20} = \omega\underline{m}$. If $\underline{A}_{20}$ is plotted *versus* the frequency, ν, a straight line should be obtained with a slope of $2\pi\underline{m}\underline{R}_1/\underline{K}^2$. A plot of this type is shown in Fig. 6. The straight line indicates that no large mechanical or electrical resonances occur over this range of frequencies. For a tube mass of 43.23 g. and a resistance $\underline{R}_1$ of 10 Ω, the slope of the straight line gives a value for $\underline{K}^2$ of $2.25(\pm .02) \times 10^4$ ohm dyne sec. cm.$^{-1}$.

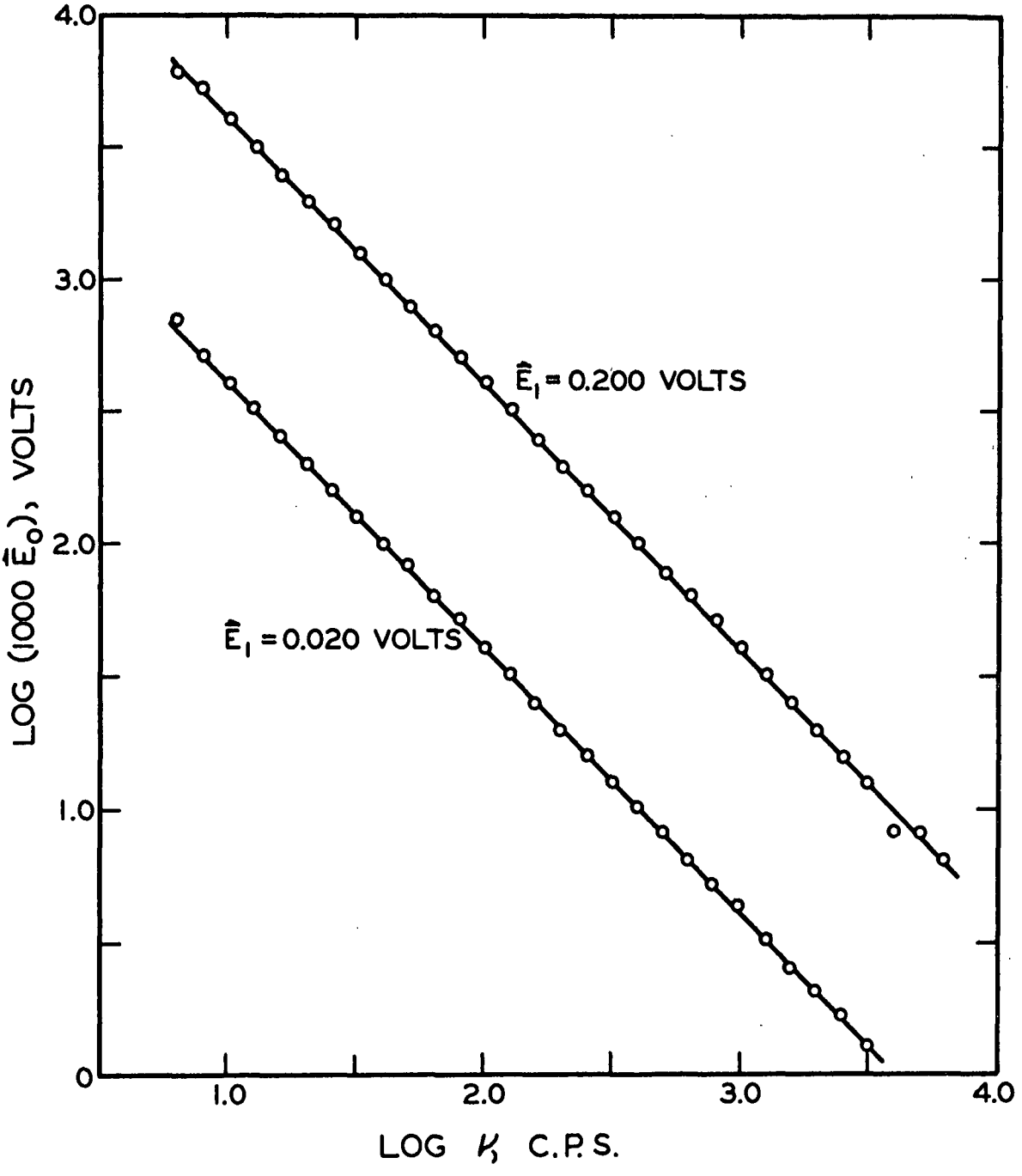

Figure 5. Frequency Response of the Integrating Circuit Used in the Double Electromagnetic Transducer

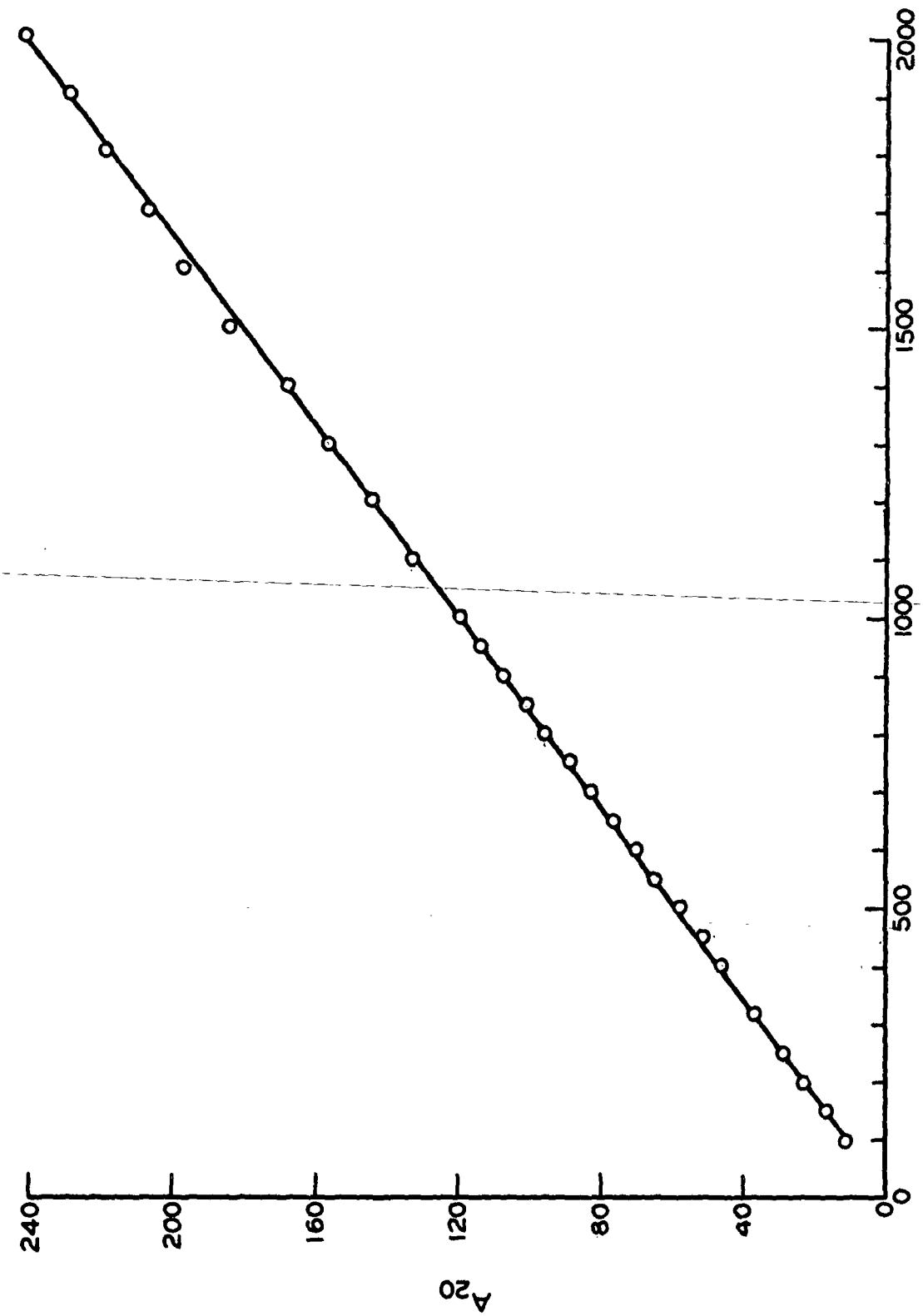

Figure 6. The Calibration Curve for the Transducer with R_1 = 10.0 ohm

The mechanical impedance of a pair of samples, $\underline{Z}_s$, is determined from the difference between the impedance of the tube with samples and without samples as indicated by Equation (33). Combining this equation with Equations (35) and (40) gives

$$Z_s = (K^2/R_1)\,[(A_1 - A_{10}) + j(A_2 - A_{20})]. \qquad (42)$$

Values of $\underline{A}_{10}$ and $\underline{A}_{20}$ for a number of frequencies are listed in Table I. Near the resonance frequency of 10 c.p.s., the value of $\underline{A}_{20}$ was found to be sensitive to changes in the tension of the supporting wires. Therefore, it was necessary to determine values of $\underline{A}_{20}$ in the range of 6 to 60 c.p.s. before or after testing each set of samples. These values are included in Table I.

Small corrections for temperature dependence and an apparent phase shift are discussed in Appendix I.

FREQUENCY LIMITS

The frequency range over which the sample impedance can be determined depends on the design of the instrument and the frequency dependence of the sample. Equation (33) indicates that the sample impedance is obtained from the difference of two impedances. Therefore, measurement of the sample impedance will become inaccurate when the magnitude of the sample impedance is small in comparison to the tube impedance. Since $\underline{A}_{20}$ increases almost linearly with frequency, this puts an upper limit on the frequency range. The limit will occur at low frequencies if the impedance of the sample is small and at higher frequencies if the impedance is large.

When the sample impedance is very large, vibration of the transducer case will interfere with the readings. In addition, the tube velocity is small, and the voltage generated in Coil 2 may be below the range of the voltmeter.

TABLE I

CALIBRATION DATA

Frequency, c.p.s.	$A_{\pm 10}$	$A_{\pm 20}$ for Polystyrene Concentrations of 52%	21%	10%	35%	5%	67%
6.	0.08	-5.55	-3.32	-3.24	-1.82	-1.57	-1.53
8.	0.08	-3.57	-2.04	-2.12	-0.95	--	--
10.	0.08	-2.55	-1.25	-1.21	-0.37	-0.209	-0.20
12.	0.08	-1.72	-0.64	-0.58	0.10	--	--
15.	0.08	-0.70	-0.172	-0.129	0.69	0.793	0.791
20.	0.08	0.60	1.09	1.08	1.50	--	--
25.	0.08	1.34	1.88	1.88	2.22	2.28	2.32
32.	0.08	2.43	2.90	2.86	3.13	--	--
40.	0.08	3.58	3.94	3.92	4.11	4.24	4.27
50.	0.08	4.85	5.10	5.16	5.34	--	--

Frequency, c.p.s.	$A_{\pm 10}$	$A_{\pm 20}$ for all Concentrations
60.	0.0	6.38
100.	-0.26	12.00
150.	-0.64	16.62
250.	-1.67	28.2
400.	-3.4	46.0
600.	-5.8	70.0
1000.	-11.9	117.0

PREPARATION OF POLYSTYRENE-TCP SOLUTIONS

The polystyrene used in this study was prepared and provided by Dr. H. W. McCormick of the Dow Chemical Company. The polymer, designated B6, was prepared by isothermal polymerization. The molecular weight distribution is shown in Fig. 7. It was determined by McCormick (27) and checked in this laboratory by Taylor (28). The polystyrene has a number average molecular weight of 152,000 and weight average of 434,000.

Practical grade o-tricresyl phosphate (TCP) was obtained from Eastman Kodak Company and purified by distillation under reduced pressure at 215 to 225°C. The distillate was a pale yellow with less than 1% impurities as determined by a phosphorus analysis (for details see Appendix V).

Six polystyrene-TCP solutions were prepared of 5, 10, 21, 35, 52, and 67% polystyrene by weight. At room temperature there was a wide latitude in the general physical properties of the solutions. The 5% solution appeared to be a viscous liquid, while at the other extreme, the 67% solution had an almost glasslike behavior.

Preparation of the solutions was much more difficult as the polystyrene concentration increased. The 5 and 10% solutions were prepared by simply heating and stirring, while the higher concentrations, in addition, required a number of extrusions through a die. Details of the mixing procedures are given in Appendix II.

PREPARATION OF TEST SAMPLES

Sample pairs suitable for testing in the transducer were prepared for each polystyrene solution. The techniques used to prepare sample pairs for the 5, 10,

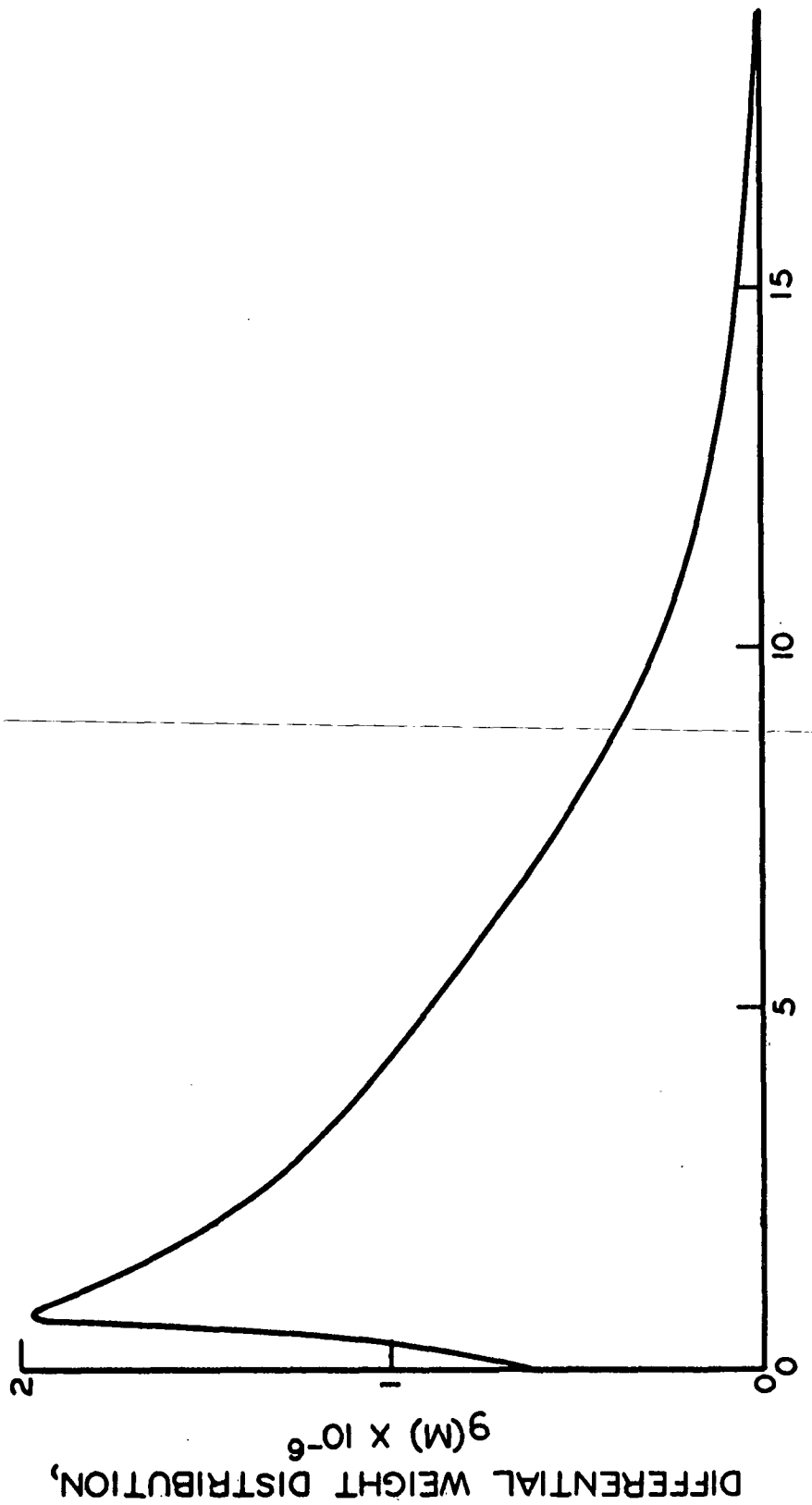

Figure 7. The Molecular Weight Distribution of the Polystyrene

and 21% solutions were entirely different than the ones used to prepare sample pairs for the 35, 52, and 67% solutions.

For the low concentrations the transducer was turned on its side. A bubble-free polystyrene solution was then carefully poured onto one of the sample support blocks to form a bead about one-half inch in diameter. The support block was immediately placed in the transducer and the sample pressed carefully against the transducer tube. If done properly, the sample formed a thick film between the support block and the transducer tube and was held in position by its surface tension. For the high concentrations bubble-free solutions were molded using heat and pressure into disk-shaped samples of about one-half inch in diameter. Specific details of these procedures are given in Appendix III.

DETERMINATION OF FORM FACTORS

It was necessary to determine a form factor for each pair of samples tested in the transducer in order to calculate the complex dynamic moduli using Equation (34). The form factor in Equation (34) is an average for the pair of samples defined by,

$$h/A = 1/[(A_1/h_1) \pm (A_2/h_2)] \qquad (43)$$

where $\underline{h}_1$ and $\underline{A}_1$ are the thickness and cross-sectional area, respectively, of one of the samples and $\underline{h}_2$ and $\underline{A}_2$ are the corresponding dimensions for the other sample. An attempt was made to keep the sample dimensions of a pair as nearly the same as possible. The procedures used to make these measurements are given in Appendix IV.

The appearance of the form factor in Equation (34) can be used to advantage. If a second set of sample pairs is prepared with sample dimensions which are much

different than the first set, the form factor can be changed by several fold. Since the range of sample impedances at which transducer measurements can be taken will remain about the same as for the first set of samples, the values of the complex shear moduli obtained will also be changed several fold. Thus, the range of values of the moduli obtained with the second set of samples can extend to temperatures or frequencies which are beyond the range of the first set. The sample coefficients, $(\underline{h}/\underline{A})(\underline{K}^2/\underline{R}_1)$, are listed in Table II for all the sample sets tested.

TABLE II

SAMPLE COEFFICIENTS

Polystyrene Concentration, %	Sample Set Number	Sample Coefficient, ohm dyne sec./cm.^{2}
5	1	39.7
10	1	194.0[a]
	2	16.2
21	1	38.9
	2	76.1[b]
	3	477.0
35	1	170.0
52	1	467.0
67	1	514.0

[a]Coefficient increased 10% to correspond with sample set number 2.
[b]Coefficient decreased 7% to correspond with first and third sample sets.

Where two or more sample sets were tested at a single concentration, the temperature ranges covered by the sets could be made to overlap. Thus, complex dynamic moduli could be calculated from more than one sample set under the same conditions of temperature and frequency. In some cases a small but constant

percentage difference was noted for the values calculated from different sample sets. This was attributed to errors in determining the form factors. Where this occurred, the sample set was selected which was thought to have the most accurately determined form factor, and the form factor of the other sample set was then adjusted so that the values calculated for the complex dynamic moduli would agree. These adjustments are noted in Table II.

PHYSICAL PROPERTIES OF POLYSTYRENE-TCP SOLUTIONS

In order to analyze the data on the mechanical properties of the solutions, it is necessary to know the concentration, glass transition temperature, density, expansion coefficient, and steady-flow viscosity. Specific details of the methods described in the following section are given in Appendix V. The results of these measurements are given in Table III.

TABLE III

SOME PHYSICAL PROPERTIES OF THE POLYSTYRENE-TCP SOLUTIONS

Concentration, wt. % PS	Glass Temperature, °C.	Density, g./ml.	Expansion Coefficient ($\times 10^4$) Above T_g	Expansion Coefficient ($\times 10^4$) Below T_g	Steady-Flow Viscosity, poise
0		1.176			1.137
5	-47	1.172			32.35
10	-45	1.167			359.0
21	-39	1.157	5.9	2.2	
35	-29	1.144			
52	-11	1.128	6.2	2.3	
67	18	1.107	5.6	1.9	

CONCENTRATION

Approximate concentrations were determined by mixing known weights of polystyrene and TCP. To avoid uncertainties due to loss of solvent or polymer during mixing, an analysis was made on each solution after it was prepared. This was accomplished by a chemical analysis of the phosphorus content of TCP using the Lieb method (29). The method involves oxidation of the organic matter in the sample to carbon dioxide and precipitation of the remaining phosphoric acid with a sulfate-molybdate reagent. The TCP content may be determined to ± 1%.

GLASS TRANSITION TEMPERATURE

Jenckel and Heusch (30) have determined the glass transition temperature for the polystyrene-TCP system over the entire concentration range. Their results are shown in Fig. 8. However, the glass transition temperatures of both the pure polystyrene and the pure TCP were found to be significantly lower than those reported by other investigators (20, 31, 32). Therefore, the data of Jenckel and Heusch were checked by determining the glass transition temperatures of the 21, 52, and 67% solutions using the procedure of Wiley and Brauer (33) which involves measuring the break in the refractive index-temperature curves.

The results are plotted in Fig. 8. The glass transition temperature for each concentration was found to be 17°C. higher than the values reported by Jenckel and Heusch. Although their data appear to be low, they are consistently low, and, therefore, the glass transition temperature of the 5, 10, and 35% solutions are also taken as being 17°C. higher than the corresponding values of Jenckel and Heusch.

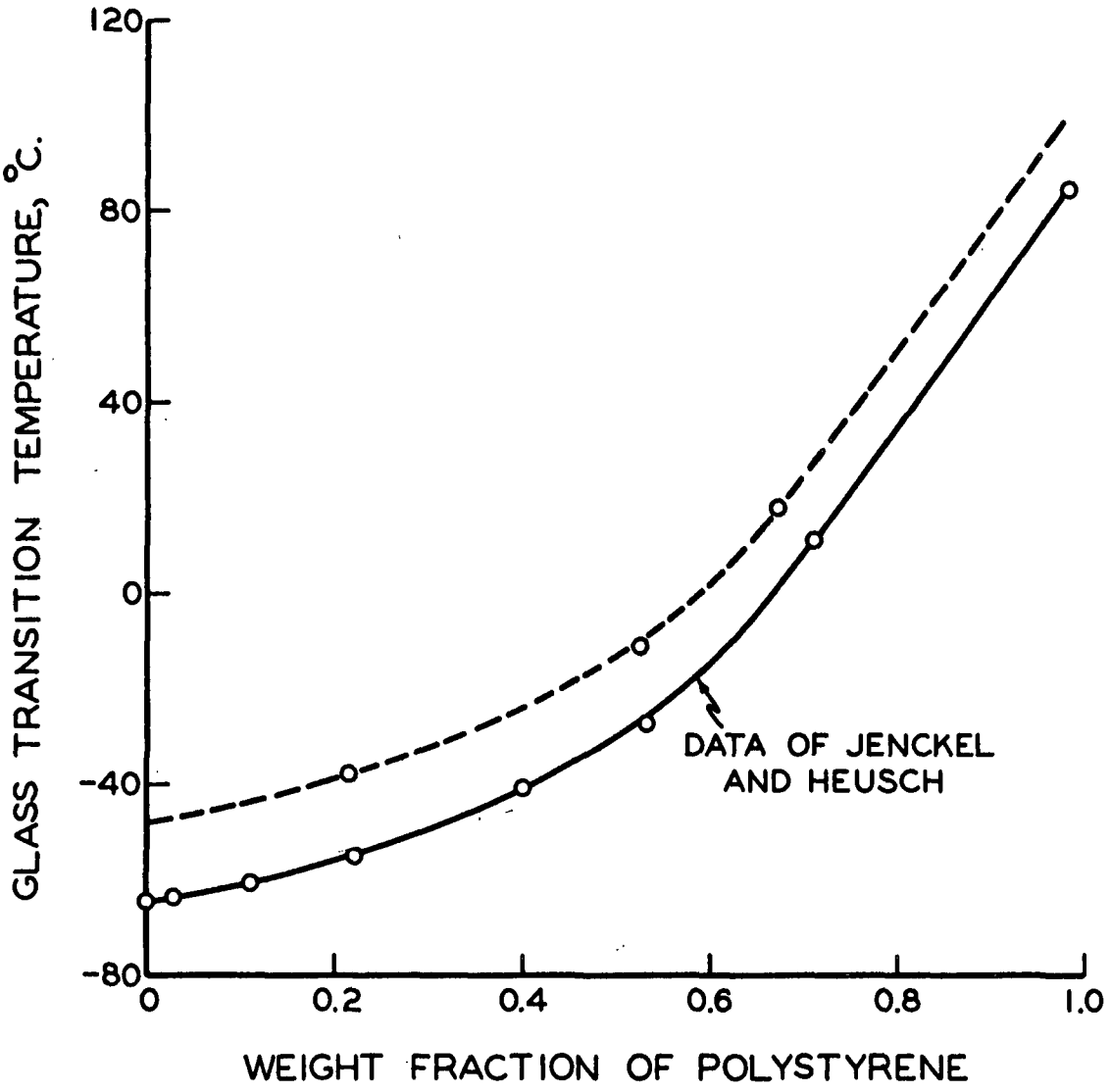

Figure 8. The Glass Transition Temperatures of Polystyrene-TCP Solutions

DENSITY

Densities were determined pycnometrically for the pure TCP, and the 10, 21, and 35% solutions. Densities of the 52 and 67% solutions were determined from a measure of their buoyancies in water.

EXPANSION COEFFICIENT

Expansion coefficients of the solutions were estimated from the refractive index-temperature data used for determining the glass transition temperatures. The relationship between the refractive index, n, and the expansion coefficient, α, may be derived from the Lorenz-Lorentz equation (34),

$$\alpha = (1/v)dv/dT = \left[\frac{-6n}{(n^2 + 2)(n^2 - 1)}\right] \left(\frac{dn}{dT}\right) \qquad (44)$$

VISCOSITY

The steady-flow viscosities of the pure TCP and the 5 and 10% solutions were determined using a Hoeppler falling ball viscometer. The viscosities at 25°C. are given in Table III.

GENERAL OPERATING PROCEDURE

After placing a pair of samples in the transducer, the instrument was mounted on a rubber cushion and completely enclosed in a water-tight stainless steel case which was immersed in a bath of water and ethylene glycol. Temperature control was maintained within one-tenth of a degree using a microset mercury thermoregulator to control electrical resistance heaters. For temperatures near and below room temperature continuous cooling was supplied by a Lehigh refrigeration unit.

A calibrated iron-constantan thermocouple was used to determine the temperature inside the case. The junction was placed in a hole drilled in one of the sample support blocks. The hole was located near the face of the block close to the sample.

The air space surrounding the instrument controlled the heat transfer rate between the instrument and the bath. This was a disadvantage when it was necessary to change the temperature of the instrument, but once the transducer had reached the desired temperature, it remained very stable.

Energy is dissipated in the samples when they are deformed, and therefore it is possible for the sample temperature to increase during a test. In some cases it was noted that the potential divider readings would change if the power to the driving coil remained on for a period of a few minutes or more. After the power was turned off for a few minutes, the original potential divider readings would be obtained. The change was in the direction of smaller modulus values which would correspond to a sample temperature increase. In order to avoid this problem, the power to the driving coil was turned on only when taking readings. This ordinarily took no more than one-half minute.

RESULTS OF DYNAMIC MEASUREMENTS

Transducer measurements were made at temperature intervals of about five degrees with frequent check runs made at the initial temperature to ensure that no changes in the sample dimensions had occurred. At each temperature, transducer measurements were taken at as many of the following 12 frequencies as possible: 6, 10, 15, 25, 40, 60, 100, 150, 250, 400, 600, and 1000 c.p.s. These frequencies are spaced at approximately equal logarithmic intervals. In a few cases where the frequency range was limited, additional data were taken at frequencies of 8, 12, 20, 32, and 50 c.p.s.

The storage modulus and loss modulus were calculated from the results of these tests using the sample coefficients given in Table II and by combining Equations (3), (34), and (42) to give,

$$G' = \omega(h/A)(K^2/R_1)(A_2 - A_{20}) ,$$

and,

$$G'' = \omega(h/A)(K^2/R_1)(A_1 - A_{10}).$$

These values are tabulated in Appendix VI, and except for a small adjustment, they are also presented in Fig. 9 through 20. The adjustment, indicated by the subscript p on the storage and loss moduli, involves a temperature reduction which is described in the section on the analysis and discussion of the results.

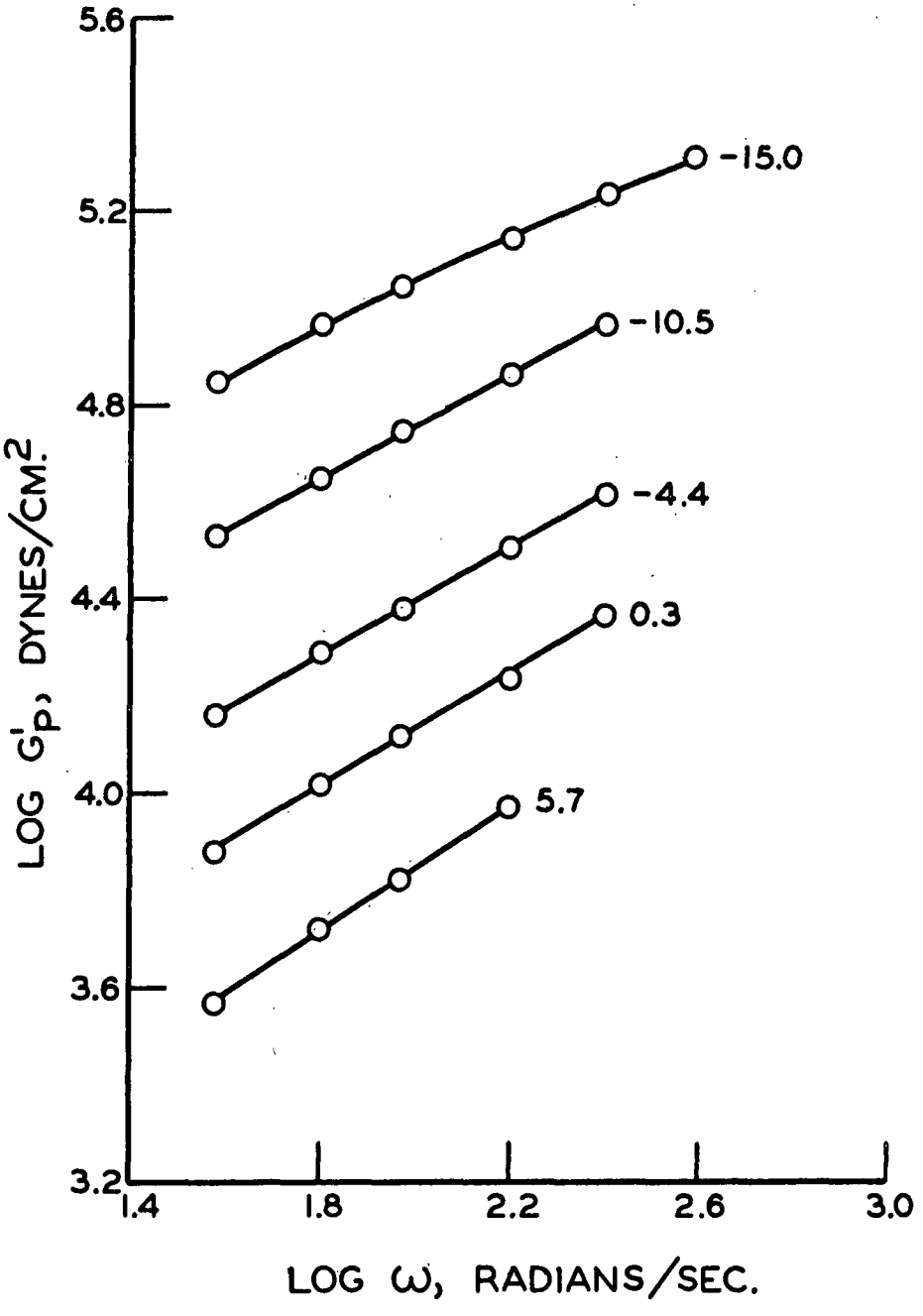

Figure 9. The Storage Modulus for a 5% Polystyrene-TCP Solution at the Temperatures Indicated

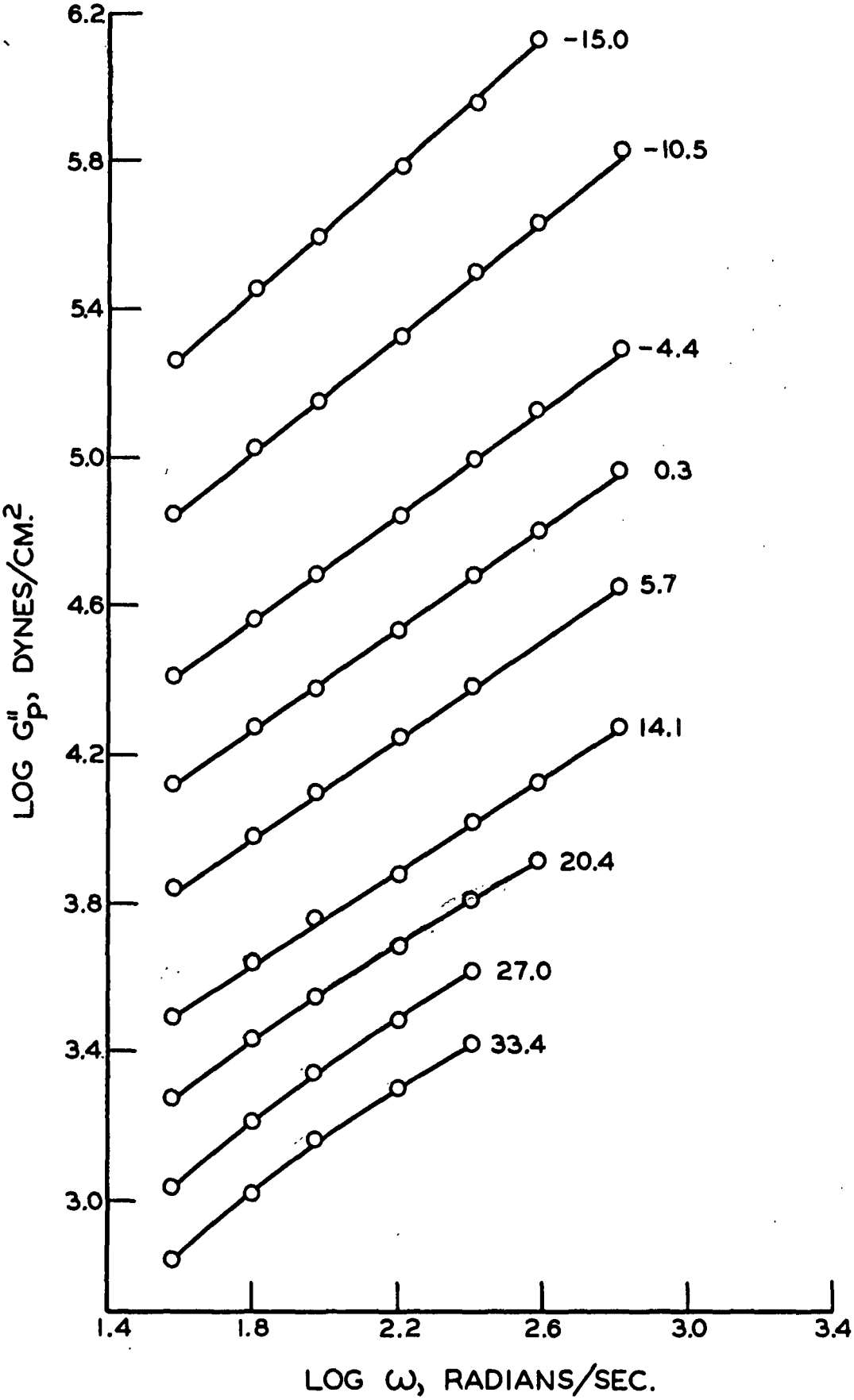

Figure 10. The Loss Modulus for a 5% Polystyrene-TCP Solution at the Temperatures Indicated

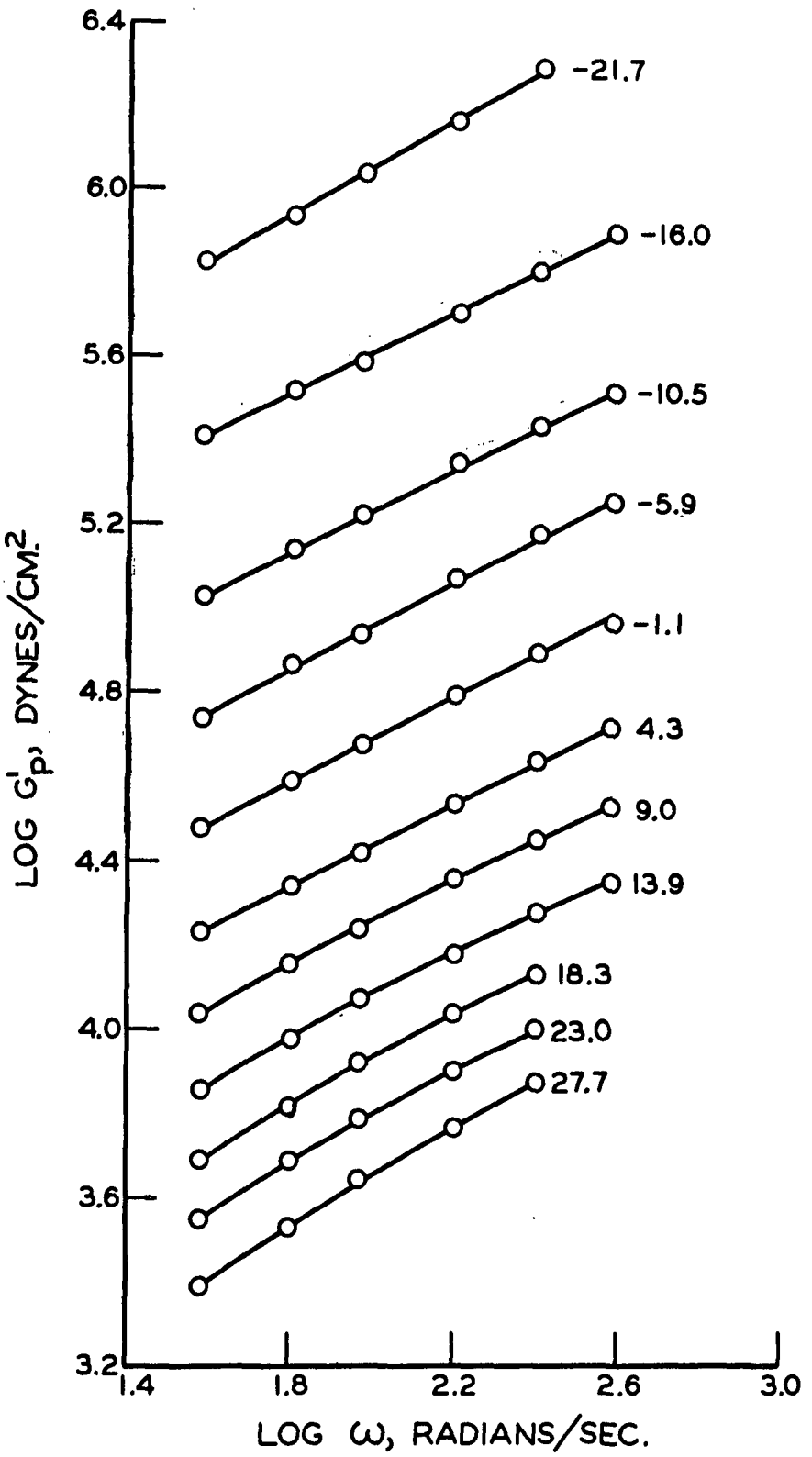

Figure 11. The Storage Modulus for a 10% Polystyrene-TCP Solution at the Temperatures Indicated

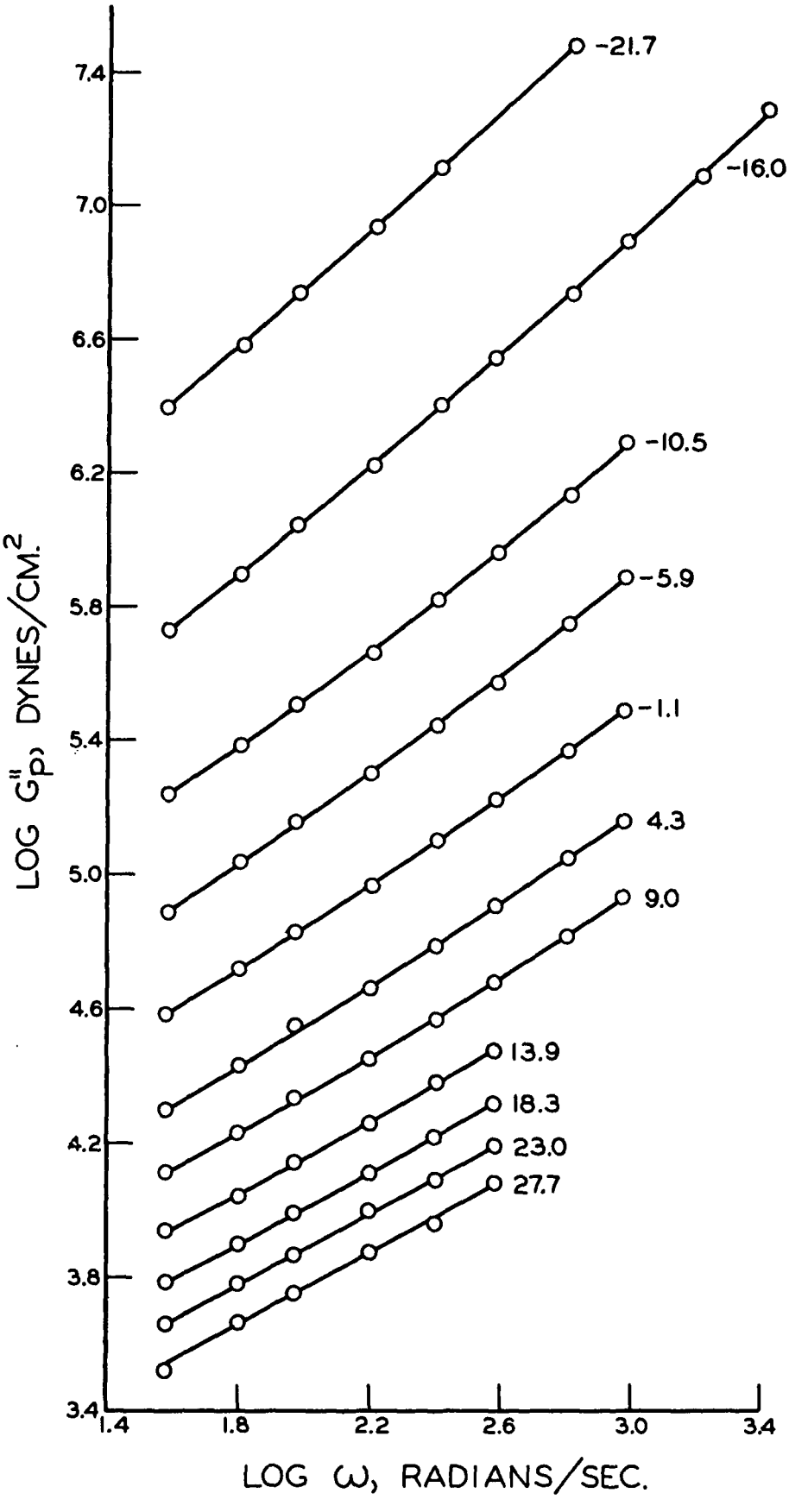

Figure 12. The Loss Modulus for a 10% Polystyrene-TCP Solution at the Temperatures Indicated

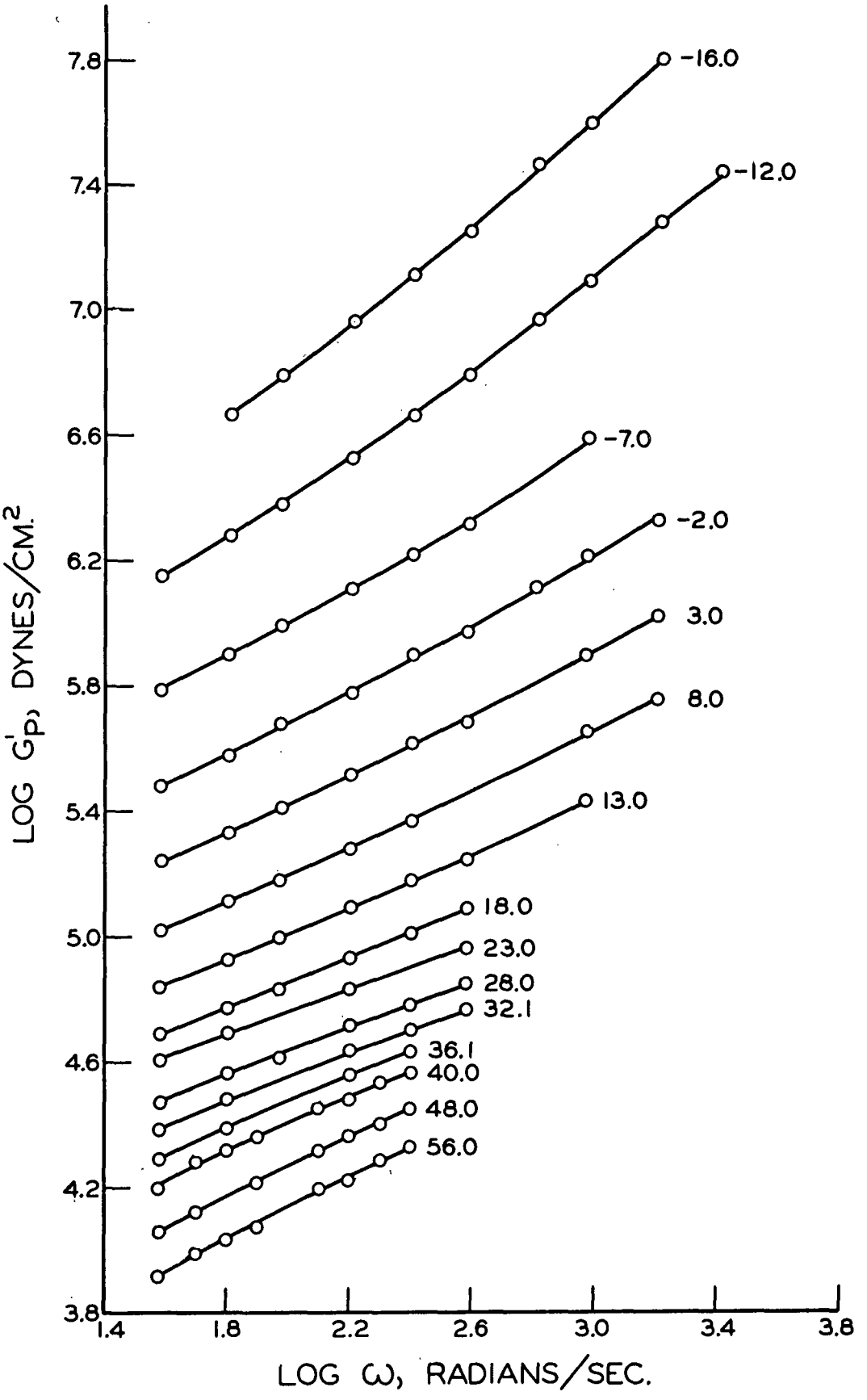

Figure 13. The Storage Modulus for a 21% Polystyrene-TCP Solution at the Temperatures Indicated

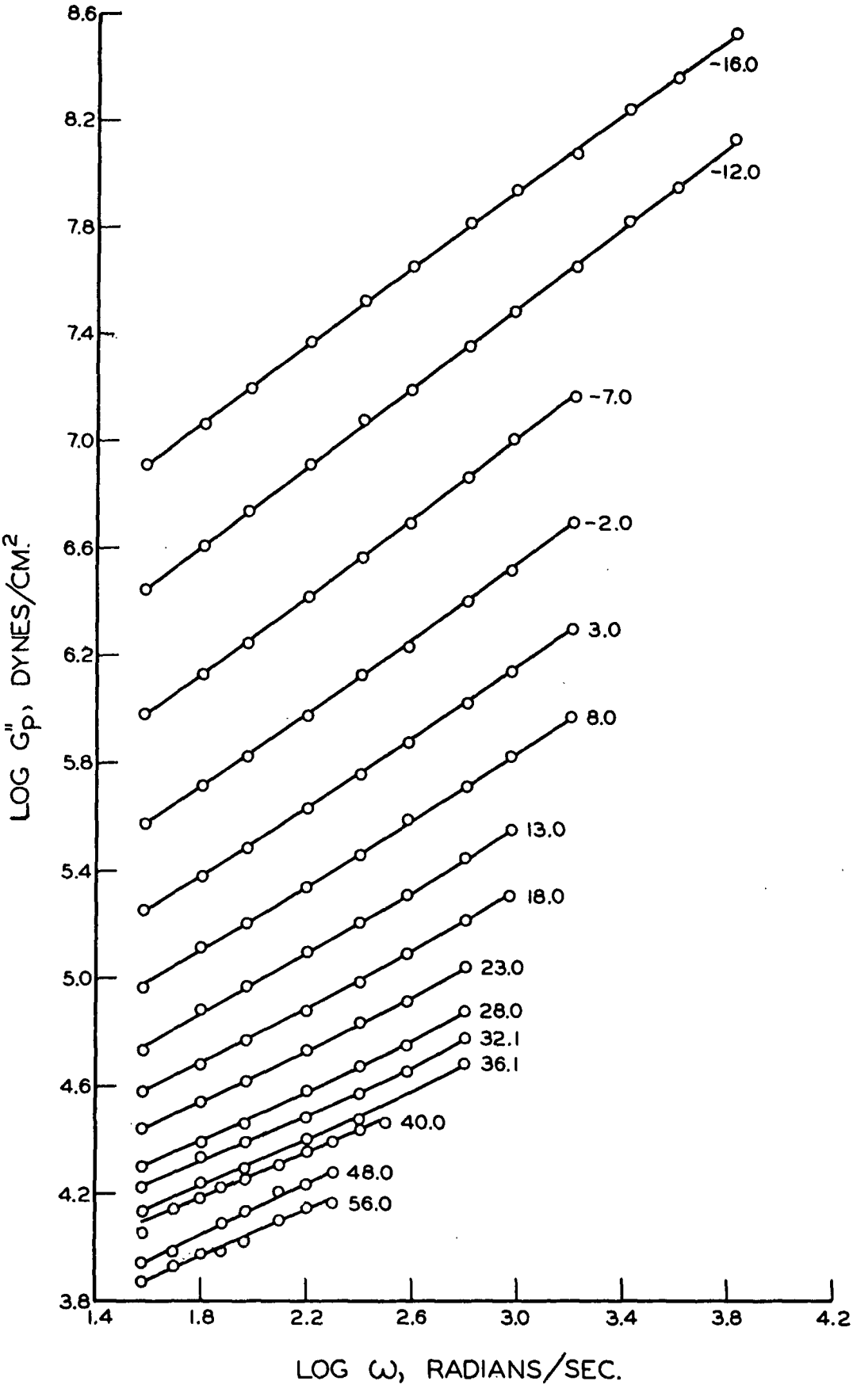

Figure 14. The Loss Modulus for a 21% Polystyrene-TCP Solution at the Temperatures Indicated

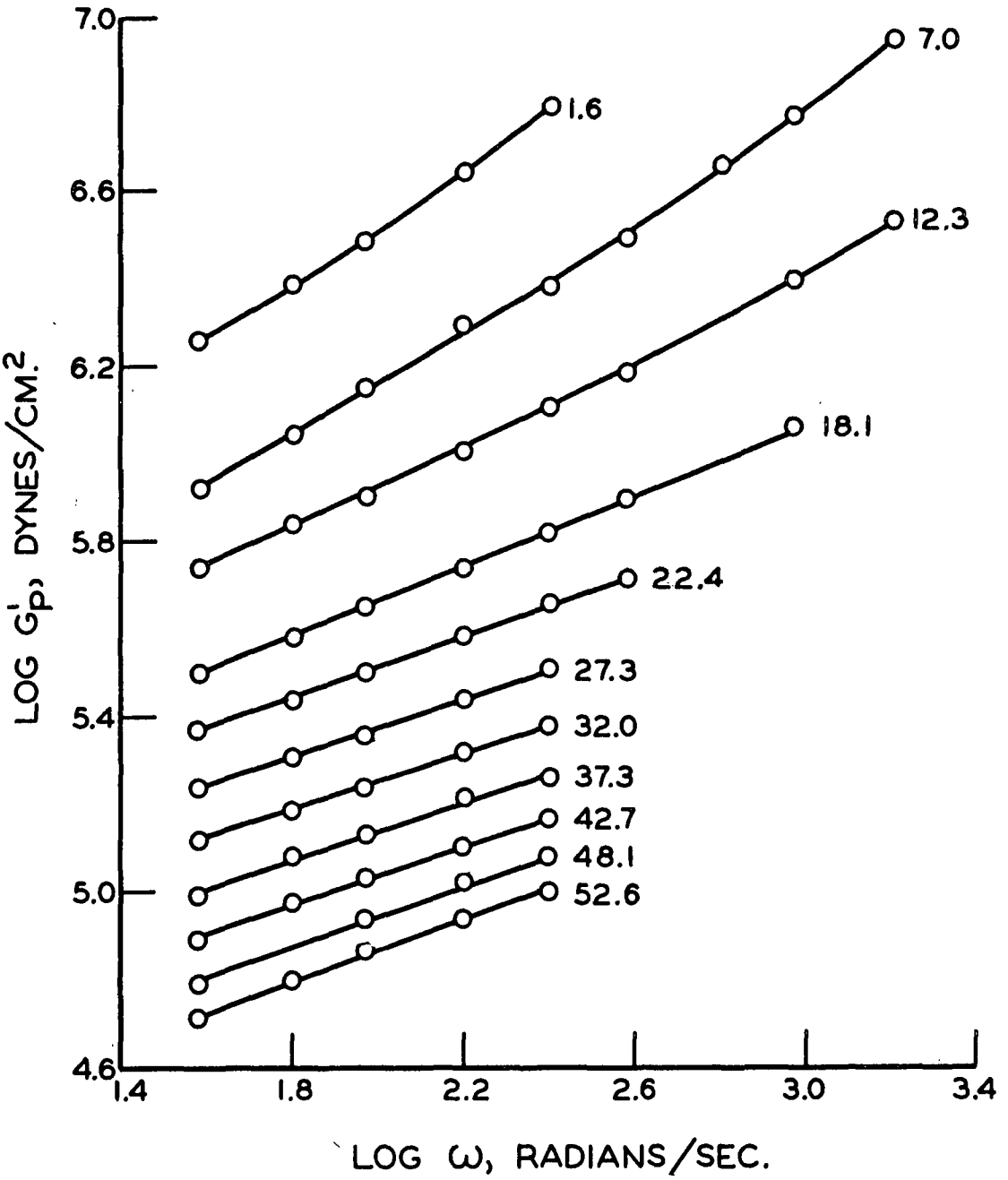

Figure 15. The Storage Modulus for a 35% Polystyrene-TCP Solution at the Temperatures Indicated

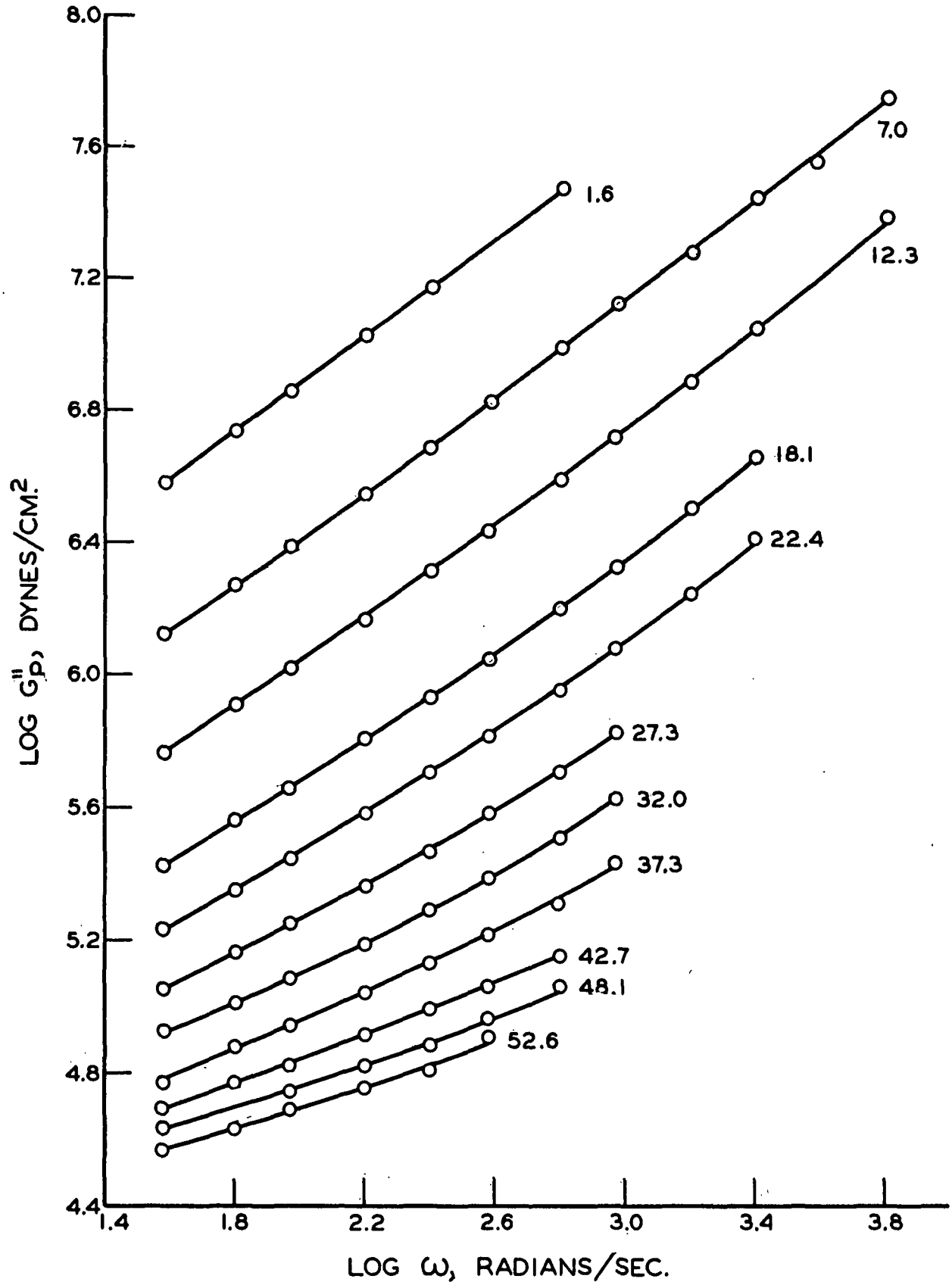

Figure 16. The Loss Modulus for a 35% Polystyrene-TCP Solution at the Temperatures Indicated

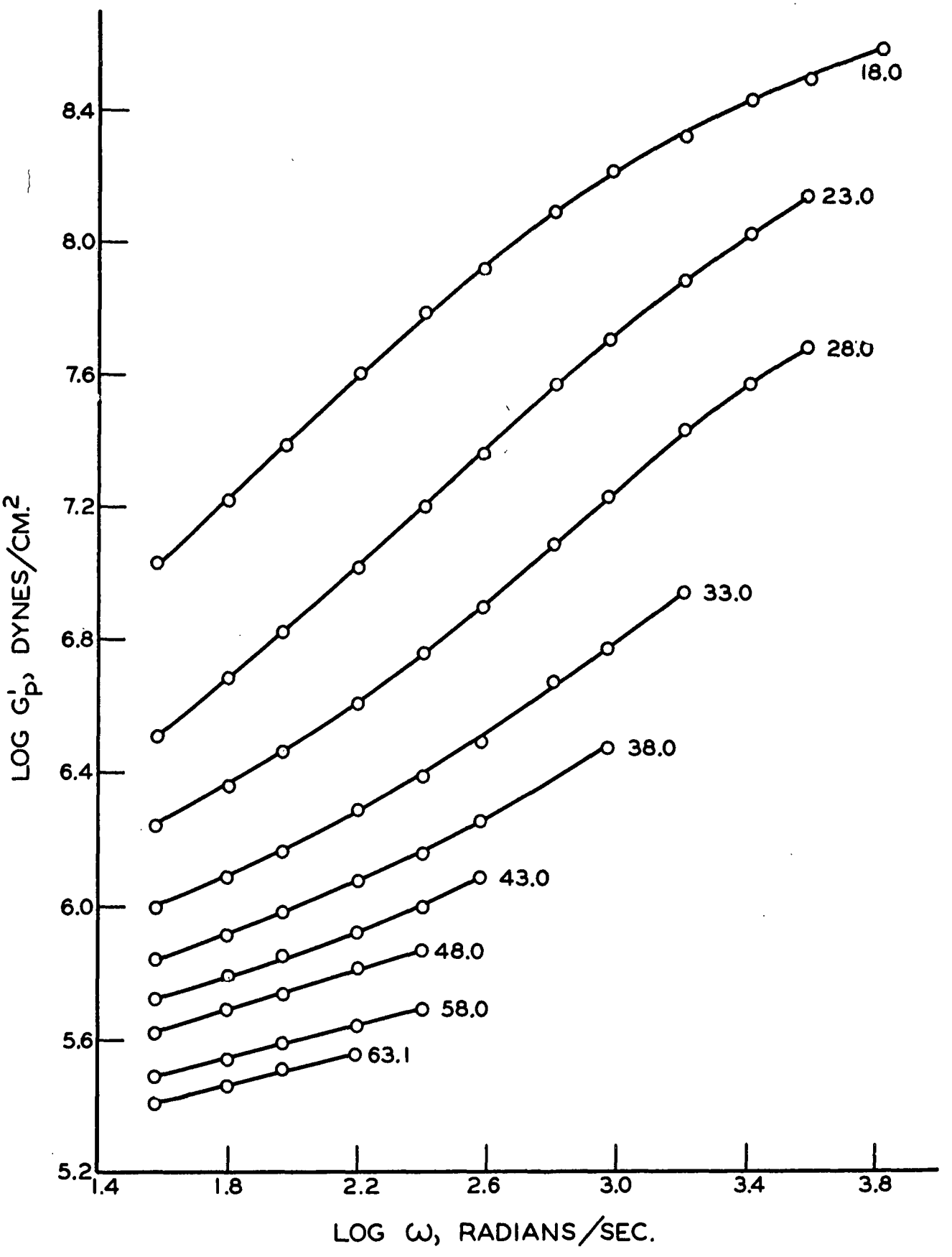

Figure 17. The Storage Modulus for a 52% Polystyrene-TCP Solution at the Temperatures Indicated

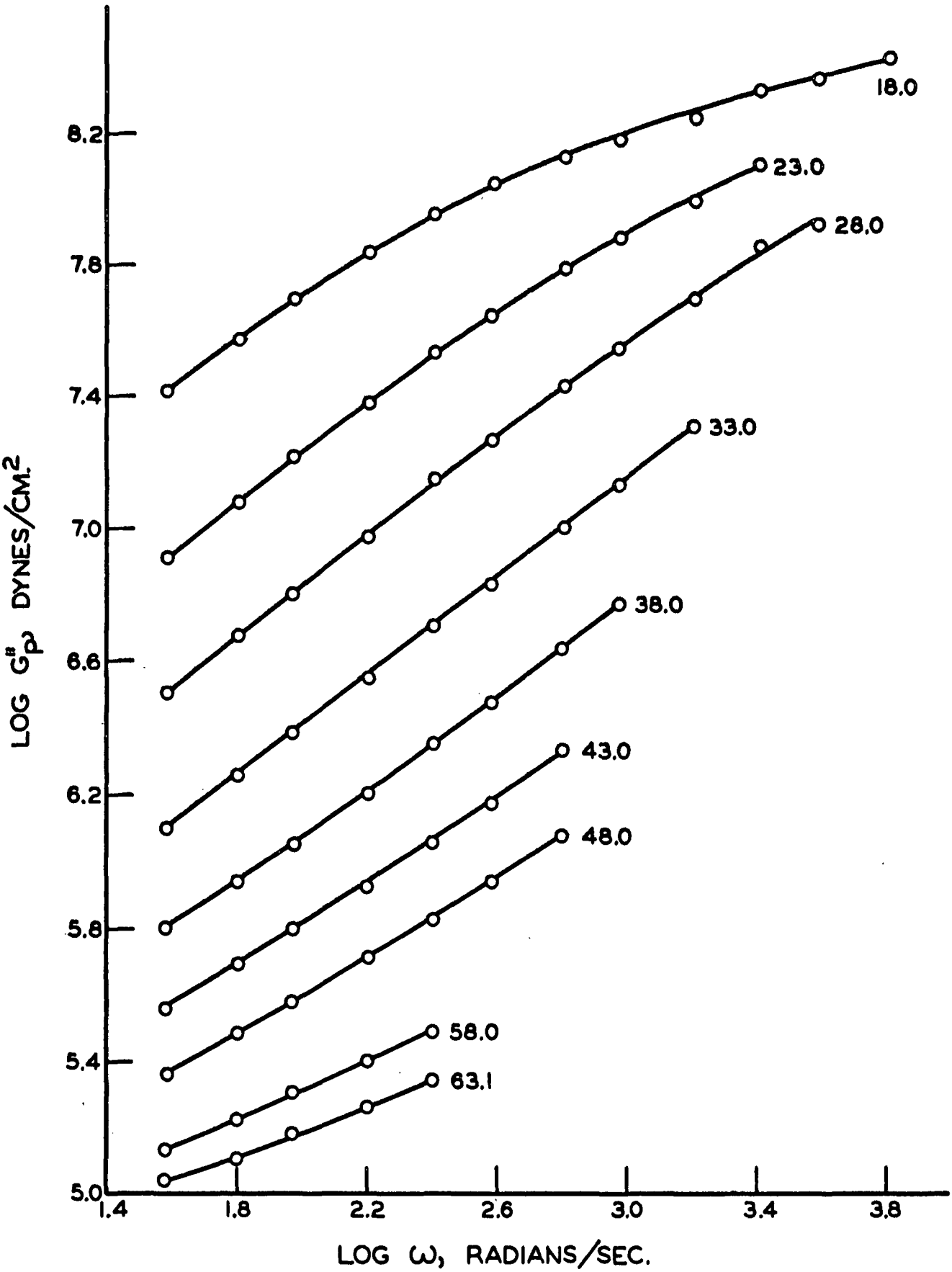

Figure 18. The Loss Modulus for a 52% Polystyrene-TCP Solution at the Temperatures Indicated

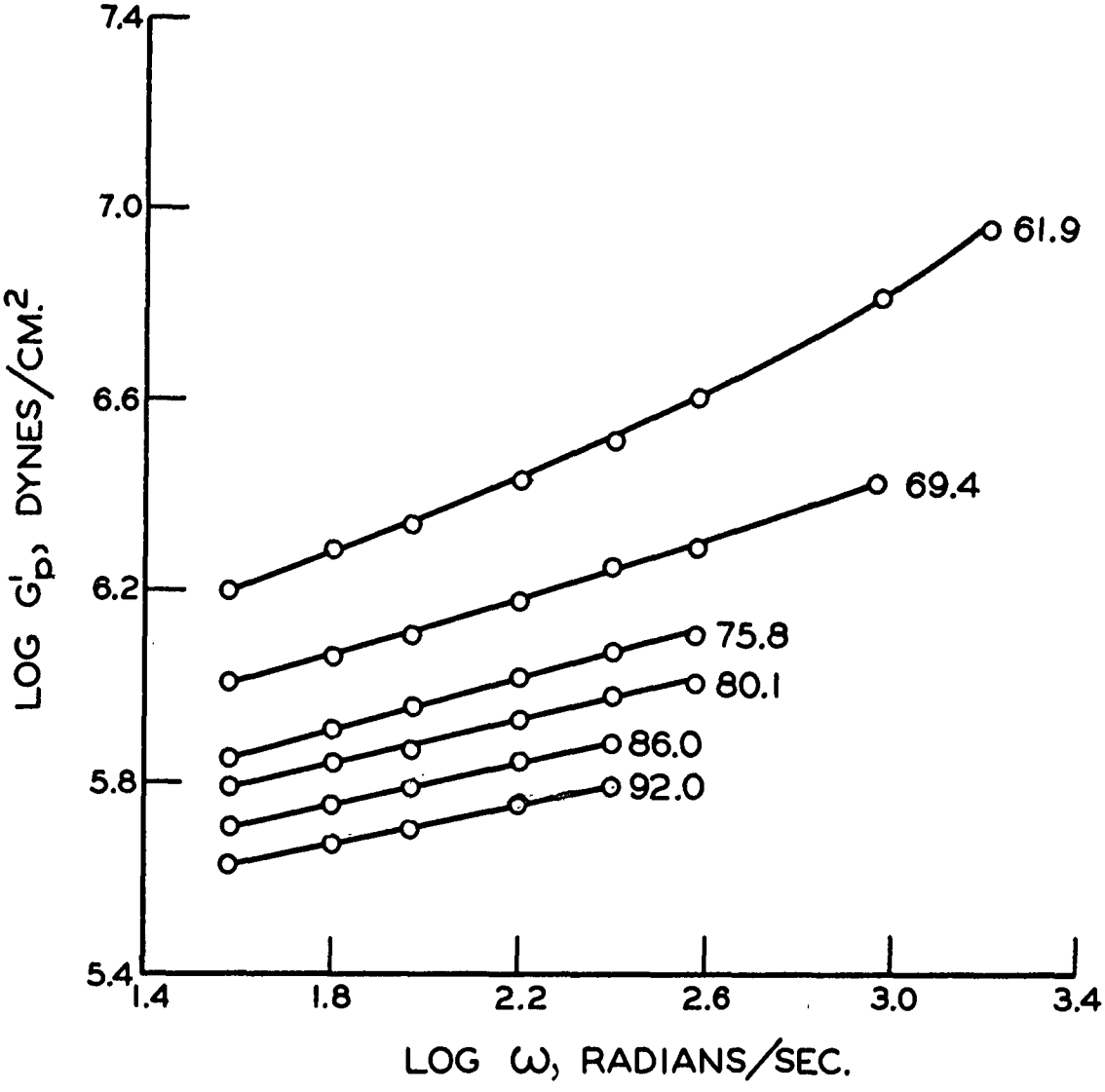

Figure 19. The Storage Modulus for a 67% Polystyrene-TCP Solution at the Temperatures Indicated

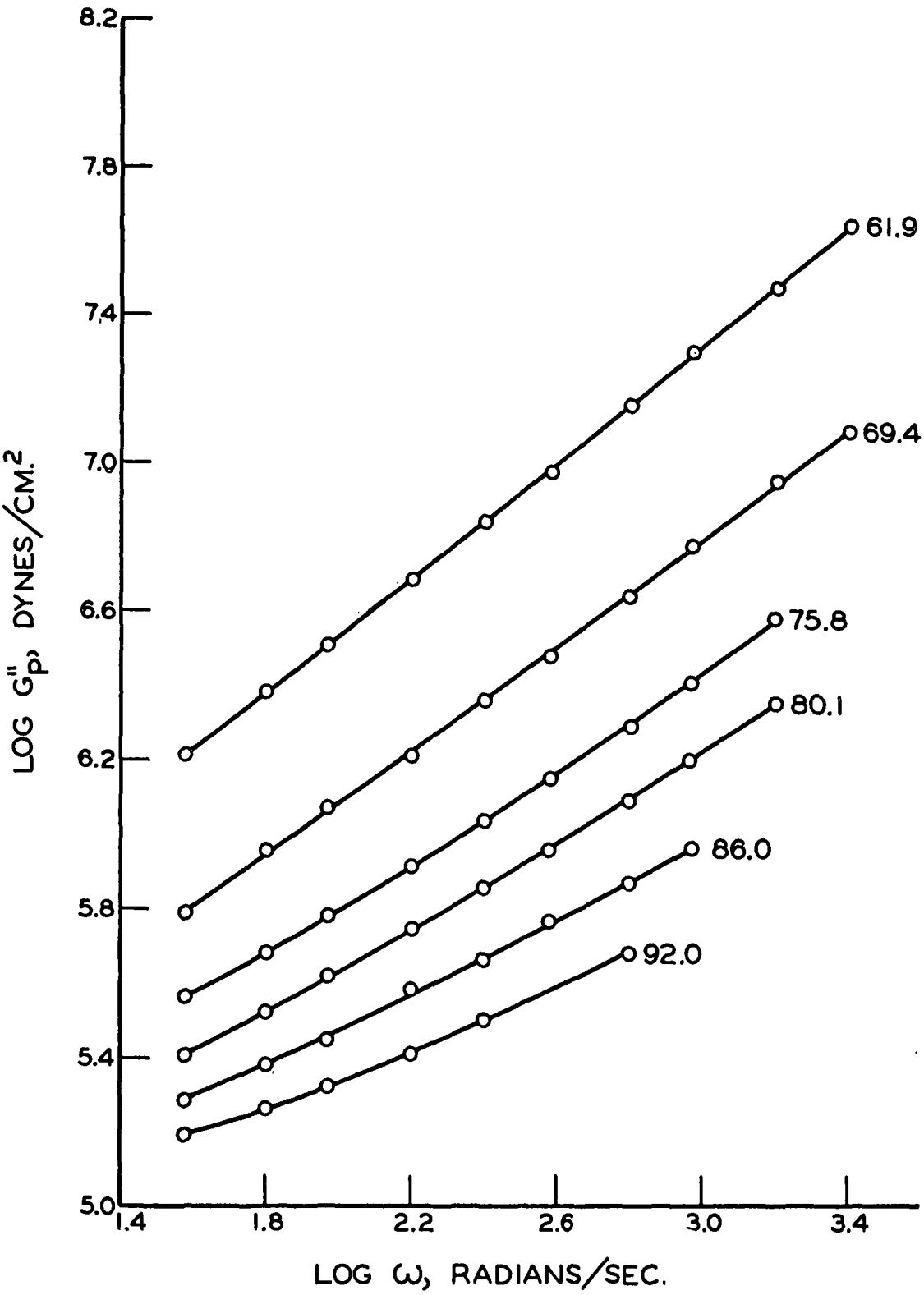

Figure 20. The Loss Modulus for a 67% Polystyrene-TCP Solution at the Temperatures Indicated

ANALYSIS AND DISCUSSION OF RESULTS

TEMPERATURE REDUCTION

The data were reduced for temperature according to the reduction scheme proposed by Ferry (1). The reduction scheme is based on the hypothesis that all the modes of motion which contribute to the relaxation spectra depend on temperature in the same way. This assumption is supported both by molecular theories and experimental results obtained for a wide variety of polymers (1).

If this assumption applies, then a curve of the storage or loss modulus plotted versus frequency on a log-log scale will be translated by a change in temperature, but its shape will remain the same. Therefore, appropriate reduced variables can be defined which incorporate the effect of temperature in their definitions, and, as a result, curves obtained at different temperatures will form a single composite curve.

The reduced variables for the storage and loss moduli are defined as,

$$G'_p = G'(T_o\rho_o/T\rho) \ , \tag{45}$$

and

$$G''_p = G''(T_o\rho_o/T\rho) \ , \tag{46}$$

where T and ρ are the temperature and density at which the modulus was measured, and T_o and ρ_o are the reference temperature, in this case 298°K, and the corresponding polymer solution density.

The reduced frequency variable is defined as,

$$\omega_p = \omega a_T \ . \tag{47}$$

where a_T is the ratio of a relaxation time at a given temperature to the corresponding relaxation time at the reference temperature T_o. The factor log a_T was determined experimentally by first plotting on a log-log scale the reduced storage modulus curves as a function of frequency as in Fig. 9 through 20. The distance along the frequency axis between each pair of adjacent curves was then measured. These distances were taken as $\Delta \log a_T$. They should be the same for both the storage modulus and loss modulus curves at each concentration. Reasonable agreement was obtained for all the curves, but where there were differences an average of the two values was used. However, in the case of the 67% solution, the curves for the storage modulus were so nearly horizontal that it was difficult to determine the distances accurately. Therefore, instead of taking averages, the values for the loss modulus were used.

By starting at the reference temperature and summing these increments of $\Delta \log a_T$, log a_T was obtained as a function of temperature. Experimentally determined log a_T-temperature functions were determined in this way for each of the six polystyrene concentrations using arbitrarily selected reference temperatures. The log a_T-temperature functions all had similar shapes and were found to nearly superimpose when a particular, though different, reference temperature was chosen for each polymer solution. As it turned out, each of these reference temperatures was a constant number of degrees above the glass temperature for the corresponding polymer solution. These results are shown in Fig. 21 where the experimental log a_T data are plotted for all six polystyrene concentrations. The reference temperature for each solution is 33 degrees above its glass temperature.

Although the data appear to fit better at the low temperature end of the curve, this is deceiving since the curves must coincide where the reference

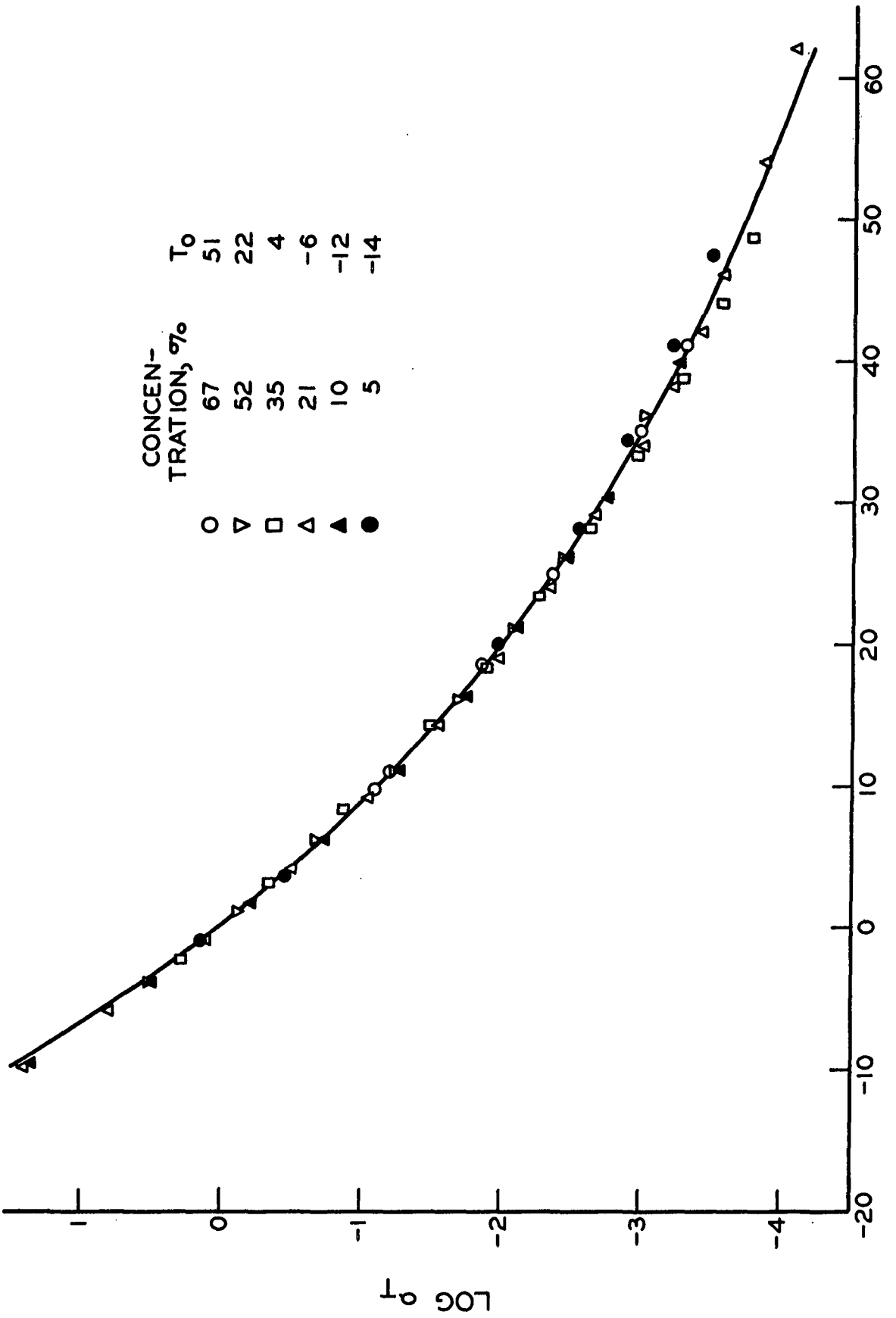

Figure 21. The Temperature Dependence of the Reduction Factor a_T for All Six Polystyrene-TCP Solutions

temperature is zero, which in this case was chosen at the low temperature end. If a reference temperature was chosen at the high temperature end, for example at T_g + 70°C., then the data at the high temperature end would appear to fit better. The deviations of the log a_T-temperature functions from exact superposition fall within the accuracy with which the log a_T data can be measured from the experimental curves and the accuracy of the glass transition temperatures of the solutions.

The data of Fig. 21 were fitted to Equation (16), the WLF equation, by the method of least squares which gave values for the constants, C_1 and C_2, of 8.93 and 69.4, respectively. The values of the constants depend on the reference temperature. If a different reference temperature is selected, the constants associated with this temperature can be calculated according to the equations (1):

$$C_2' = C_2 + T_o' - T_o \tag{48}$$

$$C_1' = C_1 C_2 / C_2' \tag{49}$$

where T_o' is the new reference temperature. When the reference temperature is chosen at the glass transition temperature, the constants become 36.4 and 17.0, respectively.

From Equations (19) and (20) the fractional free volume at the glass transition temperature is found to be 0.0255 and the expansion coefficient of the fractional free volume is 7×10^{-4}. The fractional free volume at the glass transition temperature agrees very well with the "universal" value of 0.025 (1). The expansion coefficient of the fractional free volume has sometimes been taken as equal to the difference in the thermal expansion coefficient above and below

the glass transition temperature (1). From the slopes of the refractive index curves used to determine the glass transition temperatures (Table III), this difference was estimated to be about 3.7×10^{-4} which is somewhat lower than α_f but at least of the right order of magnitude.

When the reduced storage modulus and loss modulus are plotted on a log-log plot versus the reduced frequency, composite curves are obtained for each of the polystyrene solutions as shown in Fig. 22 and 23. The reduction factors used to reduce the curves to 25°C. are given in Appendix VI.

For each solution, except the 67% solution, a least squares fit of the experimental data was used to obtain the constants for the WLF equation. The experimental data for the 67% solution was not sufficient to determine accurate constants, nor did the data extend to 25°C. Therefore, constants determined from an average of all the data were used.

Smooth curves were drawn through the data in Fig. 22 and 23. The contribution of the solvent viscosity to the loss modulus was found to be significant for the 5, 10, and 21% solutions. This contribution was eliminated by subtracting values of $\omega a_T \eta_s$ from the loss modulus curves. Points taken from the smoothed and corrected curves are tabulated in Table IX of Appendix VI.

THE RELAXATION SPECTRA

The relaxation spectra were calculated from the smoothed data (Table IX) using the second approximation method of Ferry and Williams (35). As a first approximation, the intensity function, $\omega^2\tau^2/(1+\omega^2\tau^2)$ in Equation (4), is replaced by a step function which is zero for $\omega\tau < 1$ and unity for $\omega\tau > 1$. Similarly, the factor $1/(1+\omega^2\tau^2)$ in Equation (5) is replaced by unity for $\omega\tau < 1$

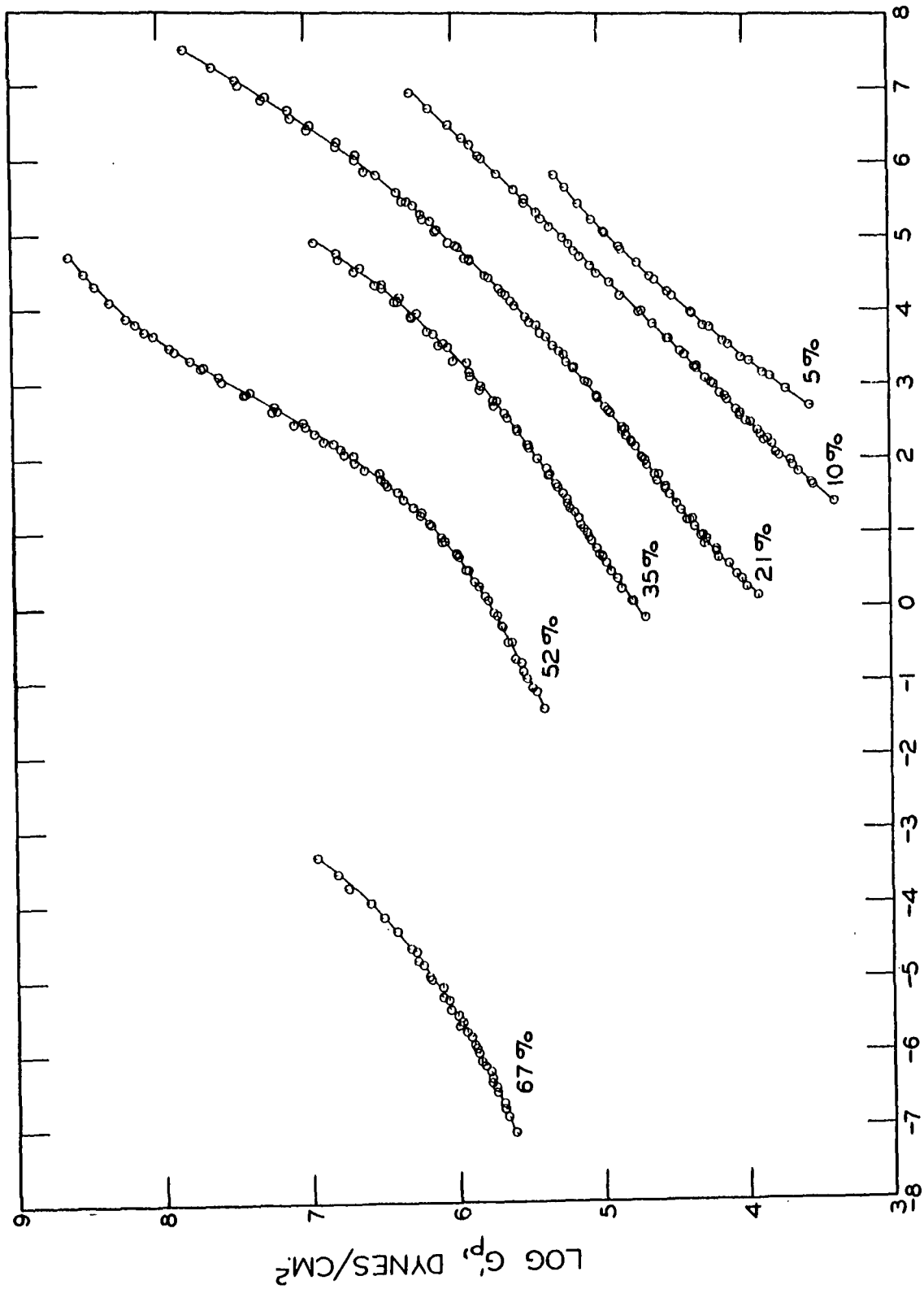

Figure 22. The Storage Modulus for Six Polystyrene-TCP Solutions Reduced to 25°C. The Pips Indicate the Temperatures at Which the Data Were Taken Starting with the Pip Up for the Lowest Temperature and Rotating 45 Degrees Clockwise According to the Temperature Sequences Given in Fig. 9 Through 20

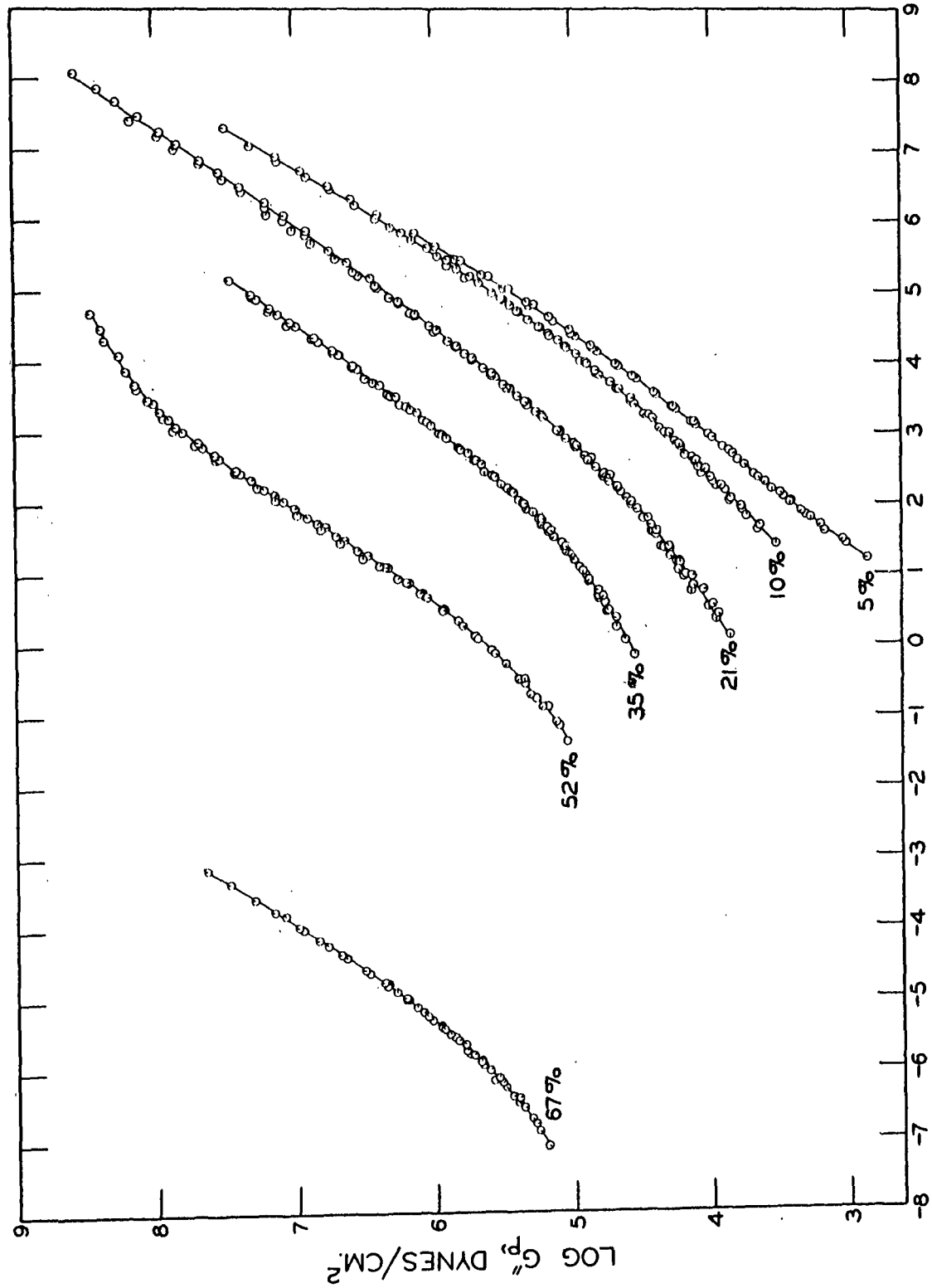

Figure 23. The Loss Modulus for Six Polystyrene-TCP Solutions Reduced to 25°C. The Pips Indicate the Temperatures at Which the Data Were Taken Starting with the Pip Up for the Lowest Temperature and Rotating 45 Degrees Clockwise According to the Temperature Sequences Given in Fig. 9 Through 20

and zero for $\omega\tau > 1$. This approximation gives,

$$H(\tau = 1/\omega) \cong G'[d(\log G')/d(\log\omega)], \tag{50}$$

and,

$$H(\tau = 1/\omega) \cong G''[1 - d(\log G'')/d(\log\omega)]. \tag{51}$$

The second approximation involves assuming an analytical expression for $\underline{H}$ which then permits the exact Equations (4) and (5) to be integrated. The relaxation spectrum, $\underline{H}$, may then be recalculated using the first approximation equations and compared with the assumed expression. The difference between the two shows what correction factors should be applied to the first approximation equations.

Assuming an analytical expression for $\underline{H}$ of the form

$$H = K\tau^{-m} \tag{52}$$

the correction factors to be applied to the first approximation equations are for Equation (6),

$$A = (2 - m)/[2\Gamma(2 - m/2)\Gamma(1 + m/2)] \; ; \; m<1 \tag{53}$$

and for Equation (7),

$$B = (1 + |m|)/[2\Gamma(3/2 - |m|/2)\Gamma(3/2 - |m|/2)], \tag{54}$$

where Γ is the gamma function.

The quantity $\underline{m}$ is determined from the slope of a log-log plot of $\underline{H}$ vs. τ obtained from the first approximation equations.

The relaxation spectra calculated from both the storage modulus and loss modulus are shown in Fig. 24. The agreement between the points calculated from

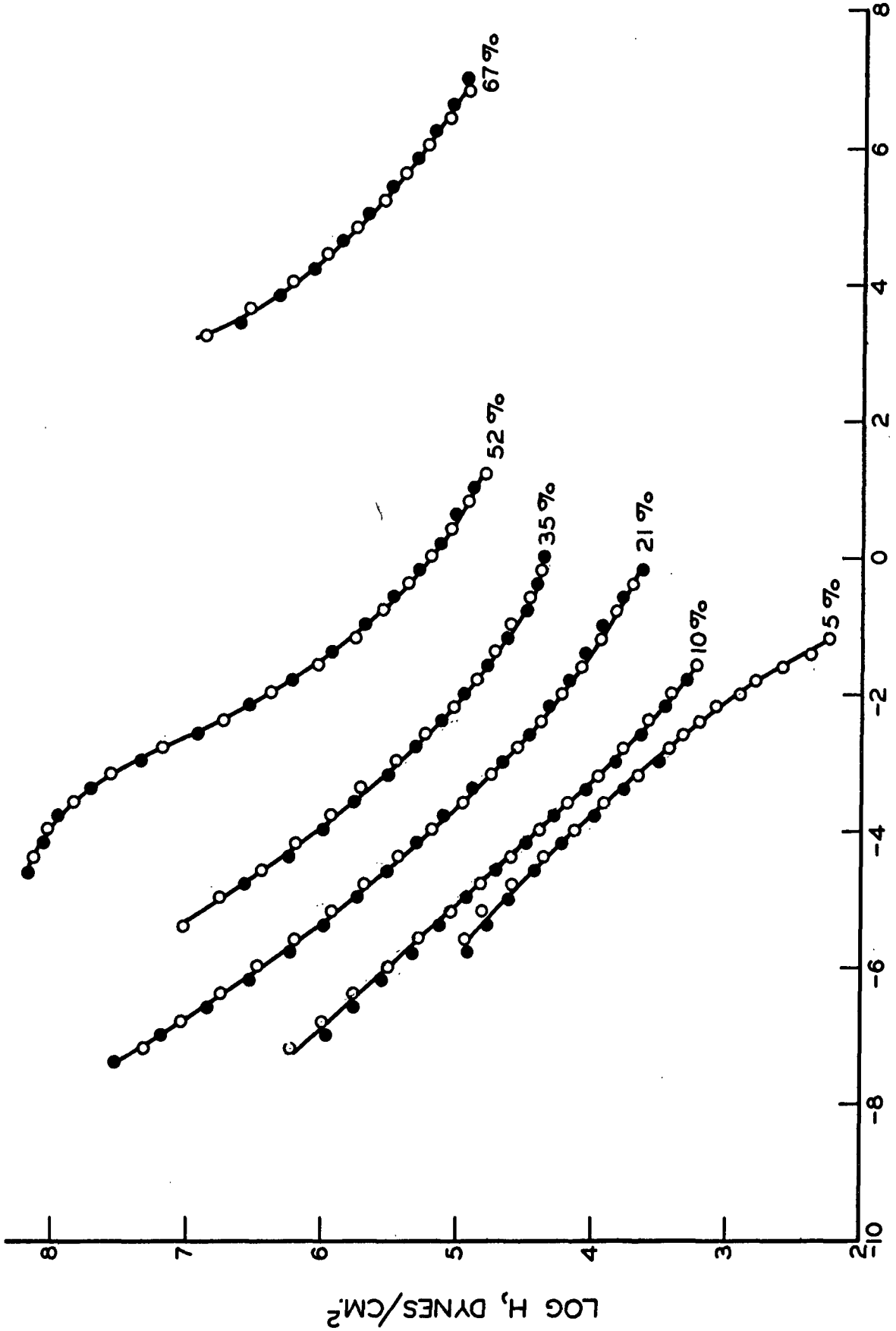

Figure 24. Comparison of the Relaxation Spectra of the Polystyrene-TCP Solutions as Calculated from the Storage Modulus (Pip Right) and Loss Modulus (Pip Up)

the two moduli is evidence that the shear strains imposed on the samples were within the linear viscoelastic region for which the Boltzmann superposition principle applies.

CONCENTRATION REDUCTION

The results of the temperature reduction indicate that the fractional free volume at the glass temperature and the expansion coefficient of the fractional free volume are independent of concentration over the range considered. These results confirm the assumptions used in deriving Equation (24). Therefore, the shift in relaxation times, log $\underline{a}_{\underline{c}}$, may be calculated with some confidence using this equation. The value of the fractional free volume in this equation, $\underline{f}(\underline{T},\underline{c}_o)$, can be calculated from Equation (22) using the results of the temperature reduction. The glass temperatures used in Equation (24) are taken from Table III. The calculated values of log $\underline{a}_{\underline{c}}$ are given in Table IV using the 52% polystyrene solution as the reference concentration, $\underline{c}_o$.

TABLE IV

CALCULATED VALUES OF LOG $\underline{a}_{\underline{c}}$ [a]

Polystyrene Concentration, %	$\underline{T}(\underline{c}_o)-\underline{T}(\underline{c})$, °C.	Log $\underline{a}_{\underline{c}}$
67	-29	5.7
52	0	--
35	18	-1.71
21	28	-2.39
10	34	-2.74
5	36	-2.84

[a] The data are calculated using Equation (24) with constants of 8.59 for $\underline{f}(\underline{T},\underline{c}_o)/2.303$ and 72.9 for $\underline{f}(\underline{T},\underline{c}_o)/\alpha_{\underline{f}}$.

The curves of Fig. 24 can be reduced by applying the calculated log a_c values to the relaxation time axis as shown in Fig. 25. Since the shapes of the curves are not identical, translations of the spectra along the log H axis will not superimpose them exactly. However, there is a portion of each spectrum where the shapes are similar. This portion includes the region where the slope is -1/2 in accordance with the Rouse theory as indicated by Equation (25). Although the Rouse theory was derived only for the case of isolated molecules, it has been proposed (1) that even in concentrated solutions there should be a region of the spectrum with slope of -1/2. Recent experimental data on moderately dilute polymer solutions support this argument (36).

In Fig. 25 slopes of -1/2 are drawn tangent to all of the spectra except the 5% solution which does not fit the Rouse theory. The reasons for this are discussed in the next section. The regions of the spectra where the slopes are -1/2 can be superimposed by appropriate translations along the log H axis. Figure 26 shows the change in log H as a function of the change in log c using the 52% solution as the reference concentration. The straight line indicates that H is proportional to $c^{2.0}$ as opposed to the first power as predicted by the Rouse theory.

Direct comparison of these results with data given in the literature is difficult since the reverse procedure has usually been used to reduce the curves. That is, assuming H was directly proportional to the concentration, values of log a_c were determined experimentally. Here, log a_c values have been calculated using Equation (24), and the effect of H on concentration was then observed from the experimental curves.

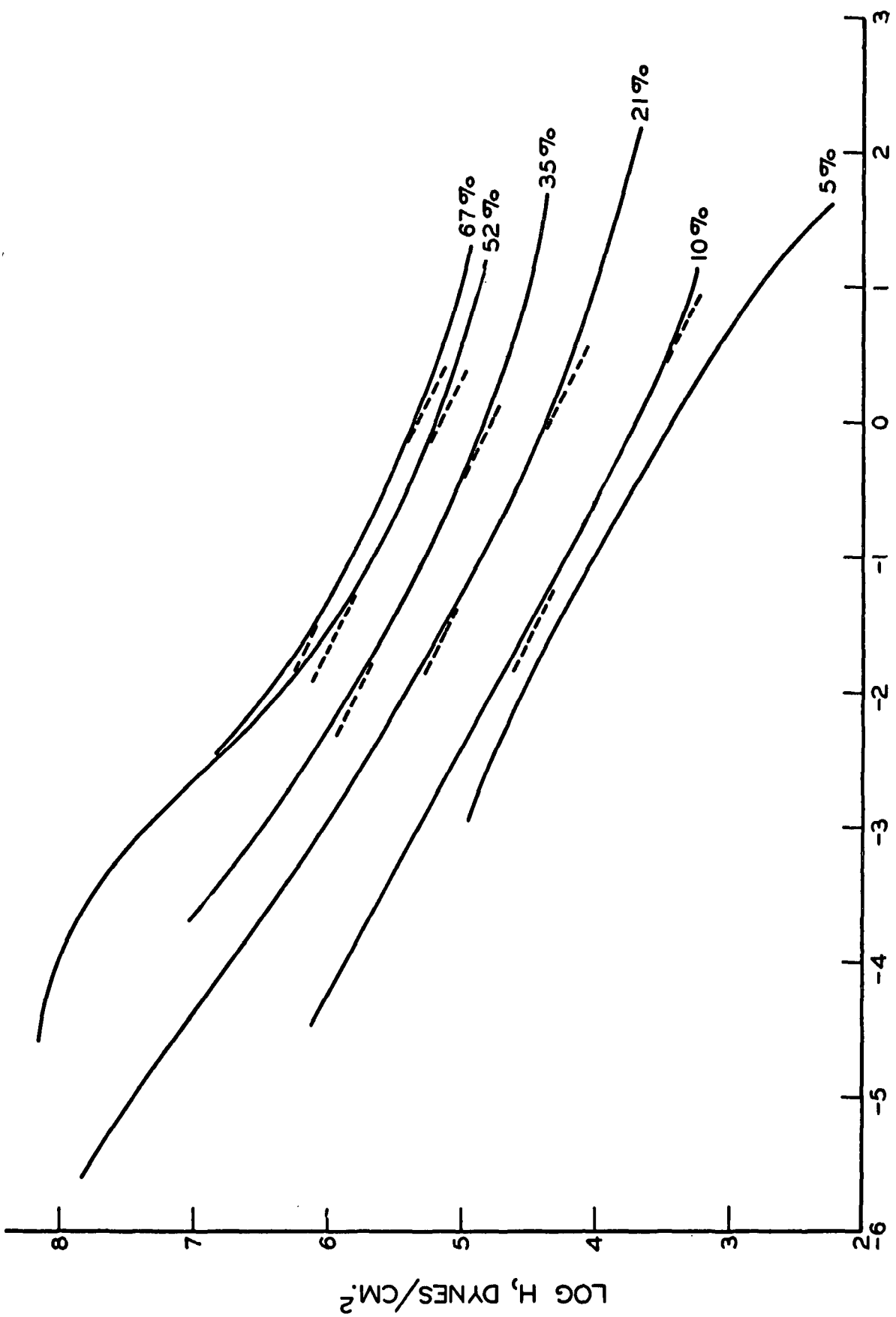

Figure 25. The Relaxation Spectra Reduced to a Concentration of 52% Using Calculated Values of log $\underline{a}_{\underline{c}}$. The Dotted Lines Have Slopes of -1/2

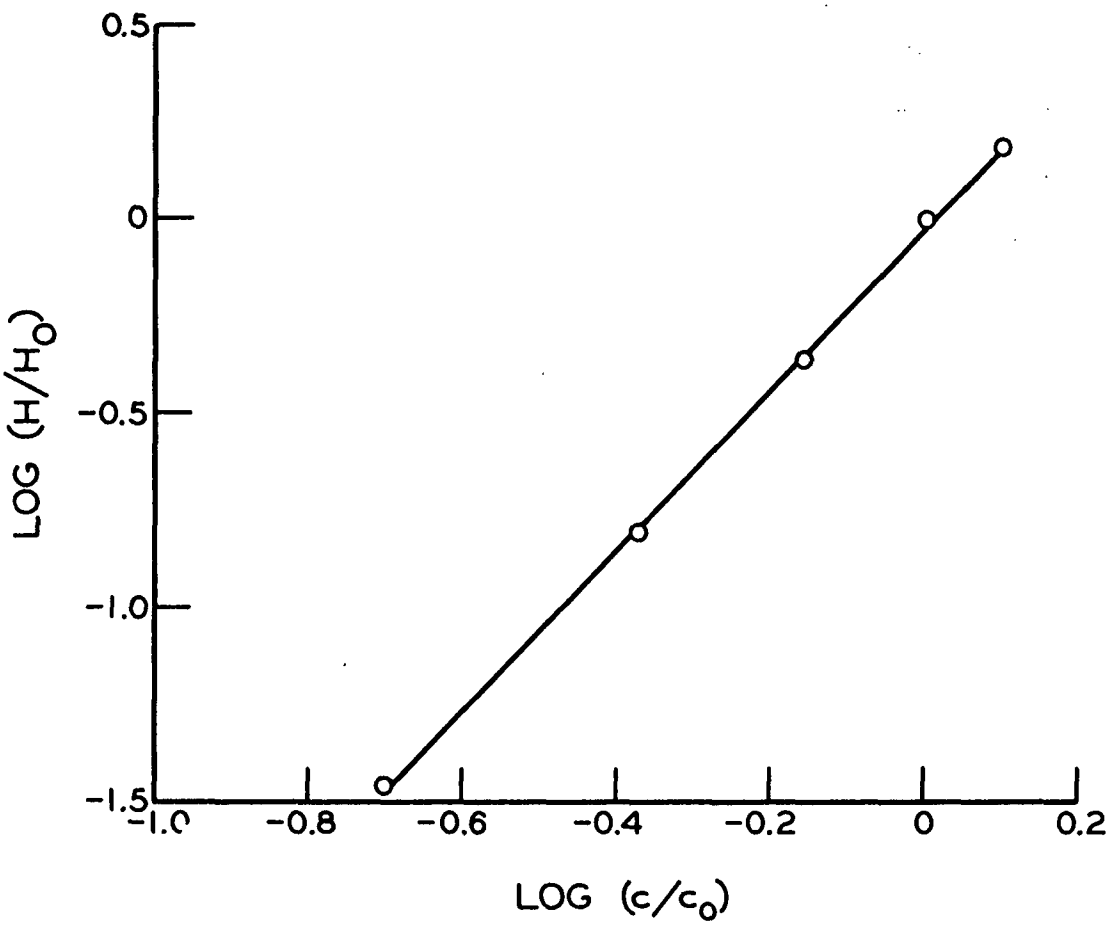

Figure 26. The Experimentally Determined Concentration Reduction Factors for the Relaxation Spectra

In the plateau region H has been found by other investigators (3,37) to depend on a higher power of concentration, presumably due to entanglement coupling. However, changes in entanglement coupling should not affect the spectra in the transition zone, which includes the region with a slope of -1/2; and, therefore, it seems unlikely that this could explain the concentration dependence found here.

EFFECTS OF ENTANGLEMENT COUPLING

The logarithm of the loss tangent, G''/G', was determined from the smoothed data (Table IX) of the reduced moduli. From the minimum points in the loss

tangent curves plotted in Fig. 27, the number of chain bonds between entanglements, Λ, can be calculated using Equation (27) and the weight average molecular weight. For the two highest concentrations, minima were not quite reached, and it was necessary to make short extrapolations. Values of log Λ are plotted versus the logarithm of the polymer concentration in Fig. 28. The 52% solution was used as the reference concentration. The slope of the straight line indicates that Λ depends on $c^{-0.75}$. According to the probability of entanglement between two juxtaposed polymer molecules the exponent should be -1 (23). However, since polymolecularity is known to affect the minimum in the loss tangent (23), the discrepancy between -0.75 and -1 may be due to the influence of the molecular weight distribution.

An exponent of -1 was reported for polyisobutylene in cetane (22). For two methacrylates, polymethyl and poly-n-butyl, in diethyl phthalate, exponents of about -2.3 to -2.6 were obtained from dynamic data (3, 38), whereas an exponent of -1.2 was obtained from viscosity data (39). However, in analyzing the dynamic data it was assumed that in the transition region H was proportional to c. If, instead, H had been taken as proportional to c^2 as has been found for the polystyrene-TCP solutions, then the exponent would be -1.3 to -1.6, which is in much better agreement with the exponent of -1.2 obtained from viscosity data.

COMPARISON WITH MOLECULAR THEORIES

The change in the theoretical Rouse curves for polymolecularity as introduced by Menefee and Peticolas (11, 12) is shown in Fig. 29. The storage modulus and loss modulus were calculated from the Rouse theory using Equations (6), (7), and (8); the weight average molecular weight of the polystyrene; and the steady-flow viscosity of the 5% polystyrene solution. The corresponding curves modified for

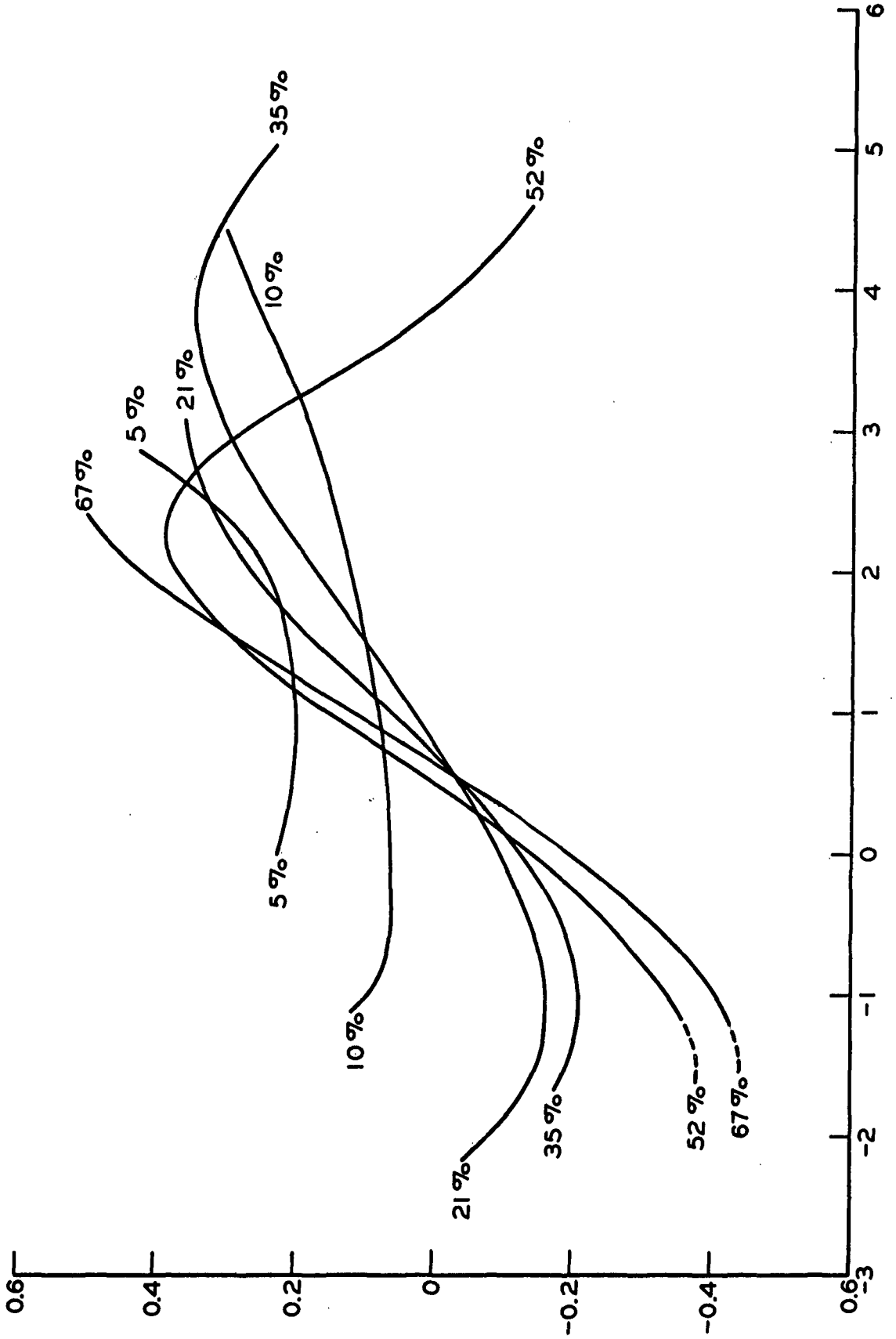

Figure 27. The Loss Tangent Curves of the Polystyrene-TCP Solutions Reduced to a Temperature of 25°C. and Concentration of 52%

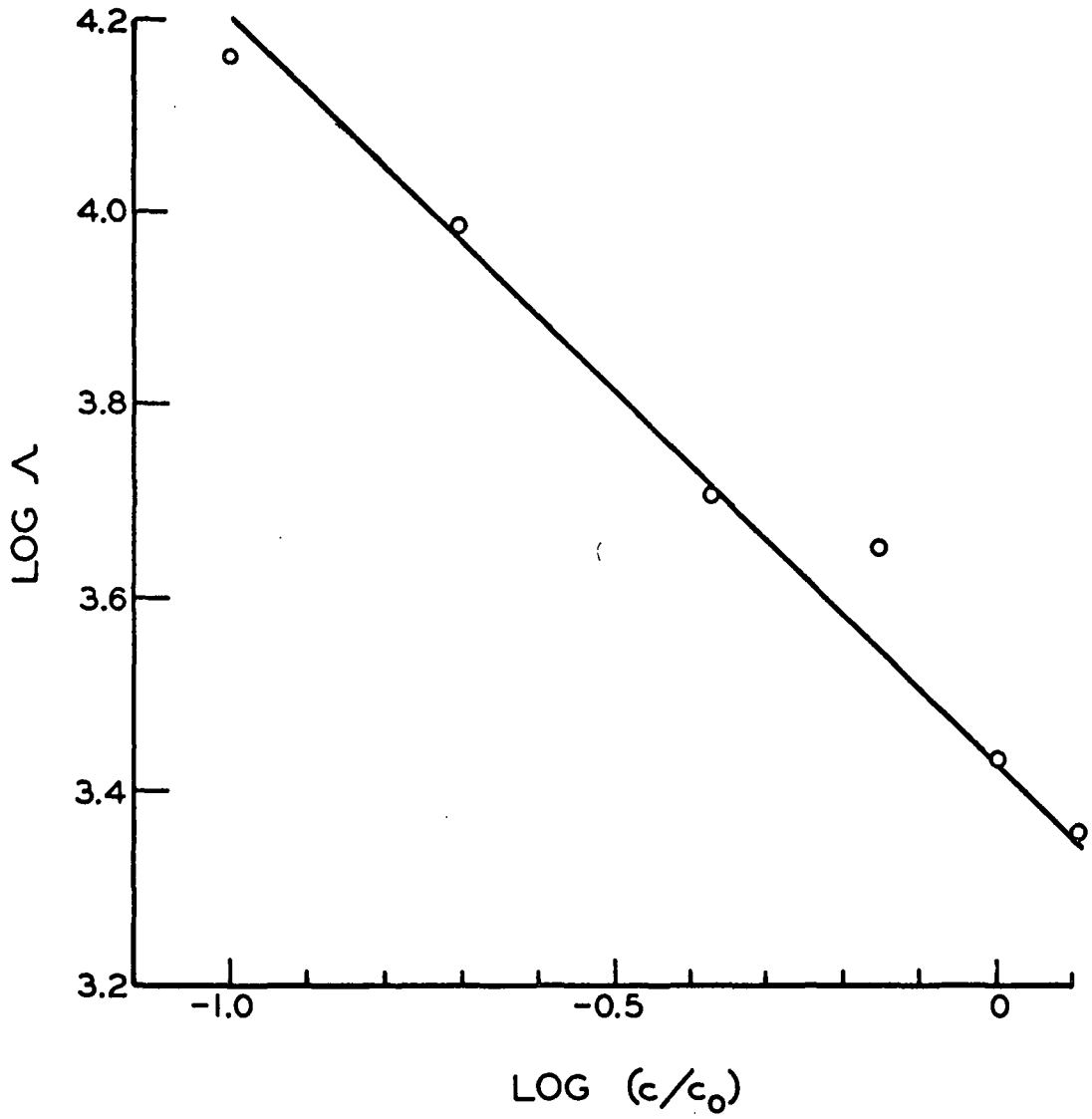

Figure 28. The Effect of Polymer Concentration on Entanglement Coupling

polymolecularity were calculated using Equations (11), (12), and (13); the molecular weight distribution given in Fig. 7; and the same steady-flow viscosity. As shown in Fig. 29 the effects of a broad molecular weight distribution are relatively small, the main effect being a more gradual change in the slope as the curves enter the flow region at low frequencies.

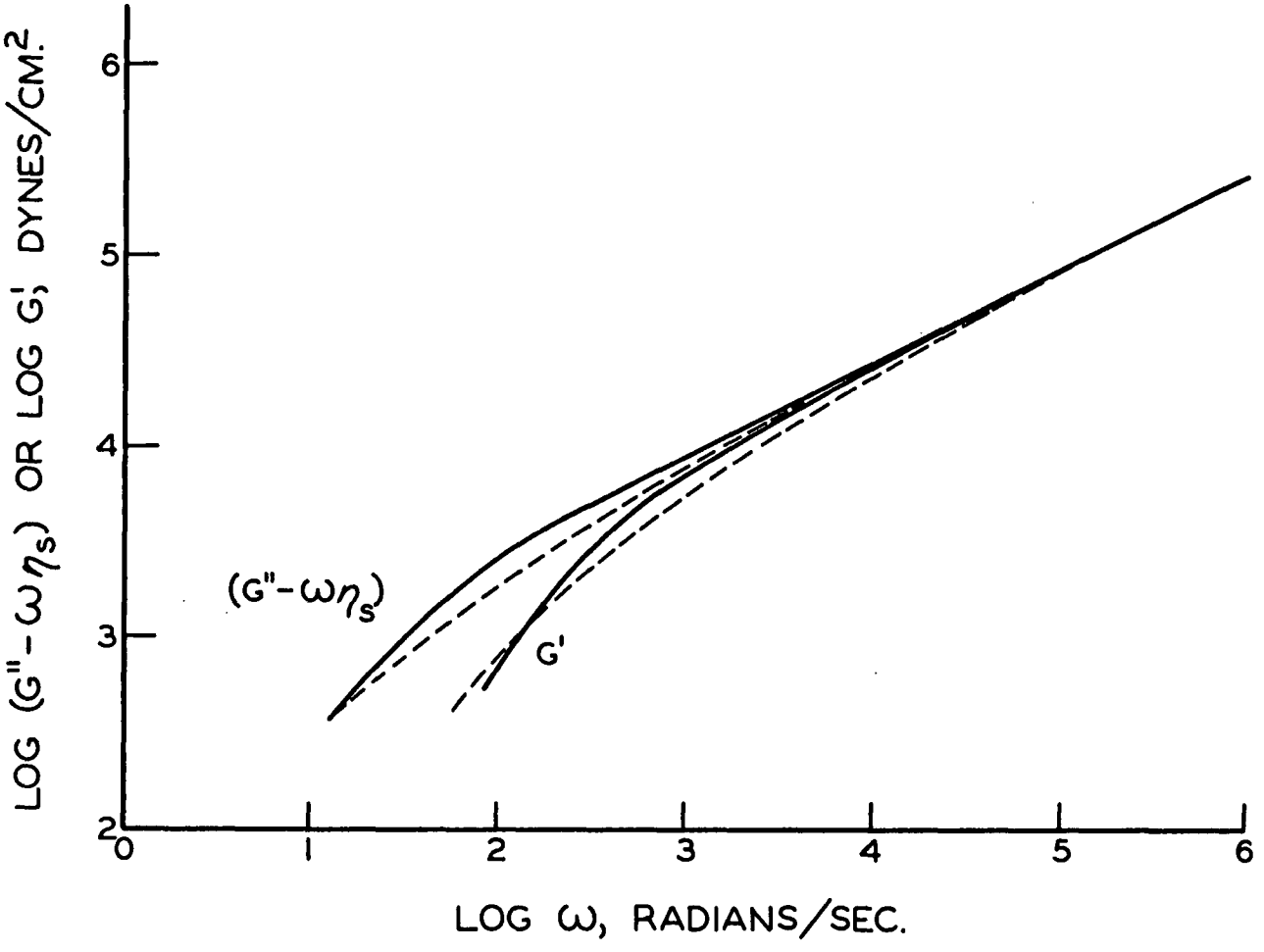

Figure 29. The Rouse Theory for a Homogeneous Polymer (Solid Lines) and Modified for a Broad Distribution Polymer (Dashed Lines)

The Rouse and Zimm theories apply only to concentrations where the polymer molecules are isolated. These concentrations are lower than the 5% polystyrene solution, and, therefore, it cannot be expected that the data for the 5% solution will follow the theories. Nevertheless, it is of interest to compare the data

with the theories in order to observe what deviations arise when interactions between the molecules occur.

Recently, DeMallie, et al. (40) have presented experimental dynamic data for dilute solutions of polystyrene fractions, and similar data have been reported by Tschoegl and Ferry (36) for polyisobutylene fractions, and a whole polymer of polyisobutylene. For both polymers, the Zimm theory was found to fit the experimental data remarkably well provided that the polymer concentration was one per cent or less. At higher concentrations two discrepancies were noted. First, the data tended to deviate from the Zimm theory toward the Rouse theory and second, the data were shifted with respect to the theoretical curves by a factor which was equivalent to increasing the molecular weight. The high molecular weight whole polymer at a concentration of 4% was found to fit the shape of the Rouse curve better than the Zimm curve.

The data for the 5 and 10% polystyrene-TCP solutions show similar discrepancies as indicated in Fig. 30 through 33. The deviation in the locations of the theoretical and experimental curves is much greater for the 10% solution than the 5%. This follows the trend noted by both DeMallie and Tschoegel. However, here there is probably an additional discrepancy, especially in the 10% solution, because the steady-flow viscosity was used in calculating the theoretical curves. Steady-flow viscosity is highly dependent on entanglement coupling, and entanglement coupling has already been shown to have some effect on both the 5 and 10% solutions.

The shapes of the storage and loss moduli curves of the 5% solution appear to be intermediate between the shapes of the Rouse and Zimm curves whereas the curves of the 10% solution have shapes which are closer to the Rouse curves. Here too, this is in agreement with the trends noted by DeMallie and Tschoegl.

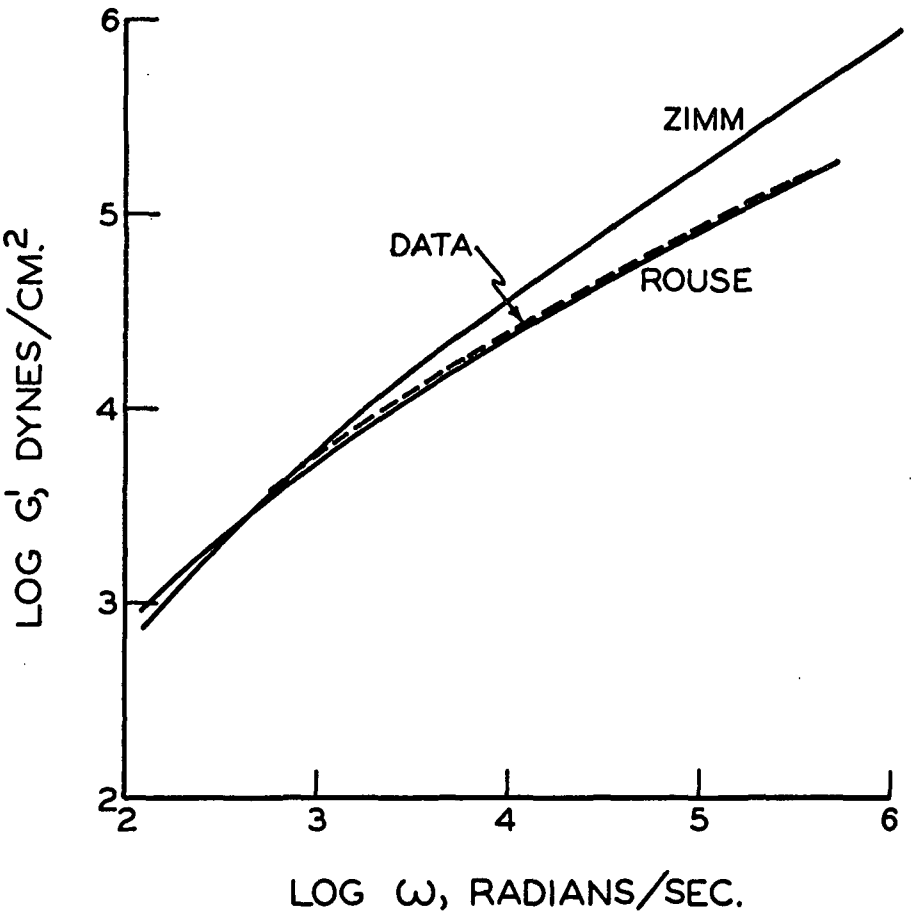

Figure 30. The Storage Modulus for the 5% Polystyrene-TCP Solution Compared with the Rouse and Zimm Curves Modified for Polymolecularity

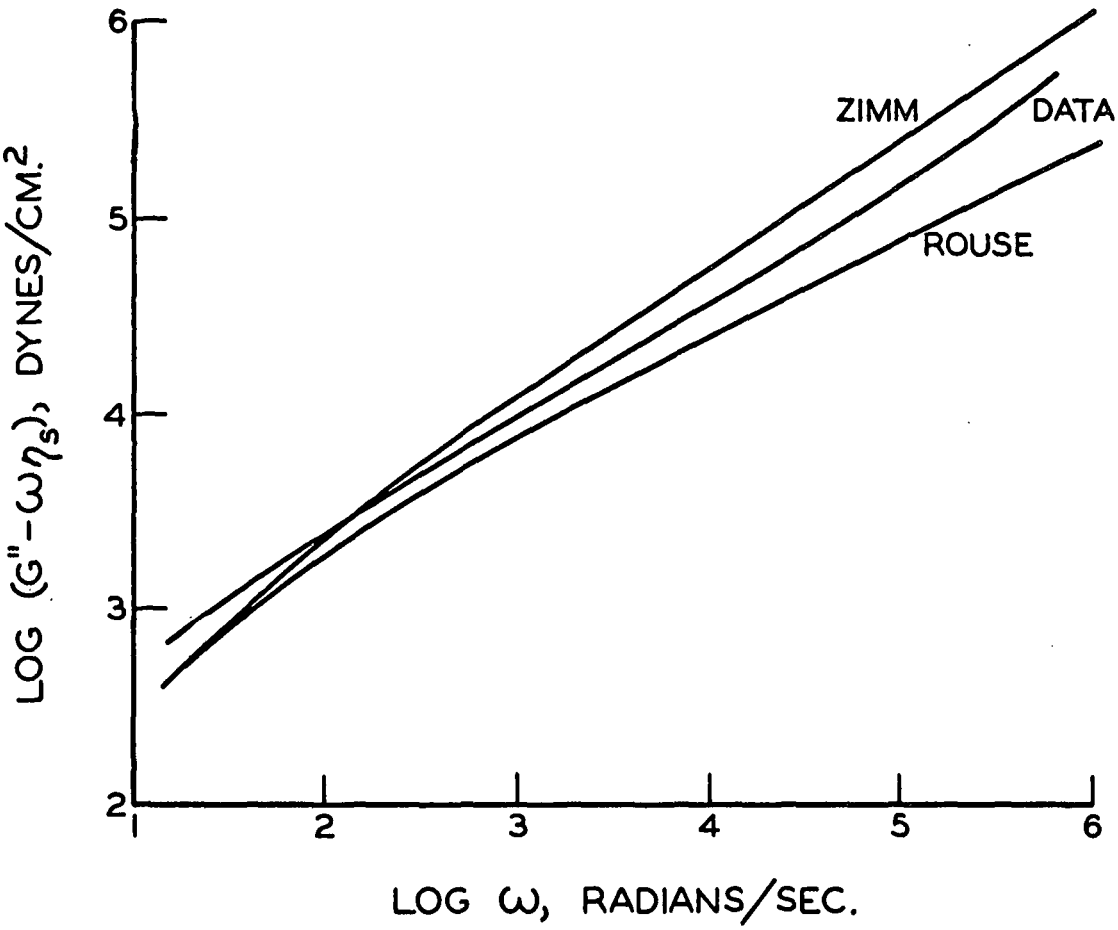

Figure 31. The Loss Modulus for the 5% Polystyrene-TCP Solution Compared with the Rouse and Zimm Curves Modified for Polymolecularity

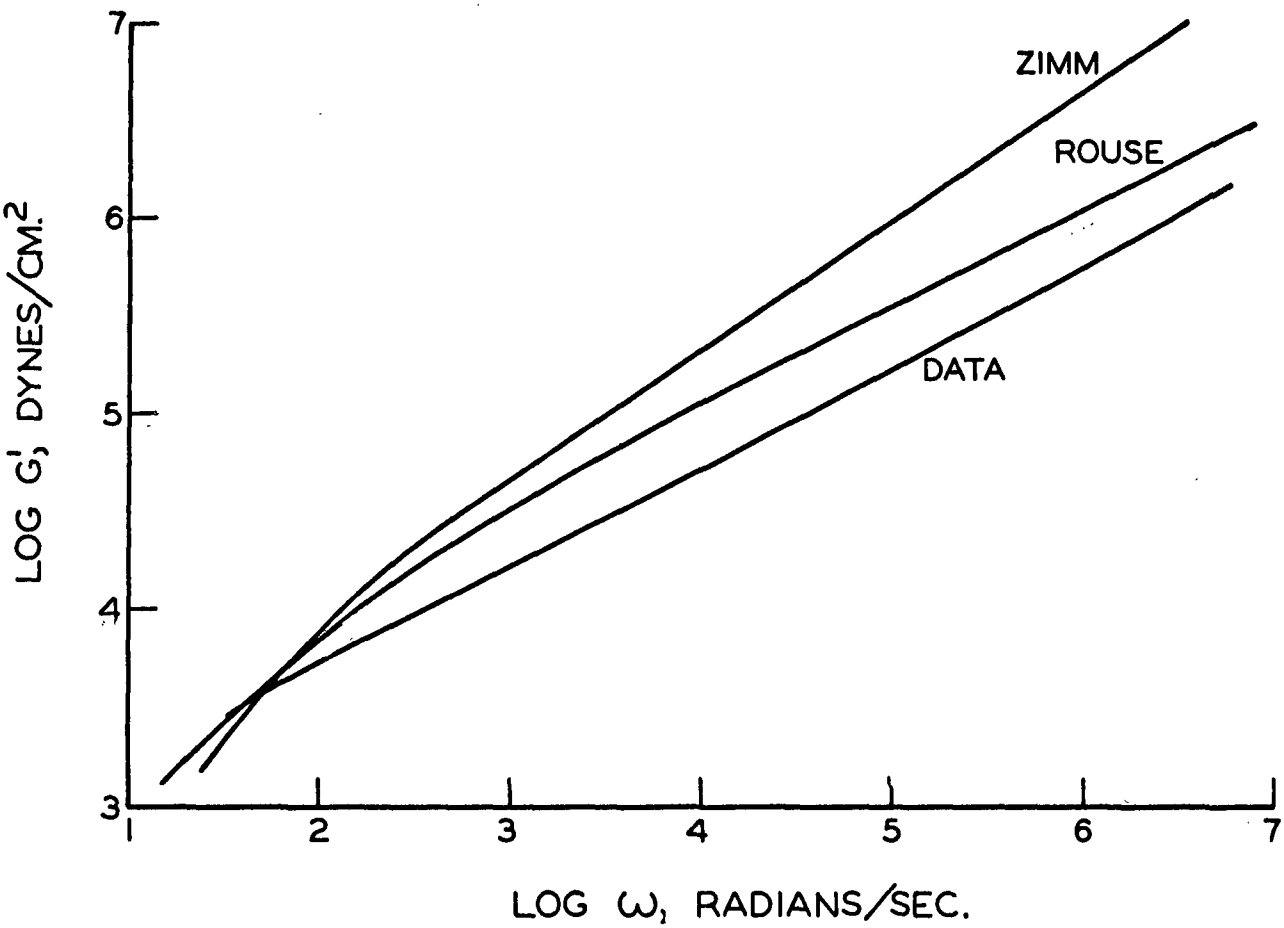

Figure 32. The Storage Modulus for the 10% Polystyrene-TCP Solution Compared with the Rouse and Zimm Curves Modified for Polymolecularity

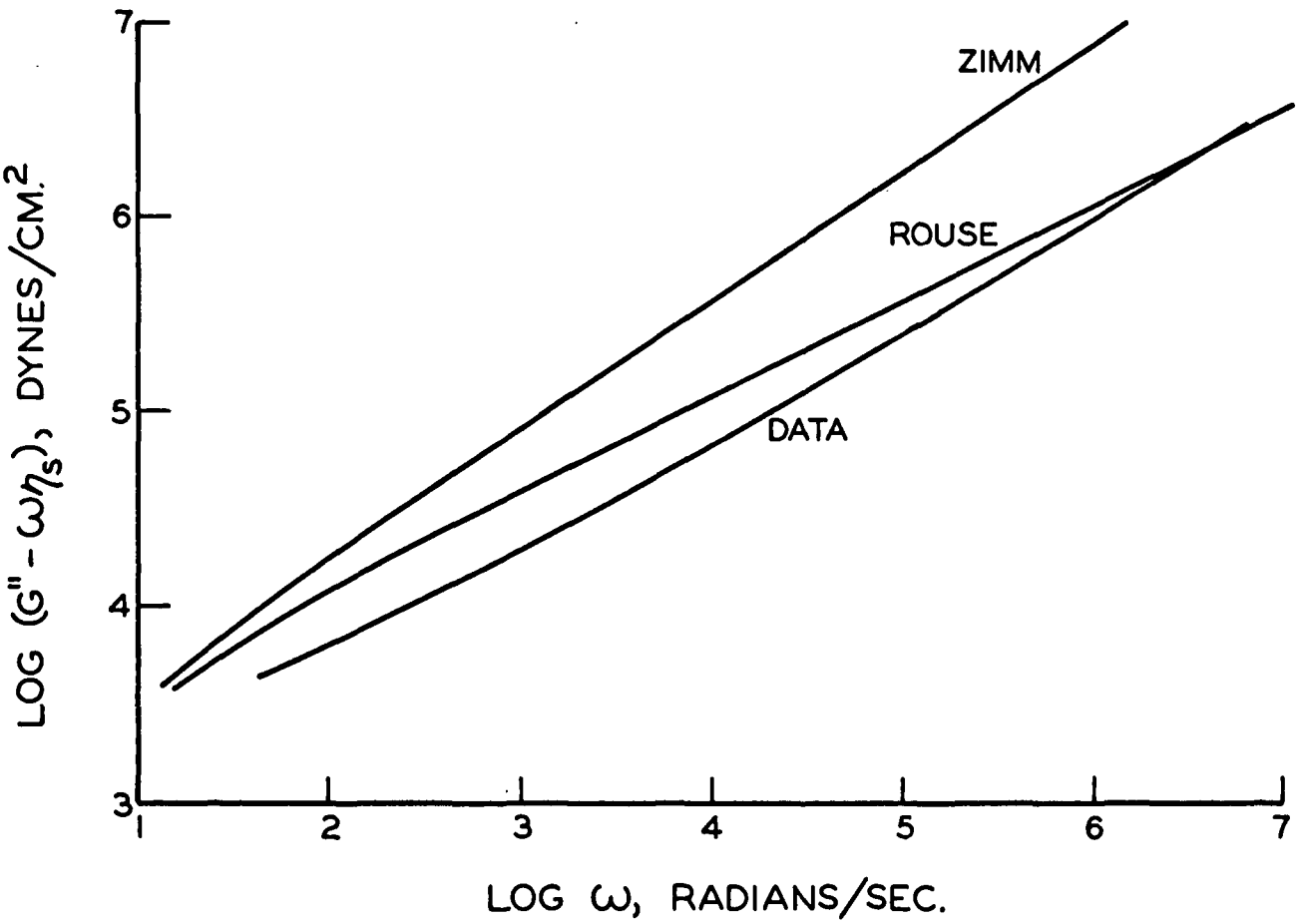

Figure 33. The Loss Modulus for the 10% Polystyrene-TCP Solution Compared with the Rouse and Zimm Curves Modified for Polymolecularity

ACKNOWLEDGMENTS

I gratefully acknowledge the guidance and encouragement of my thesis advisory committee: Dr. S. F. Kurath, Dr. R. W. Nelson, and Dr. W. P. Riemen. In particular, I would like to thank Dr. Kurath who suggested the original idea for this study and whose patience and understanding materially contributed to comprehending the subject.

GLOSSARY OF SYMBOLS

a_c	the ratio of the relaxation time at concentration c to the corresponding relaxation time at an arbitrary reference concentration c_o
a_T	the ratio of the relaxation time at temperature T to the corresponding relaxation time at an arbitrary reference temperature T_o
A	a constant in the Doolittle equation
	total cross-sectional area of a pair of transducer samples
A_1	real component of the electrical transfer admittance
	cross-sectional area of the first transducer sample of a pair
A_2	imaginary component of the electrical transfer admittance
	cross-sectional area of the second transducer sample of a pair
A_{10}	real component of the electrical transfer admittance without samples in the transducer
A_{20}	imaginary component of the electrical transfer admittance without samples in the transducer
B	a constant in the Doolittle equation
B_1, B_2	flux densities at Coils 1 and 2, respectively
c	polymer concentration in grams of polymer per milliliter of solution
c_o	reference concentration
C	capacitance of a capacitor in the integrating unit
C_1, C_2	constants in the WLF equation
c_i	instantaneous input voltage to integrating unit
e_o	instantaneous output voltage from the integrating unit
E_2	open circuit voltage generated in Coil 2
E_i	effective input voltage to the integrating unit
E_o	effective output voltage from the integrating unit
f	frictional resistance of the transducer tube
	fractional free volume

f_o	fractional free volume at the reference temperature T_o
f_g	fractional free volume at the glass transition temperature
$f(T,c)$	fractional free volume at temperature T and concentration c
F	force
G^*	complex dynamic shear modulus
G'	storage modulus or the real component of the complex dynamic shear modulus
G'_R	storage modulus reduced to a reference temperature of 25°C.
G''	loss modulus or imaginary component of the complex dynamic shear modulus
G''_R	loss modulus reduced to a reference temperature of 25°C.
h	average thickness of a pair of transducer samples
h_1, h_2	individual thicknesses of a pair of transducer samples
H	the relaxation spectrum
I_1	alternating current supplied to Coil 1
j	$\sqrt{-1}$
k	elastance of the supporting wires for the transducer tube
K^2	transducer constant
ℓ_1, ℓ_2	the lengths of wire in Coils 1 and 2, respectively
m	mass of the transducer tube
	mass of a sample
	slope of a log-log plot of H versus τ
M	molecular weight
M_o	monomer molecular weight
M_i	molecular weight of ith polymer molecule
$\overline{M}_w$	weight average molecular weight
n	refractive index
N	number of submolecules

$\underline{p}$	running index
$\underline{P}$	potential divider
$\underline{r}$	constant in the Lorenz-Lorentz equation
$\underline{R}$	gas constant
	resistance in the integrating unit
$\underline{R_1}$	resistance in the circuit of Coil 1
$\underline{RC}$	the time constant for the integrating unit
$\underline{t}$	time
$\tan \delta$	loss tangent
$\underline{T}$	temperature
$\underline{T_o}$	reference temperature
$\underline{T_g}$	glass transition temperature
$\underline{v}$	instantaneous tube velocity
	specific volume
$\underline{v_o}$	occupied volume
$\underline{v_f}$	free volume
$\underline{w_i}$	weight fraction of $\underline{i}$th polymer molecule
$\underline{Z}$	mechanical impedance
$\underline{Z_o}$	tube impedance without samples
$\underline{Z_s}$	sample impedance
α	expansion coefficient
α_1, α_2	potential divider settings
α_f	expansion coefficient of the fractional free volume
γ^*	complex dynamic shear strain
γ_o	maximum value of the complex dynamic shear strain
$\Gamma(\ )$	the gamma function

δ	phase angle between the complex dynamic stress and the complex dynamic strain
η	steady-flow viscosity
η_s	solvent viscosity
λ'_p	a numerical coefficient
Λ	the number of chain bonds between entanglement points
ν	frequency in cycles per second
ρ	density of a polymer solution
ρ_b	density of ball in Hoeppler viscosity
σ^*	complex dynamic shear stress
σ_o	maximum value of the complex dynamic shear stress
τ	relaxation time
ω	circular frequency

LITERATURE CITED

1. Ferry, J. D. Viscoelastic properties of polymers. New York, John Wiley & Sons, 1961. 482 p.

2. Fujita, H., and Kishimoto, A., J. Chem. Phys. 34:393(1961).

3. Saunders, P. R., Stern, D. M., Kurath, S. F., Sakoonkim, C., and Ferry, J. D., J. Colloid Sci. 14:222(1959).

4. Boltzmann, L., Pogg. Ann. Phys. Lpz. 7:624(1876).

5. Leaderman, H. Elastic and creep properties of filamentous materials and other high polymers. Washington, D. C., The Textile Foundation, 1943. 278 p.

6. Gross, B. Mathematical structure of the theories of viscoelasticity. Paris, Hermann et Cie, 1953. 71 p.

7. Rouse, P. E., Jr., J. Chem. Phys. 21:1272(1953).

8. Zimm, B. H., J. Chem. Phys. 24:269(1956).

9. Kirkwood, J. G., and Riseman, J., J. Chem. Phys. 16:565(1948).

10. Zimm, B. H., Roe, G. M., and Epstein, L. F., J. Chem. Phys. 24:279(1956).

11. Menefee, E., and Peticolas, W. L., J. Chem. Phys. 35:946(1961).

12. Peticolas, W. L., J. Chem. Phys. 35:2128(1961).

13. Williams, M. L., Landel, R. F., and Ferry, J. D., J. Am. Chem. Soc. 77:3701 (1955).

14. Doolittle, A. K., J. Appl. Phys. 22:1471(1951).

15. Cohen, M. H., and Turnbull, D., J. Chem. Phys. 31:1164(1959).

16. Fujita, H., and Maekawa, E., J. Phys. Chem. 66:1053(1962).

17. Teramoto, A., Okada, R., and Fujita, H., J. Phys. Chem. 67:1228(1963).

18. Fujita, H., Kishimoto, A., and Matsumoto, K., Trans. Faraday Soc. 56:424 (1960).

19. Fujita, H., and Kishimoto, A., J. Polymer Sci. 28:547(1958).

20. Fox, T. G., and Flory, P. J., J. Polymer Sci. 14:315(1954); J. Appl. Phys. 21:581(1950).

21. Marvin, R. S. In J. T. Bergen's Viscoelasticity – phenomenological aspects. p. 27. New York, Academic Press, 1960.

22. Hoberg, H., Lovell, S. E., and Ferry, J. D., Acta Chem. Scand. 14:1424(1960).

23. Richards, J. R., Ninomiya, K., and Ferry, J. D., J. Phys. Chem. 67:323(1963).

24. Marvin, R. S., Fitzgerald, E. F., and Ferry, J. D., J. Appl. Phys. 21:197 (1950).

25. Kurath, S. F., Passaglia, E., and Pariser, R., J. Appl. Polymer Sci. 1:150-7 (1959).

26. Kurath, S. F. Personal communication, 1963.

27. McCormick, H. J., J. Polymer Sci. 36:341(1959).

28. Taylor, D. L. An evaluation of column thermal diffusion as a means of polymer characterization. Doctor's Dissertation. Appleton, Wis., The Institute of Paper Chemistry, 1962. 123 p.

29. Pregl, F. Quantitative organic microanalysis. Philadelphia, P. Blakiston's Son & Co., Inc., 1937. 271 p.

30. Jenckel, E., and Heusch, R., Kolloid-Z. 130:89(1953).

31. Ueberreiter, K., and Kanig, G., J. Colloid Sci. 7:569-83(1952).

32. Ueberreiter, K., Z. Physik. Chem. B45:361(1940).

33. Wiley, R. H., and Brauer, G. M., J. Polymer Sci. 3:647(1948).

34. Lorentz, Ann. Phys. 9:641(1880); Lorenz, Ann. Phys. 11:70(1880).

35. Ferry, J. D., and Williams, M. L., J. Colloid Sci. 7:347(1952).

36. Tschoegl, N. W., and Ferry, J. D., Kolloid-Z. 189:37(1963).

37. DeWitt, T. W., Markovitz, H., Padden, F. J., Jr., and Zapas, L. J., J. Colloid Sci. 10:174(1955).

38. Stern, D. M., Berge, J. W., Kurath, S. F., Sakoonkim, C., and Ferry, J. D., J. Colloid Sci. 17:409(1962).

39. Bueche, F., Coven, C. J., and Kinzig, B. J., J. Chem. Phys. 39:128(1963).

40. DeMallie, R. B., Jr., Birnboim, M. H., Frederick, J. E., Tschoegl, N. W., and Ferry, J. D., J. Phys. Chem. 66:536(1962).

41. Tsuzuki, Y., Miwa, M., and Kobayashi, E., Anal. Chem. 23:1169(1951).

APPENDIX I

TUBE IMPEDANCE CORRECTIONS

Comparison of the real parts of Equation (41) shows that the term $\underline{A}_{10}$ depends on the frictional resistance of the tube, $\underline{f}$. This should be a small positive value at all frequencies; however, Table I shows that although $\underline{A}_{10}$ values are small and positive at low frequencies, above 60 c.p.s. they become negative. Negative friction values have no physical meaning, and, therefore, some other factor must be influencing the $\underline{A}_{10}$ values.

In order to determine what effect these negative values had on determining sample impedance, tests were made on samples of glycerin. For a Newtonian liquid like glycerin, the values of $(\underline{A}_1 - \underline{A}_{10})$ should be constant for all frequencies. Figure 34 shows this to be the case even though both $\underline{A}_1$ and $\underline{A}_{10}$ are negative. This indicates that the factor causing the negative values is the same whether samples are in the transducer or not, and it cancels out when taking the difference between the two terms.

However, after using these negative values for calculating the dynamic shear moduli for several concentrations, it became apparent that the loss modulus, $\underline{G}''$, calculated from $(\underline{A}_1 - \underline{A}_{10})$ tended to become too large as the frequency increased, while in some cases the storage modulus tended to be too low. A logical explanation consistent with these facts is that a small phase shift occurred which increased with the frequency. If the frictional resistance is assumed to be essentially zero, then the phase shift, θ, would be $\tan^{-1}(\underline{A}_{10}/\underline{A}_{20})$. The corrected values after phase shifting are

$$A_1' - A_{10}' = (A_1 - A_{10}) \cos\theta + (A_2 - A_{20}) \sin\theta \ , \qquad (55)$$

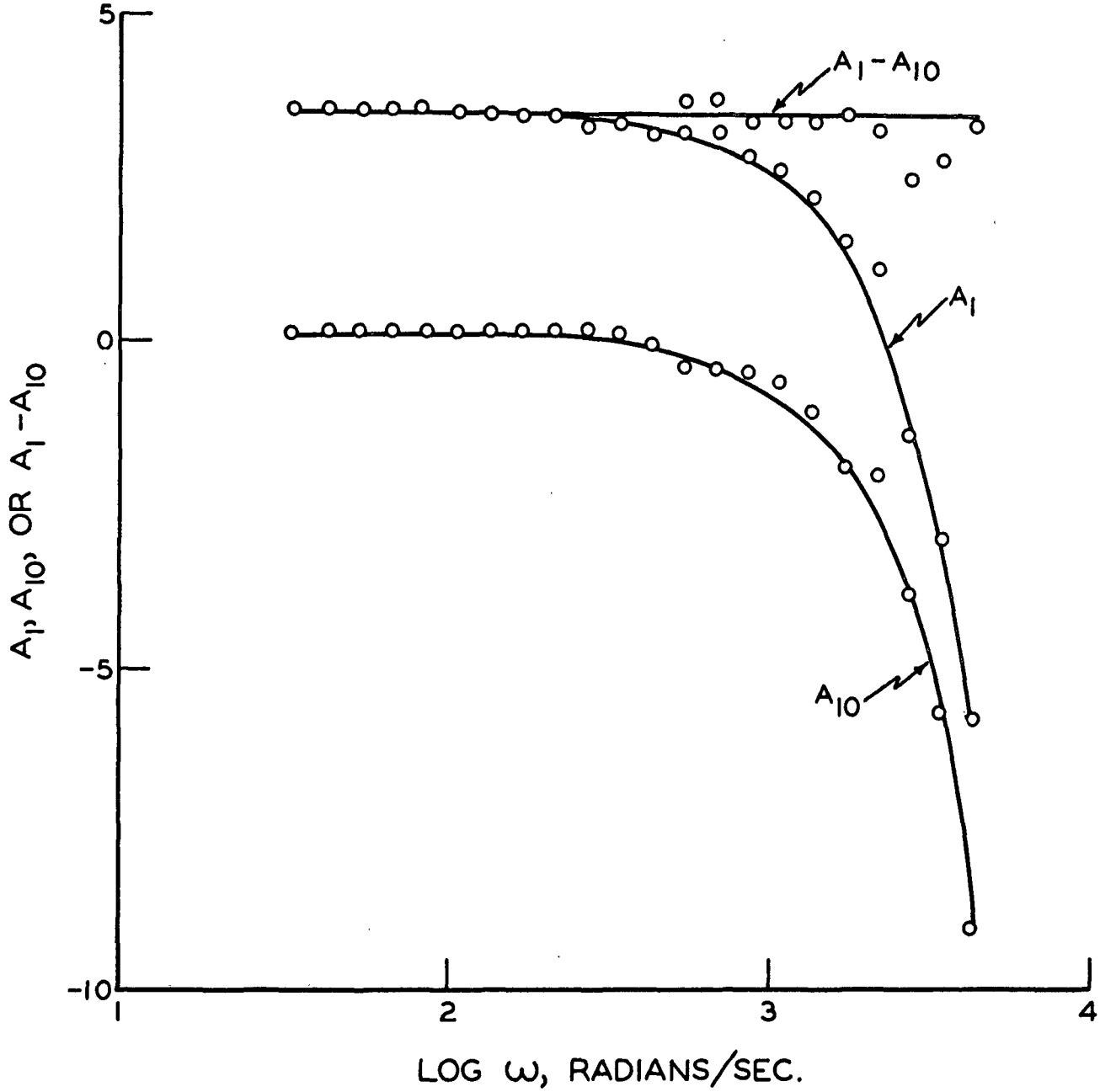

Figure 34. Transducer Tests on Glycerin at -12.7°C.

and,

$$A_2' - A_{20}' = -(A_1 - A_{10}) \sin\theta + (A_2 - A_{20}) \cos\theta \ . \qquad (56)$$

This correction is significant only at high frequencies, and then it amounts to only a few per cent. However, it does help to make the data more consistent, and, therefore, it was used in all the calculations of the dynamic moduli.

A second correction involves the effect of temperature on the elastance $\underline{k}$. This is significant only near the resonance frequency. Rather than determine $\underline{A}_{20}$ values for every temperature at which $\underline{A}_2$ values were measured, linear temperature coefficients were used to convert $\underline{A}_{20}$ values to the proper temperature. The temperature coefficients given in Table V were determined from $\underline{A}_{20}$ data taken over a temperature range of 70°C.

TABLE V

THE TEMPERATURE COEFFICIENTS FOR $\underline{A}_{20}$

Frequency, c.p.s.	Temperature Coefficient, $(d\underline{A}_{20}/d\underline{T}) \times 10^2$
6	-1.84
8	-1.33
10	-1.10
12	-0.843
15	-0.714
20	-0.500
25	-0.372
32	-0.214
40	-0.214

APPENDIX II

PREPARATION OF POLYSTYRENE-TCP SOLUTIONS

For the 5 and 10% solutions, the pure polystyrene and TCP were weighed out and mixed together in a small beaker. The mixtures were heated in an oven with occasional stirring until a homogeneous solution was obtained. The conditions of temperature and time required to prepare the solutions are given in Table VI.

TABLE VI

MIXING AND EXTRUDING CONDITIONS

Polystyrene Concn., %	Mixing Time, hr.	Mixing Temp., °C.	Number of Extrusions	Extruding Temp., °C.
5	12	150		
10	5	150		
	48	50		
21	12	140	4	25
	72	50		
35	72	140		
52	6	140	6	100
67	20	150	2	150
			2	100
			1	80

For the higher concentrations, the polystyrene and TCP were first mixed together and heated under the conditions indicated in the table. When the polystyrene was sufficiently softened by diffusion of the TCP, the mixture was removed from the oven and extruded through a die. The extruder consisted of a 1/2-inch diameter piston which fit into a stainless steel cylinder 1-3/4 inches in length. Three 1/16-inch holes were drilled in the closed end of the cylinder. The mixture was placed in the cylinder, heated and then extruded through the holes by

applying pressure to the piston with a hydraulic press. This procedure was repeated a number of times as indicated in Table VI until a homogeneous solution was obtained. In the case of the 35% solution, the mixture was heated for a longer period than the other solutions and extrusion was not necessary.

APPENDIX III

PREPARATION OF TEST SAMPLES

Bubbles were removed from the solutions by heating under reduced pressure. The solutions of low concentrations were heated for about an hour at 100°C. while the solutions of high concentration were heated at 150°C., also for about an hour. The temperature of a low concentration solution was then adjusted until the solution would barely pour. This required cooling the 5% solution and heating the 21% solution. The sample support block, on which the test sample was to be poured, was cooled with dry ice to a temperature well below that of the solution. When this temperature was below the dew point of the atmosphere, this procedure was carried out in a dry box to prevent moisture from condensing on the block. The viscous solution was then poured onto the block to form a bead. The weight of the sample was determined by difference. The support block with the bead was immediately placed in the transducer. The sample was carefully pressed against the transducer tube to form a thick film which was held in place by its surface tension.

Test samples for the high concentrations were prepared by molding the solutions into disks. The extruder used for mixing the solutions was also used as a mold for the samples. The end of the extruder containing the holes was removed and replaced by a piece without holes. A sample of known weight was then placed in the cylinder and heated under vacuum to 150°C. The mold was set up so that, while it was still under vacuum in the oven, the piston could be pressed down by hand into the cylinder. The vacuum was then released and the mold removed from the oven and placed in a hydraulic press where the piston was placed under pressure while the mold cooled. The mold was cooled to near the glass temperature

of the solution before the sample was pressed out. This prevented the shape of the sample from being deformed. If the sample was free of bubbles it was placed in the transducer for testing. Before transducer tests were made the samples were heated in the transducer to temperatures well above the glass transition temperature to relieve internal stresses which might have formed during the molding process.

APPENDIX IV

DETERMINATION OF FORM FACTORS

The cross-sectional area of a sample was determined indirectly from its thickness, density, and mass;

$$A_i = m_i(\rho h_i) .$$

Equation (43) for the form factor then becomes,

$$h/A = \rho/[(m_1/h_1^2) + (m_2/h_2^2)].$$

The thickness of a sample was determined after being placed in the transducer as follows: After placing the first sample in the transducer, the face of the support block for the second sample was pressed against the transducer tube. The distance between the faces of the two support blocks was then measured using a telescope gage and a micrometer. This distance was equal to the thickness of the sample plus the thickness of the transducer tube. By subtracting the thickness of the transducer tube from the measured distance, the thickness of the first sample was obtained. The second sample was then placed in the transducer and the distance measured again. The increase in the distance was the thickness of the second sample.

APPENDIX V

PHYSICAL PROPERTIES OF POLYSTYRENE-TCP SOLUTIONS

CONCENTRATION

The sulfate-molybdate reagent was prepared as follows: 50 g. of ammonium sulfate were dissolved in 500 ml. of concentrated nitric acid, and 150 g. of ammonium molybdate were dissolved in 400 ml. of boiling water. After cooling, the ammonium molybdate solution was poured slowly into the ammonium sulfate solution. The solution was then transferred to a liter volumetric flask and filled to the mark.

The form of the complex formed with the phosphoric acid is not known, but the composition is constant and the phosphorus content has been accurately determined by Tsuzuki, et al. (41) to be 1.442% phosphorus. The procedure of Lieb in Pregl (29) was followed except that the analysis was made on a larger scale using samples containing a few hundredths of a gram of TCP to give precipitates of a few tenths of a gram.

Five analyses were made on the purified TCP used to make up the polystyrene solutions. The results showed that the phosphorus content of the TCP was 8.35% (± 0.05). The stoichiometric quantity of phosphorus in TCP is 8.40%; therefore, the impurities in the TCP amount to less than 0.7%, assuming that they are all nonphosphorus compounds. This is a reasonable assumption, since the main impurity is probably o-cresol, one of the reactants used in the production of TCP.

Samples from each of the six solutions were analyzed by this method. Concentrations were calculated using 8.35% as the phosphorus content of TCP.

GLASS TRANSITION TEMPERATURE

The glass temperatures were determined from the break in the refractive index-temperature curves. The technique was essentially that described by Wiley and Brauer (33). An Abbé refractometer was used to make the measurements. Ethanol was pumped through a copper coil immersed in a dry ice acetone bath before being circulated around the prisms of the refractometer. By adding dry ice to the acetone bath by hand, the temperature could be held constant within one degree centigrade. The temperature was held constant for approximately five minutes at each point before making a refractive index reading, and then dropped rapidly to the next point. The data for the 21, 52, and 67% solutions are plotted in Fig. 35. The intersection of the straight lines was taken as the glass temperature with an estimated accuracy of $\pm$ 2 degrees.

DENSITY

The density is used to calculate the form factor of the test samples and it is also used in the reduction of the shear moduli. Two methods were used to determine the densities of the solutions. For the low polystyrene concentrations, bubble-free samples were poured into a pycnometer and the remaining free space filled with water. For the high concentrations, samples, usually the same ones used for the transducer tests, were suspended from an analytical balance by a fine wire and weighed in air and then in water to determine their buoyancies.

The densities are plotted in Fig. 36 as a function of concentration. The curve seems to be linear except for the 67% solution. The glass temperature for this concentration is 18°C. which is only about ten degrees below the temperature at which the density was measured. Since the relaxation processes slow

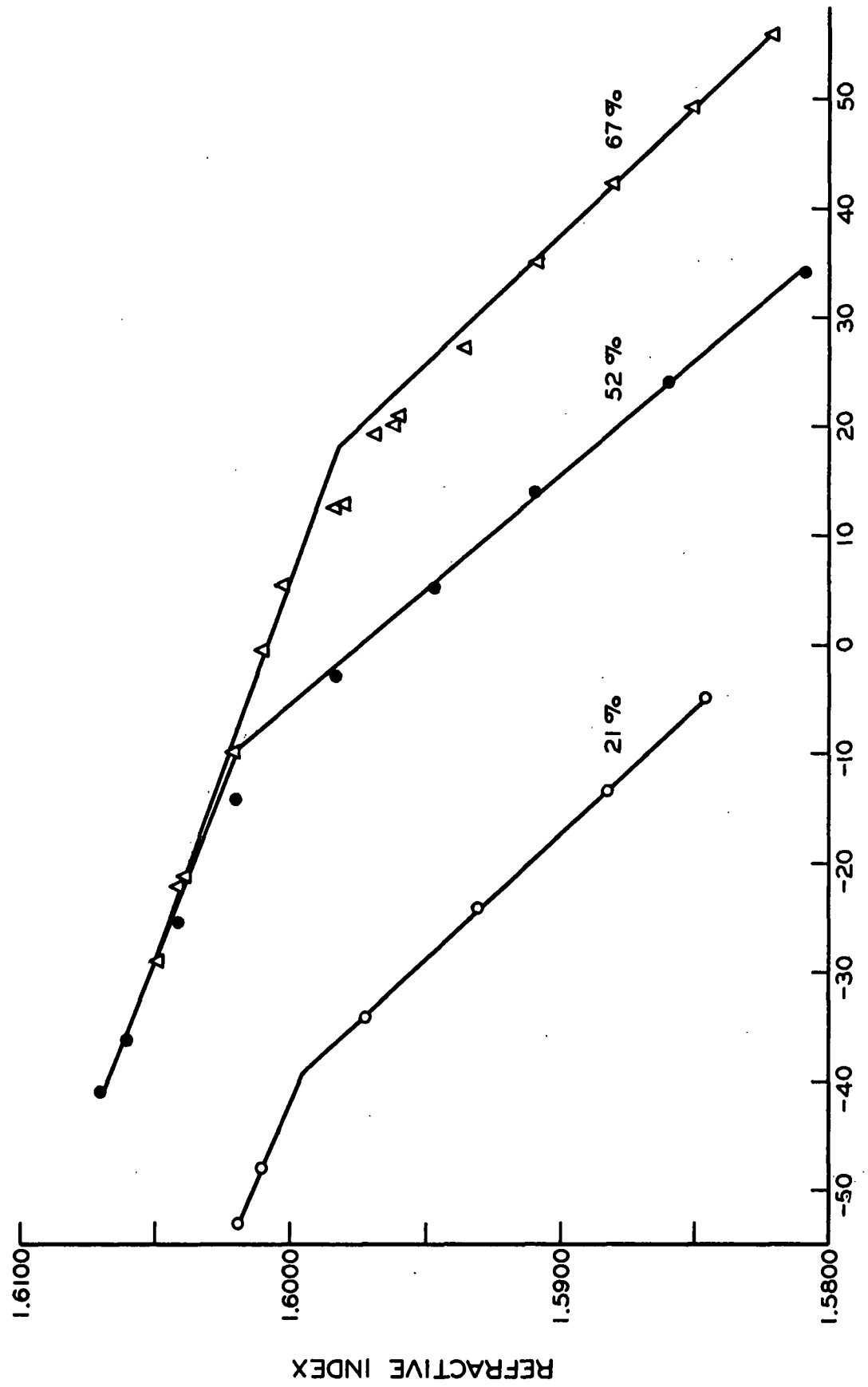

Figure 35. The Determination of the Glass Transition Temperatures for Three Polystyrene-TCP Solutions

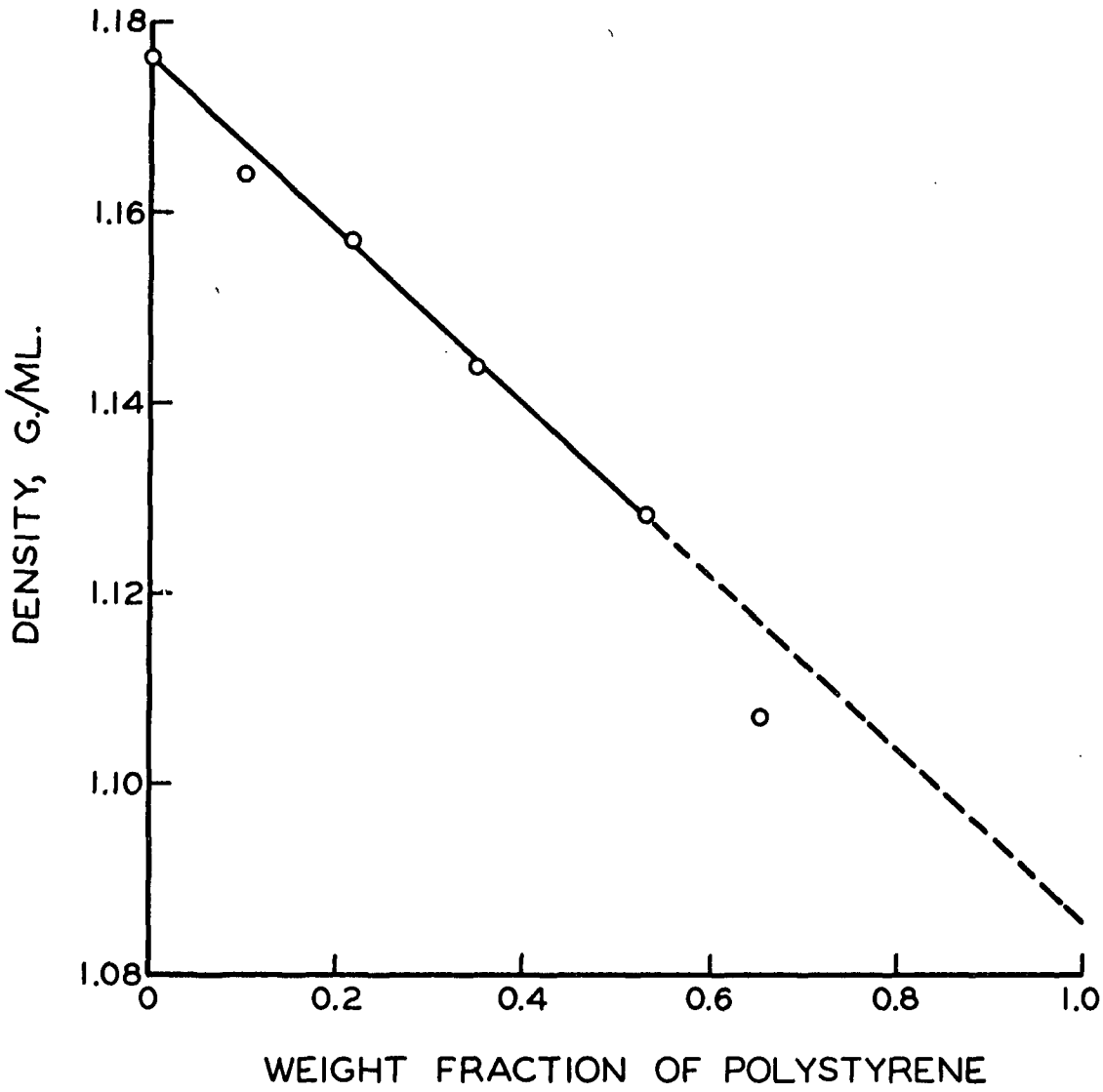

Figure 36. Densities of Polystyrene-TCP Solutions

down drastically as the glass temperature is approached, it may be that the sample on which the density was measured was not at equilibrium.

EXPANSION COEFFICIENT

The Lorenz-Lorentz equation (34) is given by,

$$v = r[(n^2 + 2)/n^2 - 1)]$$

where v is the specific volume, n the refractive index, and r is a constant. Taking the derivative of this equation with respect to temperature and dividing by v gives Equation (44).

Expansion coefficients were calculated for the 21, 52, and 67% solutions using Equation (44) and the data given in Fig. 35. The refractive index was taken at the glass transition temperature. The calculated expansion coefficients, both above and below the glass transition temperature are given in Table III.

Density is required for calculation of the form factor, and also for a temperature reduction of the data. In both cases the densities of the solutions at 25°C. given in Table III were adjusted to the required temperature using an expansion coefficient of 5.5×10^{-4}.

VISCOSITY

The steady-flow viscosities of the pure TCP, and the 5 and 10% solutions were determined using a Hoeppler falling ball viscometer. About 30 ml. of solution were degassed by heating under vacuum. The solution was then carefully poured into the viscometer and the ball inserted. The temperature of the water circulating through the jacket was maintained at 25°C. within $\pm$ 0.1°C. The times

for the ball to pass between the marks was determined a number of times. The viscosity in poise was calculated from the equation,

$$\eta_s = t(\rho_b - \rho)k$$

where t is the time in seconds, k is a calibration constant, and ρ_b and ρ are the densities of the ball and solution, respectively. The times were reproducible within about 0.2%.

APPENDIX VI

TABLE VII

THE STORAGE AND LOSS MODULI FOR SIX POLYSTYRENE-TCP SOLUTIONS

	Frequency, c.p.s.	Log G'', ^{2} dynes/cm.	Log G', ^{2} dynes/cm.
Run Number F-17[a]	6.	6.252	6.245
Temperature 61.9°C.	10.	6.421	6.324
	15.	6.552	6.380
	25.	6.725	6.470
	40.	6.887	6.561
	60.	7.024	6.646
	100.	7.205	--
	150.	7.352	6.866
	250.	7.526	7.009
	400.	7.690	--
Run Number F-12	6.	5.842	6.057
Temperature 69.4°C.	10.	5.995	6.112
	15.	6.115	6.161
	25.	6.263	6.231
	40.	6.408	6.299
	60.	6.530	6.344
	100.	6.694	--
	150.	6.831	6.477
	250.	7.002	--
	400.	7.135	--
Run Number F-13	6.	5.615	5.910
Temperature 75.8°C.	10.	5.737	5.965
	15.	5.840	6.013
	25.	5.964	6.071
	40.	6.090	6.130
	60.	6.202	6.169
	100.	6.342	--
	150.	6.468	--
	250.	6.639	--

[a]Letters refer to polystyrene concentrations. F = 67%; A = 52%; D = 35%; B = 21%; C = 10%; and E = 5%.

TABLE VII (Continued)

	Frequency, c.p.s.	Log $\overline{G''}$, ^{2} dynes/cm.^{2}	Log $\overline{G'}$, ^{2} dynes/cm.^{2}
Run Number F-14	6.	5.468	5.847
Temperature 80.1°C.	10.	5.582	5.896
	15.	5.678	5.935
	25.	5.798	5.989
	40.	5.909	6.044
	60.	6.018	6.072
	100.	6.147	---
	150.	6.263	--
	250.	6.408	--
Run Number F-15	6.	5.351	5.766
Temperature 86.0°C.	10.	5.444	5.817
	15.	5.519	5.851
	25.	5.650	5.907
	40.	5.727	5.947
	60.	5.832	--
	100.	5.938	--
	150.	6.030	--
Run Number F-16	6.	5.263	5.700
Temperature 92.0°C.	10.	5.332	5.746
	15.	5.389	5.774
	25.	5.484	5.826
	40.	5.575	5.864
	100.	5.753	--
	150.	5.899	--
Run Number A-101	6.	7.414	7.024
Temperature 18.0°C.	10.	7.571	7.220
	15.	7.691	7.382
	25.	7.842	7.599
	40.	7.960	7.783
	60.	8.048	7.922
	100.	8.135	8.099
	150.	8.193	8.222
	250.	8.244	8.336
	400.	8.347	8.439
	600.	8.379	8.508
	1000.	8.449	8.603

TABLE VII (Continued)

	Frequency, c.p.s.	Log G'', dynes/cm.^{2}	Log G', dynes/cm.^{2}
Run Number A-100	6.	6.909	6.508
Temperature 23.0°C.	10.	7.085	6.678
	15.	7.222	6.826
	25.	7.391	7.017
	40.	7.540	7.204
	60.	7.662	7.363
	100.	7.800	7.578
	150.	7.900	7.721
	250.	8.013	7.900
	400.	8.137	8.047
	600.	--	8.160
Run Number A-14	6.	6.518	6.252
Temperature 28.0°C.	10.	6.681	6.360
	15.	6.816	6.465
	25.	6.989	6.614
	40.	7.149	6.763
	60.	7.282	6.900
	100.	7.443	7.102
	150.	7.566	7.242
	250.	7.717	7.443
	400.	7.877	7.583
	600.	7.952	7.707
Run Number A-15	6.	6.113	6.007
Temperature 33.0°C.	10.	6.272	6.103
	15.	6.402	6.181
	25.	6.561	6.297
	40.	6.716	6.403
	60.	6.850	6.515
	100.	7.018	6.692
	150.	7.151	6.789
	250.	7.329	6.965
Run Number A-16	6.	5.814	5.856
Temperature 38.0°C.	10.	5.952	5.931
	15.	6.070	5.999
	25.	6.221	6.088
	40.	6.367	6.176
	60.	6.496	6.278
	100.	6.658	--
	150.	6.796	6.477

TABLE VII (Continued)

	Frequency, c.p.s.	Log $\overline{G''}$, dynes/cm.^{2}	Log $\overline{G'}$, dynes/cm.^{2}
Run Number A-17	6.	5.585	5.745
Temperature 43.0°C.	10.	5.711	5.811
	15.	5.816	5.868
	25.	5.951	5.944
	40.	6.084	6.016
	60.	6.204	6.115
	100.	6.361	--
Run Number A-19	6.	5.383	5.651
Temperature 48.0°C.	10.	5.514	5.721
	15.	5.611	5.770
	25.	5.733	5.835
	40.	5.857	5.899
	60.	5.966	--
	100.	6.111	--
Run Number A-21	6.	5.167	5.525
Temperature 58.0°C.	10.	5.255	5.583
	15.	5.342	5.631
	25.	5.435	5.680
	40.	5.525	5.726
Run Number A-22	6.	5.087	5.452
Temperature 63.1°C.	10.	5.149	5.503
	15.	5.228	5.556
	25.	5.306	5.599
	40.	5.388	--
Run Number D-6	6.	6.544	6.223
Temperature 1.6°C.	10.	6.700	6.350
	15.	6.821	6.454
	25.	6.992	6.610
	40.	7.148	6.767
	60.	7.290	--
	100.	7.440	--

TABLE VII (Continued)

	Frequency, c.p.s.	Log $\underline{G}''$, ^{2} dynes/cm.^{2}	Log $\underline{G}'$, ^{2} dynes/cm.^{2}
Run Number D-5	6.	6.090	5.893
Temperature 7.0°C.	10.	6.243	6.018
	15.	6.363	6.121
	25.	6.523	6.273
	40.	6.664	6.363
	60.	6.798	6.475
	100.	6.964	6.648
	150.	7.090	6.762
	250.	7.249	6.936
	400.	7.420	--
	600.	7.536	--
	1000.	7.684	--
Run Number D-4	6.	5.741	5.720
Temperature 12.3°C.	10.	5.890	5.818
	15.	6.000	5.882
	25.	6.151	5.985
	40.	6.291	6.088
	60.	6.415	6.166
	100.	6.572	--
	150.	6.699	6.393
	250.	6.861	6.522
	400.	7.032	--
	600.	7.170	--
	1000.	7.294	--
Run Number D-3	6.	5.412	5.489
Temperature 18.1°C.	10.	5.545	5.564
	15.	5.646	5.633
	25.	5.793	5.724
	40.	5.923	5.810
	60.	6.037	5.885
	100.	6.187	6.037
	150.	6.312	6.069
	250.	6.482	--
	400.	6.656	--

TABLE VII (Continued)

	Frequency, c.p.s.	Log G", dynes/cm.^{2}	Log G', dynes/cm.^{2}
Run Number D-2	6.	5.224	5.357
Temperature 22.4°C.	10.	5.340	5.427
	15.	5.438	5.490
	25.	5.573	5.575
	40.	5.696	5.652
	60.	5.809	5.712
	100.	5.948	--
	150.	6.074	--
	250.	6.231	--
	400.	6.432	--
Run Number D-1	6.	5.048	5.233
Temperature 27.3°C.	10.	5.157	5.303
	15.	5.245	5.359
	25.	5.357	5.435
	40.	5.470	5.505
	60.	5.578	--
	100.	5.707	--
	150.	5.831	--
Run Number D-8	6.	4.930	5.126
Temperature 32.0°C.	10.	5.009	5.189
	15.	5.083	5.244
	25.	5.189	5.319
	40.	5.294	5.381
	60.	5.393	--
	100.	5.523	--
	150.	5.645	--
Run Number D-9	6.	4.776	5.001
Temperature 37.3°C.	10.	4.887	5.087
	15.	4.944	5.142
	25.	5.051	5.214
	40.	5.138	5.271
	60.	5.222	--
	100.	5.334	--
	150.	5.468	--

TABLE VII (Continued)

	Frequency, c.p.s.	Log G'', dynes/cm.^{2}	Log G', dynes/cm.^{2}
Run Number D-11	6.	4.703	4.904
Temperature 42.7°C.	10.	4.785	4.989
	15.	4.832	5.045
	25.	4.922	5.119
	40.	5.008	5.172
	60.	5.078	--
	100.	5.189	--
Run Number D-10	6.	4.650	4.813
Temperature 48.1°C.	15.	4.765	4.963
	25.	4.842	5.036
	40.	4.908	5.090
	60.	4.976	--
	100.	5.111	--
Run Number D-12	6.	4.590	4.737
Temperature 52.6°C.	10.	4.653	4.824
	15.	4.715	4.894
	25.	4.779	4.969
	40.	4.839	5.023
	60.	4.934	--
Run Number B-34	6.	6.858	--
Temperature -16.0°C.	10.	7.008	6.601
	15.	7.149	6.735
	25.	7.329	6.914
	40.	7.480	7.062
	60.	7.611	7.208
	100.	7.776	7.421
	150.	7.900	7.566
	250.	8.050	7.773
	400.	8.214	--
	600.	8.336	--
	1000.	8.509	--

TABLE VII (Continued)

	Frequency, c.p.s.	Log G", dynes/cm.^{2}	Log G', dynes/cm.^{2}
Run Number B-33	6.	6.399	6.104
Temperature -12.0°C.	10.	6.564	6.229
	15.	6.698	6.333
	25.	6.868	6.478
	40.	7.028	6.617
	60.	7.155	6.750
	100.	7.323	6.934
	150.	7.454	7.058
	250.	7.622	7.250
	400.	7.802	7.411
	600.	7.931	--
	1000.	8.116	--
Run Number B-32	6.	5.934	5.748
Temperature -7.0°C.	10.	6.085	5.858
	15.	6.210	5.943
	25.	6.373	6.071
	40.	6.529	6.182
	60.	6.662	6.283
	100.	6.834	--
	150.	6.975	6.561
	250.	7.152	--
Run Number B-2	6.	5.536	5.446
Temperature -2.0°C.	10.	5.678	5.549
	15.	5.794	5.640
	25.	5.943	5.748
	40.	6.091	5.862
	60.	6.207	5.945
	100.	6.372	6.087
	150.	6.503	6.184
	250.	6.671	6.307
Run Number B-3	6.	5.224	5.202
Temperature 3.0°C.	10.	5.356	5.297
	15.	5.464	5.382
	25.	5.603	5.487
	40.	5.733	5.583
	60.	5.853	5.664
	100.	6.001	--
	150.	6.123	5.882
	250.	6.285	6.004

TABLE VII (Continued)

	Frequency, c.p.s.	Log G", dynes/cm.^{2}	Log G', dynes/cm.^{2}
Run Number B-4	6.	4.942	5.000
Temperature 8.0°C.	10.	5.085	5.088
	15.	5.186	5.160
	25.	5.318	5.261
	40.	5.442	5.351
	60.	5.568	--
	100.	5.691	--
	150.	5.810	5.636
	250.	5.961	5.739
Run Number B-6	6.	4.714	4.823
Temperature 13.0°C.	10.	4.866	4.918
	15.	4.956	4.982
	25.	5.080	5.075
	40.	5.192	5.162
	60.	5.299	5.237
	100.	5.432	--
	150.	5.541	5.420
Run Number B-12	6.	4.567	4.710
Temperature 18.0°C.	10.	4.666	4.788
	15.	4.761	4.843
	25.	4.859	4.938
	40.	4.975	5.015
	60.	5.077	5.077
	100.	5.206	--
	150.	5.304	--
	250.	5.464	--
Run Number B-11	6.	4.434	4.611
Temperature 23.0°C.	10.	4.535	4.684
	15.	4.605	--
	25.	4.729	4.825
	40.	4.824	--
	60.	4.905	4.965
	100.	5.039	--

TABLE VII (Continued)

	Frequency, c.p.s.	Log G", dynes/cm.^{2}	Log G', dynes/cm.^{2}
Run Number B-13	6.	4.301	4.474
Temperature 28.0°C.	10.	4.393	4.561
	15.	4.461	4.609
	25.	4.579	4.717
	40.	4.676	4.784
	60.	4.749	4.859
	100.	4.883	--
Run Number B-15	6.	4.231	4.394
Temperature 32.1°C.	10.	4.334	4.486
	15.	4.401	--
	25.	4.490	4.637
	40.	4.582	4.706
	60.	4.661	4.778
	100.	4.776	--
Run Number B-14	6.	4.145	4.307
Temperature 36.1°C.	10.	4.238	4.393
	15.	4.306	--
	25.	4.416	4.573
	40.	4.481	4.641
	100.	4.693	--
Run Number B-17	6.	4.069	4.219
Temperature 40.0°C.	8.	4.153	4.296
	10.	4.193	4.332
	12.	4.240	4.376
	15.	4.265	--
	20.	4.319	4.467
	25.	4.368	4.501
	32.	4.410	4.547
	40.	4.446	4.577
	50.	4.478	--

TABLE VII (Continued)

	Frequency, c.p.s.	Log G", dynes/cm.^{2}	Log G', dynes/cm.^{2}
Run Number B-20	6.	3.972	--
Temperature 48.0°C.	8.	4.012	4.145
	10.	4.007	4.157
	12.	4.112	4.235
	15.	4.156	--
	20.	4.223	4.344
	25.	4.260	4.384
	32.	4.301	4.430
	40.	--	4.468
Run Number B-24	6.	3.902	3.950
Temperature 56.0°C.	8.	3.961	4.029
	10.	4.001	4.061
	12.	4.016	4.103
	15.	4.050	--
	20.	4.121	4.227
	25.	4.176	4.256
	32.	4.198	4.320
	40.	--	4.351
Run Number C-5	6.	6.335	5.769
Temperature -21.7°C.	10.	6.525	5.879
	15.	6.685	5.980
	25.	6.886	6.111
	40.	7.069	6.235
	100.	7.443	6.644
Run Number C-4	6.	5.674	5.354
Temperature -16.0°C.	10.	5.847	5.464
	15.	5.991	5.533
	25.	6.176	5.652
	40.	6.352	5.757
	60.	6.503	5.841
	100.	6.701	--
	150.	6.861	--
	250.	7.069	--
	400.	7.264	--

TABLE VII (Continued)

	Frequency, c.p.s.	Log G'', dynes/cm.^{2}	Log G', dynes/cm.^{2}
Run Number C-3	6.	5.189	4.986
Temperature -10.5°C.	10.	5.341	5.098
	15.	5.460	5.178
	25.	5.626	5.301
	40.	5.782	5.397
	60.	5.922	5.478
	100.	6.107	--
	150.	6.260	--
Run Number C-2	6.	4.850	4.698
Temperature -5.9°C.	10.	4.999	4.826
	15.	5.120	4.899
	25.	5.269	5.033
	40.	5.410	5.136
	60.	5.537	5.221
	100.	5.721	--
	150.	5.859	--
Run Number C-29	6.	4.552	4.450
Temperature -1.1°C.	10.	4.685	4.558
	15.	4.796	4.648
	25.	4.938	4.764
	40.	5.071	4.870
	60.	5.197	4.940
	100.	5.346	--
	150.	5.468	--
Run Number C-28	6.	4.275	4.202
Temperature 4.3°C.	10.	4.400	4.312
	15.	4.523	4.394
	25.	4.636	4.517
	40.	4.764	4.617
	60.	4.879	4.697
	100.	5.025	--
	150.	5.146	--

TABLE VII (Continued)

	Frequency, c.p.s.	Log $\frac{G''}{2}$, dynes/cm.^{2}	Log $\frac{G'}{2}$, dynes/cm.^{2}
Run Number C-27	6.	4.087	4.021
Temperature 9.0°C.	10.	4.207	4.135
	15.	4.307	4.223
	25.	4.431	4.336
	40.	4.552	4.435
	60.	4.661	4.509
	100.	4.801	--
	150.	4.920	--
Run Number C-26	6.	3.923	3.842
Temperature 13.9°C.	10.	4.029	3.962
	15.	4.127	4.055
	25.	4.250	4.168
	40.	4.363	4.266
	60.	4.465	4.333
Run Number C-16	6.	3.776	3.685
Temperature 18.3°C.	10.	3.892	3.813
	15.	3.982	3.913
	25.	4.104	4.029
	40.	4.213	4.125
	60.	4.308	--
Run Number C-17	6.	3.654	3.546
Temperature 23.0°C.	10.	3.778	3.683
	15.	3.863	3.788
	25.	3.985	3.903
	40.	4.090	4.003
	60.	4.186	--
Run Number C-19	6.	3.527	3.391
Temperature 27.7°C.	10.	3.661	3.534
	15.	3.753	3.642
	25.	3.868	3.768
	40.	3.968	3.873
	60.	4.070	--

TABLE VII (Continued)

	Frequency, c.p.s.	Log G", dynes/cm.^{2}	Log G', dynes/cm.^{2}
Run Number E-5	6.	5.219	4.799
Temperature -15.0°C.	10.	5.398	4.913
	15.	5.545	4.998
	25.	5.737	5.096
	40.	5.920	5.186
	60.	6.082	5.264
Run Number E-4	6.	4.807	4.485
Temperature -10.5°C.	10.	4.970	4.608
	15.	5.106	4.703
	25.	5.282	4.821
	40.	5.450	4.924
	60.	5.598	--
	100.	5.792	--
Run Number E-3	6.	4.371	4.118
Temperature -4.4°C.	10.	4.524	4.249
	15.	4.651	4.340
	25.	4.810	4.470
	40.	4.962	4.584
	60.	5.098	--
	100.	5.270	--
Run Number E-2	6.	4.087	3.845
Temperature 0.3°C.	10.	4.236	3.989
	15.	4.353	4.083
	25.	4.507	4.209
	40.	4.650	4.335
	60.	4.780	--
	100.	4.940	--
Run Number E-1	6.	3.820	3.542
Temperature 5.7°C.	10.	3.960	3.695
	15.	4.080	3.798
	25.	4.223	3.944
	40.	4.364	--
	100.	4.640	--

TABLE VII (Continued)

	Frequency, c.p.s.	Log $\underline{G}''$, dynes/cm.^{2}	Log $\underline{G}'$, dynes/cm.^{2}
Run Number E-6	6.	3.482	--
Temperature 14.1°C.	10.	3.630	--
	15.	3.745	--
	25.	3.865	--
	40.	4.002	--
	60.	4.121	--
	100.	4.265	--
Run Number E-7	6.	3.267	--
Temperature 20.4°C.	10.	3.420	--
	15.	3.545	--
	25.	3.676	--
	40.	3.803	--
	60.	3.911	--
Run Number E-8	6.	3.042	--
Temperature 27.0°C.	10.	3.210	--
	15.	3.346	--
	25.	3.482	--
	40.	3.612	--
Run Number E-9	6.	2.863	--
Temperature 33.4°C.	10.	3.024	--
	15.	3.171	--
	25.	3.314	--
	40.	3.424	--

TABLE VIII

TEMPERATURE REDUCTION FACTORS

Temperature, °C.	Log $\frac{T_o \rho_o}{T \rho}$	Log a_T
67% PS		
61.9	0.042	-6.55
69.4	0.050	-7.21
75.8	0.056	-7.69
80.1	0.060	-7.98
86.0	0.066	-8.34
92.0	0.072	-8.66
52%		
18.0	0.009	0.90
23.0	0.002	0.23
28.0	-0.004	-0.35
33.0	-0.010	-0.86
38.0	-0.016	-1.31
43.0	-0.022	-1.70
48.0	-0.027	-2.06
58.0	-0.038	-2.67
63.1	-0.044	-2.95
35%		
1.6	0.030	2.37
7.0	0.023	1.71
12.3	0.016	1.23
18.1	0.008	0.57
22.4	0.003	0.20
27.3	-0.003	-0.19
32.0	-0.008	-0.53
37.3	-0.015	-0.88
42.7	-0.021	-1.20
48.1	-0.027	-1.50
52.6	-0.032	-1.72

TABLE VIII (Continued)

Temperature, °C.	Log $\frac{T_o \rho_o}{T \rho}$	Log a_T
21%		
-16.0	0.054	4.28
-12.0	0.049	3.61
-7.0	0.042	2.88
-2.0	0.035	2.26
3.0	0.028	1.72
8.0	0.021	1.24
13.0	0.015	0.83
18.0	0.009	0.45
23.0	0.002	0.12
28.0	-0.004	-0.18
32.1	-0.008	-0.41
36.1	-0.013	-0.61
40.0	-0.018	-0.80
48.0	-0.027	-1.14
56.0	-0.035	-1.43
10%		
-21.7	0.063	4.51
-16.0	0.054	3.64
-10.5	0.047	2.98
-5.9	0.040	2.40
-1.1	0.034	1.91
4.3	0.026	1.42
9.0	0.020	1.05
13.9	0.014	0.69
18.3	0.008	0.40
23.0	0.002	0.11
27.7	-0.003	-0.15
5%		
-15.0	0.053	3.25
-10.5	0.047	2.66
-4.4	0.038	2.00
0.3	0.032	1.57
5.7	0.024	1.14
14.1	0.014	0.58
20.4	0.006	0.22
27.0	-0.002	-0.10
33.4	-0.010	-0.37

TABLE IX

THE SHEAR MODULI SMOOTHED AND CORRECTED FOR SOLVENT VISCOSITY

67% Solution			52% Solution		
Log ωa_T	Log $(G''_p - \omega a_T \eta_s)$	Log G'_p	Log ωa_T	Log $(G''_p - \omega a_T \eta_s)$	Log G'_p
-7.0	5.21	5.64	-1.2	5.09	5.45
-6.8	5.27	5.68	-1.0	5.16	5.49
-6.6	5.34	5.72	-0.8	5.24	5.54
-6.4	5.43	5.77	-0.6	5.32	5.60
-6.2	5.52	5.82	-0.4	5.42	5.65
-6.0	5.62	5.87	-0.2	5.52	5.71
-5.8	5.73	5.92	0.0	5.63	5.76
-5.6	5.84	5.98	0.2	5.74	5.83
-5.4	5.95	6.04	0.4	5.86	5.89
-5.2	6.08	6.10	0.6	6.00	5.96
-5.0	6.21	6.17	0.8	6.14	6.04
-4.8	6.35	6.25	1.0	6.28	6.12
-4.6	6.50	6.32	1.2	6.43	6.22
-4.4	6.65	6.41	1.4	6.59	6.32
-4.2	6.80	6.50	1.6	6.75	6.44
-4.0	6.96	6.59	1.8	6.90	6.56
-3.8	7.12	6.69	2.0	7.06	6.69
-3.6	7.28	6.81	2.2	7.22	6.83
-3.4	7.44	6.94	2.4	7.37	6.99
-3.2	7.61	--	2.6	7.52	7.16
			2.8	7.66	7.34
			3.0	7.79	7.52
			3.2	7.90	7.70
			3.4	8.01	7.87
			3.6	8.10	8.02
			3.8	8.18	8.16
			4.0	8.25	8.28
			4.2	8.31	8.38
			4.4	8.37	8.47
			4.6	8.42	8.56

TABLE IX (Continued)

35% Solution			21% Solution		
Log ωa_T	Log $(G''_p - \omega a_T \eta_s)$	Log G'_p	Log ωa_T	Log $(G''_p - \omega a_T \eta_s)$	Log G'_p
0.0	4.59	4.76	0.0		
0.2	4.64	4.83	0.2	3.90	3.94
0.4	4.70	4.90	0.4	3.97	4.05
0.6	4.76	4.97	0.6	4.03	4.14
0.8	4.83	5.03	0.8	4.10	4.24
1.0	4.90	5.09	1.0	4.16	4.32
1.2	4.97	5.15	1.2	4.24	4.40
1.4	5.06	5.22	1.4	4.32	4.48
1.6	5.17	5.28	1.6	4.40	4.55
1.8	5.24	5.35	1.8	4.48	4.63
2.0	5.35	5.43	2.0	4.56	4.70
2.2	5.46	5.50	2.2	4.66	4.77
2.4	5.57	5.57	2.4	4.76	4.85
2.6	5.69	5.65	2.6	4.86	4.92
2.8	5.82	5.73	2.8	4.96	5.00
3.0	5.95	5.82	3.0	5.07	5.08
3.2	6.08	5.90	3.2	5.18	5.17
3.4	6.21	6.00	3.4	5.29	5.26
3.6	6.34	6.10	3.6	5.41	5.35
3.8	6.48	6.20	3.8	5.54	5.45
4.0	6.62	6.31	4.0	5.67	5.55
4.2	6.76	6.43	4.2	5.79	5.65
4.4	6.90	6.55	4.4	5.93	5.75
4.6	7.05	6.69	4.6	6.05	5.85
4.8	7.20	6.84	4.8	6.19	5.96
5.0	7.35	--	5.0	6.32	6.06
5.2	7.49	--	5.2	6.45	6.17
			5.4	6.59	6.29
			5.6	6.74	6.40
			5.8	6.87	6.53
			6.0	7.00	6.66
			6.2	7.15	6.79
			6.4	7.28	6.94
			6.6	7.42	6.09
			6.8	7.56	7.25
			7.0	7.70	7.41
			7.2	7.84	7.58
			7.4	7.98	7.75
			7.6	8.11	--
			7.8	8.26	--
			8.0	8.38	--

TABLE IX (Continued)

10% Solution			5% Solution		
Log ωa_T	Log $(G''_p - \omega a_T \eta_s)$	Log G'_p	Log ωa_T	Log $(G''_p - \omega a_T \eta_s)$	Log G'_p
1.6	3.58	3.46	1.2	2.83	--
1.8	3.66	3.58	1.4	2.98	--
2.0	3.76	3.69	1.6	3.13	--
2.2	3.85	3.79	1.8	3.26	--
2.4	3.95	3.89	2.0	3.38	--
2.6	4.05	3.99	2.2	3.52	--
2.8	4.14	4.08	2.4	3.63	--
3.0	4.25	4.18	2.6	3.75	--
3.2	4.35	4.28	2.8	3.86	3.63
3.4	4.45	4.38	3.0	3.98	3.76
3.6	4.56	4.48	3.2	4.09	3.89
3.8	4.67	4.59	3.4	4.22	4.02
4.0	4.79	4.69	3.6	4.34	4.14
4.2	4.90	4.80	3.8	4.46	4.26
4.4	5.02	4.91	4.0	4.57	4.39
4.6	5.14	5.02	4.2	4.71	4.50
4.8	5.25	5.12	4.4	4.83	4.62
5.0	5.37	5.23	4.6	4.95	4.73
5.2	5.47	5.33	4.8	5.06	4.84
5.4	5.59	5.44	5.0	5.21	4.94
5.6	5.70	5.54	5.2	5.34	5.04
5.8	5.82	5.64	5.4	5.46	5.12
6.0	5.95	5.75	5.6	5.62	5.21
6.2	6.06	5.86	5.8	5.78	5.30
6.4	6.21	5.96			
6.6	6.32	6.07			
6.8	6.45	6.17			
7.0	6.58	6.28			
7.2	6.69	--			